Final Report

FDOT Contract No.: BDK75-977-68
UF Contract No.: 00100800

Pile/Shaft Designs Using Artificial Neural Networks (i.e., Genetic Programming) with Spatial Variability Considerations

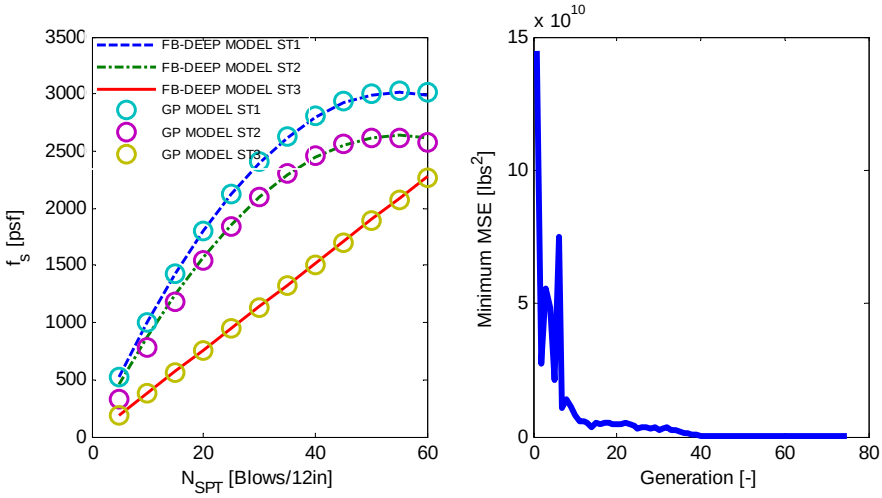

Principal Investigators: Michael C. McVay
Harald Klammler
Khiem Tran
Primary Researcher: Michael Faraone
Student Assistants: Nathan Dodge
Nilses Vera
Le Yuan

Department of Civil and Coastal Engineering
Engineering School of Sustainable Infrastructure and Environment
University of Florida
P.O. Box 116580
Gainesville, Florida 32611-6580

Developed for the

Rodrigo Herrera, P.E., Project Manager; Peter Lai (Retired)

February 2014

DISCLAIMER

The opinions, findings, and conclusions expressed in this publication are those of the authors and not necessarily those of the Florida Department of Transportation or the U.S. Department of Transportation.

Prepared in cooperation with the State of Florida Department of Transportation and the U.S. Department of Transportation.

SI (MODERN METRIC) CONVERSION FACTORS (from FHWA)

APPROXIMATE CONVERSIONS TO SI UNITS

SYMBOL	WHEN YOU KNOW	MULTIPLY BY	TO FIND	SYMBOL
LENGTH				
in	inches	25.4	millimeters	mm
ft	feet	0.305	meters	m
yd	yards	0.914	meters	m
mi	miles	1.61	kilometers	km

SYMBOL	WHEN YOU KNOW	MULTIPLY BY	TO FIND	SYMBOL
AREA				
in^2	square inches	645.2	square millimeters	mm^2
ft^2	square feet	0.093	square meters	m^2
yd^2	square yard	0.836	square meters	m^2
ac	acres	0.405	hectares	ha
mi^2	square miles	2.59	square kilometers	km^2

SYMBOL	WHEN YOU KNOW	MULTIPLY BY	TO FIND	SYMBOL
VOLUME				
fl oz	fluid ounces	29.57	milliliters	mL
gal	gallons	3.785	liters	L
ft^3	cubic feet	0.028	cubic meters	m^3
yd^3	cubic yards	0.765	cubic meters	m^3
NOTE: volumes greater than 1000 L shall be shown in m^3				

SYMBOL	WHEN YOU KNOW	MULTIPLY BY	TO FIND	SYMBOL
MASS				
oz	ounces	28.35	grams	g
lb	pounds	0.454	kilograms	kg
T	short tons (2000 lb)	0.907	megagrams (or "metric ton")	Mg (or "t")

SYMBOL	WHEN YOU KNOW	MULTIPLY BY	TO FIND	SYMBOL
TEMPERATURE (exact degrees)				
°F	Fahrenheit	5 (F-32)/9 or (F-32)/1.8	Celsius	°C

SYMBOL	WHEN YOU KNOW	MULTIPLY BY	TO FIND	SYMBOL
ILLUMINATION				
fc	foot-candles	10.76	lux	lx
fl	foot-Lamberts	3.426	candela/m^2	cd/m^2

SYMBOL	WHEN YOU KNOW	MULTIPLY BY	TO FIND	SYMBOL
FORCE and PRESSURE or STRESS				
Lbf*	poundforce	4.45	newtons	N
kip	kip force	1000	pounds	lbf
lbf/in^2	poundforce per square inch	6.89	kilopascals	kPa

APPROXIMATE CONVERSIONS TO SI UNITS

SYMBOL	WHEN YOU KNOW	MULTIPLY BY	TO FIND	SYMBOL
		LENGTH		
mm	millimeters	0.039	inches	in
m	meters	3.28	feet	ft
m	meters	1.09	yards	yd
km	kilometers	0.621	miles	mi

SYMBOL	WHEN YOU KNOW	MULTIPLY BY	TO FIND	SYMBOL
		AREA		
mm^2	square millimeters	0.0016	square inches	in^2
m^2	square meters	10.764	square feet	ft^2
m^2	square meters	1.195	square yards	yd^2
ha	hectares	2.47	acres	ac
km^2	square kilometers	0.386	square miles	mi^2

SYMBOL	WHEN YOU KNOW	MULTIPLY BY	TO FIND	SYMBOL
		VOLUME		
mL	milliliters	0.034	fluid ounces	fl oz
L	liters	0.264	gallons	gal
m^3	cubic meters	35.314	cubic feet	ft^3
m^3	cubic meters	1.307	cubic yards	yd^3

SYMBOL	WHEN YOU KNOW	MULTIPLY BY	TO FIND	SYMBOL
		MASS		
g	grams	0.035	ounces	oz
kg	kilograms	2.202	pounds	lb
Mg (or "t")	megagrams (or "metric ton")	1.103	short tons (2000 lb)	T

SYMBOL	WHEN YOU KNOW	MULTIPLY BY	TO FIND	SYMBOL
		TEMPERATURE (exact degrees)		
°C	Celsius	1.8C+32	Fahrenheit	°F

SYMBOL	WHEN YOU KNOW	MULTIPLY BY	TO FIND	SYMBOL
		ILLUMINATION		
lx	lux	0.0929	foot-candles	fc
cd/m^2	candela/m^2	0.2919	foot-Lamberts	fl

SYMBOL	WHEN YOU KNOW	MULTIPLY BY	TO FIND	SYMBOL
		FORCE and PRESSURE or STRESS		
N	newtons	0.225	poundforce	lbf
kPa	kilopascals	0.145	poundforce per square inch	lbf/in^2

*SI is the symbol for International System of Units. Appropriate rounding should be made to comply with Section 4 of ASTM E380.
(Revised March 2003)

Symbol List

A_{Tip} – Cross-sectional area used for tip resistance calculation

B – Pile or Shaft diameter/width

COV – Covariance

CV – Coefficient of variation, standard deviation / mean

CV_M –Error for a method

CV_R – Total prediction resistance error

CV_s –Error from site variability

CV_{SPT} – Error in SPT measurements

E – Elastic Modulus

f_s – Mobilized side resistance

$f_{s,ult}$ – Ultimate side resistance

$\bar{f}_{ST}$ – Mean side resistance for specific soil type

k – Generalized mean averaging factor

L_i – SPT N attributed length along pile

L – Total pile length

L_{ST_i}- Total length of specific soil type alongside a pile

M – Measured value

MSE – Mean squared error, eq. 3.1

MSE_{Ln} – Mean squared error evaluated in log space, eq. 3.1

N – SPT blowcount

$\mathbb{R}$ - GP generated random constant

R – Resistance

r – Percent deflection z/B

REC - Recovery

RMSE – Root mean squared error, eq 3.1

RQD – Rock quality index

P – Predicted value

p – Boring foundation resistance prediction

Prm – Pile perimeter

$\overline{q_T}$ – Mean unit tip resistance

q_t – Split tension

Q_{TIP} – Tip Resistance

q_u – Unconfined compression

T – Mobilized side shear resistance

t – Load test prediction

W_i – Weighting factor for averaging

Z – Displacement

β – Reliability index

Δ – Pile segment deflection

λ – Method bias

Φ – LRFD resistance factor

σ_ε^2 – Error variance between load test and borings

σ'^2_ε – Error variance between borings

σ_m^2 – Method error

σ_A^2 – Error from mean prediction of borings and load tests

σ_B^2 – Error from random construction issues and construction method between sites

σ_C^2 – Error from site specific variability

σ_D^2 – Error from random construction issues within a site

σ_E^2 – Error from measurement errors between sites

σ_F^2 – Error from random measurement within a site

σ_{LF}^2 – Method error determined from scatter about a linear trend

TECHNICAL REPORT DOCUMENTATION PAGE

1. Report No.	2. Government Accession No.	3. Recipient's Catalog No.
4. Title and Subtitle Pile/Shaft Designs Using Artificial Neural Networks (i.e., Genetic Programming) with Spatial Variability Considerations		5. Report Date March 2014 6. Performing Organization Code
7. Author(s) Michael C. McVay, Harald Klammler, Khiem Tran, Michael Faraone, Nathan Dodge, Nilses Vera and Le Yaun		8. Performing Organization Report No.
9. Performing Organization Name and Address University of Florida – Dept. of Civil and Coastal Engineering Engineering School of Sustainable Infrastructure and Environment 365 Weil Hall – P.O. Box 116580 Gainesville, FL 32611-6580		10. Work Unit No. (TRAIS) 11. Contract or Grant No. BDK75-977-68
12. Sponsoring Agency Name and Address Florida Department of Transportation 605 Suwannee Street, MS 30 Tallahassee, FL 32399		13. Type of Report and Period Covered Final Report 10/15/12 – 5/15/14 14. Sponsoring Agency Code
15. Supplementary Notes		

16. Abstract

The work focused on the improvement of FB-DEEP's prediction of skin and tip resistance of concrete piles and drilled shafts in Florida. For the work, data from 19 concrete pile sites and 18 drilled shaft sites were collected. This included 458 standard penetration test, SPT, borings on the pile sites and 815 borings on the drilled shaft sites. A total of 64 static pile load tests and 66 drilled shaft tests were acquired. For the piles, 48 tests reached Davisson Capacity, of which 28 had separation of skin and tip resistance. All of the drilled shafts were instrumented with strain gauges from which unit skin transfer (T–Z) was assessed for Florida limestone. All of the data were uploaded into the FDOT online database based on position (i.e., station + offset, or GPS).

In the case of piles, the data (e.g., boring vs. measured skin friction) were analyzed with a genetic program (GP) algorithm to construct equations for unit skin friction and tip resistance based on soil type (USCS) and SPT N values. The resulting GP skin friction curves were found to be similar to FB-DEEP; the tip resistance curves had higher unit tip resistance vs. blow count values, as well as being only averaged 4 diameters/widths beneath the piles. In addition, the practice of setting SPT N to zero for N< 5 was found to be conservative, and the use of N=5 for N< 5 is recommended. For both current FB-DEEP and GP curves, load resistance factor design, LRFD Φ, were obtained for borings within 100 ft. In the case of borings outside this distance or for site-specific conditions, method error (CV_m) for FB-DEEP and the GP curves is presented from which LRFD Φ may be found.

In the case of drilled shaft, the GP algorithm a developed normalized unit skin friction vs. displacement curve for limestone, which were similar to Kim (2001). In the case of ultimate skin friction in limestone, the GP algorithm was used to validate the FDOT relationship between unit skin friction and rock strength (unconfined compression, split tension).

17. Key Words	18. Distribution Statement
Genetic Programming, Deep Foundations, LRFD ϕ, Spatial Variability, Prestressed Concrete Piles, Skin, Tip, and Total Resistance	No restrictions.

19. Security Classif. (of this report)	20. Security Classif. (of this page)	21. No. of Pages	22. Price
Unclassified	Unclassified	133	

Form DOT F 1700.7 (8-72) Reproduction of completed page authorized

ACKNOWLEDGMENTS

The researchers would like to thank the Florida Department of Transportation (FDOT) for the financial support to carry out this research, the State Materials Office (SMO) for providing laboratory results, and the district offices for plans and geotechnical reports.

EXECUTIVE SUMMARY

Current length estimates of driven prestressed concrete test piles and drilled shafts in Florida uses the FB-DEEP program, developed more than 20 years ago, which is known to be typically conservative. For instance, Styler (2006) reported that FB-DEEP's bias (measured/ predicted) was 1.4 for prestressed concrete piles in Florida soils and rock at Davisson Capacity. Similarly, in early design of drilled shafts, limited rock strength (q_u and q_t) data were available on sites with load tests when the original unit skin friction curves were developed.

Consequently, the focus of this work was to improve both unit skin friction and tip resistances curves for estimating pile and shaft capacities. To accomplish this, data from 18 pile sites in Florida and one in Louisiana as well as 18 drilled shaft sites in Florida were collected. In the case of in situ data, 458 standard penetration test, SPT, borings on the pile sites and 815 borings on the drilled shaft sites were obtained from geotechnical reports and plans obtained from the FDOT districts. A total of 64 static pile load tests and 66 drilled shaft tests (33 Osterberg, 15 top-down static, and 15 Statnamic) was acquired. For the piles, 48 tests reached Davisson Capacity, of which 28 had separation of skin and tip resistance. All of the drilled shafts were instrumented with strain gauges from which unit skin transfer (T –Z) was assessed for Florida limestone. All of the in situ data (borings, rock strengths – q_u and q_t) was uploaded into the FDOT online database based on position (i.e., station + offset, or GPS). For the load tests (piles and shafts), all of the data (load test and T-Z curves) were digitized and also uploaded into the database.

To analyze the data (e.g., boring vs. unit skin friction), a genetic program (GP) algorithm was written. The GP program used concepts of genetic evolution (cross-over, mutation and reproduction) to construct equations (unit skin friction and tip resistance), which result in the

minimum mean square error, MSE, (reduces bias and its variance) between the predicted and measured values. In development of the unit curves, different forms of averaging (arithmetic, harmonic and geometric) were considered. For soil/rock delineation, the Unified Soil Classification System (USCS) was used to separate the material into 4 general types: 1) clays; 2) silty-sands or sandy silts; 3) clean sands; and 4) limestone rock. For the 4 soil types, the following unit skin friction curves (tsf – tons/ft^2, psf - lbs/ft^2) were obtained for piles:

$$f_s(tsf) = USF = 0.051 * N + 0.098 \quad < 1.5tsf\ (3000\ psf), (Soil\ Type\ 1)$$

$$f_s(tsf) = USF = 0.037 * N \quad < 1.375tsf\ (2750\ psf) \quad (Soil\ Type\ 2)$$

$$f_s(tsf) = USF = 0.0125 * N + 0.175 \quad (Soil\ Type\ 3)$$

$$f_s(tsf) = USF = 0.0125 * N \quad (Soil\ Type\ 4)$$

In the case of pile tip resistance, the following linear representations were developed:

$$q_T(tsf) = 0.58325 * N \quad (Soil\ Type\ 1)$$

$$q_T(tsf) = 1.08 * N \quad (Soil\ Type\ 2)$$

$$q_T(tsf) = 1.25 * N \quad (Soil\ Types\ 3\ \&\ 4)$$

In the case of averaging, arithmetic (vs. geometric and harmonic) was found to result in the lowest MSE, (i.e., variance plus bias) for both skin and tip resistance assessment. Also, it was discovered that FB-DEEP's estimate of pile tip resistance was very conservative, attributed not only to the unit tip resistance curves, but also the averaging process of 8B above and 3.5B below the tip. In order to increase the mean SPT blow count, as well as reduce the error, averaging only 4B below the tip was found to result in the lowest error for the unit tip resistance curves. Note, the GP development for unit tip resistance was for predominately cohesionless soils. Finally, for both FB-DEEP and the GP proposed curves, current practice of setting SPT N to zero for N< 5 increased the bias by 18 % (FB-DEEP and GP) versus using N=5 for N< 5.

Using borings within 100 ft of the test piles resulted in LRFD resistance,Φ, values of 0.66 (side) and 0.49 (Davisson) for the GP curves and 0.65 (side) and 0.61 (Davisson) for FB-DEEP (for N <5, N=5) with β=2.5. Note, for comparison for existing FB-DEEP tip resistance see section 5.4. For comparison (without bias), the Φ/λ values were 0.62 (side) and 0.52 (Davisson) for the GP and 0.54 (side) and 0.43 (Davisson) for FB-DEEP (for N <5, N=5). Note, these values considered both spatial and method error and are recommended for borings within 100 ft.

To improve the LRFD Φ assessment (e.g., borings closer to pile to reduce spatial uncertainty; required for tip assessment), the method error for side, tip, and Davisson capacity was assessed for each method's (GP and FB-DEEP) side and tip resistance curves. Using both the boring and load tests, the error between prediction and load test, σ_{ε}^2, as well the prediction error between borings, $\sigma_{\varepsilon\prime}^2$, was found, from which the method error σ_m^2 (or CV_m) was assessed for both the GP and FB-DEEP algorithms based on distance (100 ft, 500 ft and 1000 ft). Adding the method error to the spatial error, e.g., using borings at distances of interest with the algorithms (e.g., GP and FB-DEEP) to find CV_s, then the total uncertainty, CV_R, and LRFD Φ was found on a site-specific basis.

In the case of the drilled shafts, a normalized mobilized unit skin friction vs. displacement was developed with the GP algorithm based on 33 T-Z curves of limestone,

$$\frac{f_s}{f_{s,ult}} = \left[\frac{4 * r}{4 * r + 1}\right]^{0.5}$$

where, r = z (displacement) / B (shaft diameter). A comparison between FB-DEEP's (Kim, 2001) mobilized unit skin friction vs. displacement curve with the GP results are quite similar on average; however, the mean square error (MSE) for the GP curve (0.0198) is slightly better than Kim (2001) curve (0.1359).

For estimating ultimate skin friction of limestone, the following equation was developed,

$$f_{s,bias\_corrected} = 0.768\left(\frac{1}{2}\sqrt{q_u}\sqrt{q_t}\ x\ Recovery\right)$$

where q_u and q_t are unconfined and split tension strength, and recovery is for the whole site.

The method error for this analysis was quantified by a constant error, σ_{LF} , (spread of data about linear trend line). For the equation above, it was found to be σ_{LF} equal to1.96 tsf.

TABLE OF CONTENTS

page

LIST OF TABLES

LIST OF FIGURES

Figure page

CHAPTER 1
INTRODUCTION

1.1 Background

The Florida Department of Transportation, FDOT, supports the majority of their structures (bridges, sound walls, sign, lighting, etc.) on deep foundations (driven piles, drilled shafts and auger-cast piles). The designs of such foundations usually employ, standard penetration test, SPT, borings in the vicinity of the foundation and the use of FDOT's FB-DEEP software. Recently, AASHTO and FDOT adopted Load Resistance Factor Design, LRFD, or reliability based design as the standard design method. FDOT developed and intent to improve the LRFD Φ factors. Impacting the LRFD Φ factor (used to set pile/shaft length) is uncertainty (CV_R) associated with spatial variability (e.g., borings 50 to 100 ft from the foundation) as well as error associated with design methodology. For instance, FDOT "BDK-75-977-23" (LRFD Φ Factors for Deep Foundation Design due to Site Variability) has developed analytical approaches (e.g., software) for assessing spatial uncertainty based on SPT N values in the footprint or from nearby borings (i.e., spatial variability). However, also contributing to the LRFD Φ resistances variability is the uncertainty of the method, i.e., the empirical methods of assessing skin or tip resistance on the pile/shaft. For instance, Chung et al. (2011) showed that the tip resistance of a drilled shaft embedded in limestone is influenced not only by the modulus of rock beneath the tip, but also by its variability (CV_E^2).

Recently, a number of authors [Nawari et al. (1999), Shahin and Jaksa (2005)] have reported Artificial Neural Network (ANN) software, which was trained on a database of measured foundation response having coefficient of variation, CV_R, equal to or better than established design approaches. For instance, for shallow foundations, Shahin and Jaksa (2005)

used 150 footings in granular soil to train the ANN algorithm. Comparison with traditional methods (e.g., Schmertmann, Meyerhof) showed correlation coefficient of 0.9 for ANN, 0.44 for Meyerhof, and 0.798 for Schmertmann. Using the ANN algorithm, Shahin and Jaksa (2005) developed design charts based on contact stress, footing dimension, and SPT N for predicting settlements. Also in the paper, Shahin and Jaksa (2005) incorporated spatial variability in the proposed design. Specifically, using the expected SPT N beneath the footing and associated variability, the ANN code was run approximately 1000 times to identify the mean expected settlement, as well as its variability from which LRFD Φ was assessed. Similarly, Nawari et al. (1999) developed an ANN code for estimating axial and lateral capacities/movements of driven piles (concrete, pipe, etc.). Using a database of 60 piles loaded axially and 25 piles loaded laterally, Nawari et al. (1999) showed ANN comparisons with traditional methods (SPT 91, Coyle & Costello, Reese p-y). Generally, the ANN had correlation coefficients between 0.88 (axial) and 0.94 (lateral) vs. 0.65 (Coyle) and 0.78 (SPT 91). More recently, Rezania and Javadi (2007) improved Artificial Neural Networks (ANN) approach with Genetic Programming (GP). In the latter case, the neural network of weighting values (ANN) was replaced with a genetic program (variables, and function statements – sqrt, log, division, etc.), which was trained through genetic evolution (i.e., cross-over, mutation) on a database to evolve an analytical model (i.e., equation) to predict shallow foundation settlements. Rezania and Javadi (2007) was able to reproduce Shahin and Jaksa (2005) ANN correlation coefficient (0.9) with the GP analytical expression developed on the same database and test cases.

Therefore, with the recent advances in geospatial analyses (FDOT BDK-75-977-23), artificial neural network software (ANN or GP), databases (i.e., FDOT/UF: as built and load tests), and reliability based design (e.g., LRFD), improvements in current deep foundation design

may be possible. Specifically, prior geospatial research, i.e., BDK-75-977-23, has identified that LRFD resistance factors, Φ, for a specific prediction method are impacted by bias (i.e., measured/predicted resistances) and its variability (i.e., coefficient of variation CV_R = standard deviation / mean bias). Contributing to the variability (i.e., CV_R) is: 1) spatial variability, e.g., boring nearby vs. 200ft away; and 2) prediction method error, i.e., uncertainty of the method if the boring was in the footprint of the pile/shaft. Since, the spatial uncertainty (e.g., variability of SPT N values in a layer) are site to site specific, as well as a function of foundation dimension (e.g., diameter and length), further reductions in CV_R can only occur through reduction in method error (i.e., prediction method).

Therefore, using ANN/GP, both driven prestressed concrete piles and drilled shafts may be analyzed with site borings, to obtain the best fit unit skin friction and end bearing representation with the static load tests, which minimizes both the bias (measured and predicted resistances), and the total variability, i.e., CV_R (combined spatial and method). Next, using the multiple borings on a site with the ANN/GP determined side and tip resistance curves, the spatial variability contribution to the site's CV_R may be established and subtracted from the total CV_R to obtain the method error, which may be used subsequently for any future design with the new side and tip resistance curves.

1.2 Objective and Supporting Tasks

The primary objective of the research is to improve axial prediction of skin and tip resistance for deep foundations using SPT, and laboratory data (e.g., rock strength). Past research (BDK-75-977-23) has shown that the method error (expressed as $CV_\varepsilon = \sigma_\varepsilon/m_\varepsilon$) varies from 0.25 to 0.6 as function of foundation type. Contributing to the error in the original development (e.g., SPT91) was that only one boring (e.g., 10ft to 50ft away) was used (i.e., provides limited SPT N

– effects mean and variance), along with spatial uncertainty. Also contributing to the method error (CV_ε) is the uncertainty of the layer boundaries, i.e., location of bearing layer relative to pile tip. Finally, when the original equations (skin & tip) were developed, simple evaluation techniques (i.e., scatterplots with no use of any minimization techniques) were employed.

As identified in the background, significant improvements in data mining, e.g., Artificial Neural Network (ANN) and recently Genetic Programming (GP) have occurred for the development of improved design charts or algorithms in assessing foundation (shallow & deep) design. Trained with databases of measured response (e.g., settlement, capacity, etc.) along with insitu boring data, loads, etc., newer skin and tip resistance curves may be developed for Florida conditions (e.g., specific soil and foundation types) with consideration given for spatial and method uncertainty variability. The research work will be accomplished through five tasks as described below:

1.2.1 Task 1 – Collection of Borings, and Load Test Data for Driven Concrete Piles and Drilled Shafts

FDOT is storing all static load tests on piles and shafts in the new FDOT online (Microsoft SQL) database vs. the older Microsoft access database used to develop SPT91. The newer database contains recent FDOT sites (17^{th}, Dixie Highway, Jewfish Creek, etc.), which contains multiple boring, laboratory and load test data. In the case of boring data, some of the drilled shaft data may be in the footprint of the shafts. In the case of the older Microsoft Access Database (PC based), over 400 piles and drilled shaft load test data is available; however, only one set of boring data (nearest) with pile driving record was recorded. In addition, the older database has data (approximately 50%) from commercial (e.g., hotels, condos, etc.) sites. Consequently, the older FDOT bridge Access Database information needs to be ported over to the newer online FDOT SQL database. In addition, nearby boring data reported in the plans (i.e.,

legacy data) needs to be coded and uploaded into the newer online database. For instance, it is estimated that over 100 static pile/shaft load test data needs to be transferred from the Access to the online database; and hundreds of borings will need to be collected from plan sheets and uploaded to online database. All of the data will be used by the Genetic program to improve design resistance (i.e., improve skin and tip resistance) and for validation of such.

1.2.2 Task 2 – Development of Genetic Code to Improve Pile/Shaft Capacity Predictions

A Genetic program (GP) will be written to develop analytical equations to predict pile/shaft capacity (skin friction and tip resistance) as a function of soil types, SPT blow count, pile/shaft diameter, pile/shaft type, and loads.

To form the best possible solution, it is expected that the GP will begin with functions of a few variables, such as common arithmetic operators (like +, -, x, and /), will be used to develop the simple relationship between the SPT N, and the pile/shaft skin and tip resistance. The simple relationship can provide general ideas of important factors/parameters in calculation of the capacity. Also investigated will be averaging distances, e.g., 8B above and 3.5B below pile tip of for tip resistance calculation as well as critical depths for various soil types.

Evaluation of the functionality and accuracy of the GP will be undertaken by 1) generating hundreds of estimated side and tip resistance from FB-DEEP using borings that are randomly generated with multiple layers and 2) using the same SPT borings and FB-DEEP predicted side and tip resistance to identify if the GP can reconstruct FB-DEEP side and tip resistance curves (i.e., Unit skin and tip resistance vs. SPT blow count). For the evaluation of all four soil types and rock materials will be considered.

1.2.3 Task 3 – Inclusion of Spatial Variability in Assessment of Pile/Shaft Capacity Equations

Generally, to develop any analytical equations or charts for design, insitu data in the footprint of the foundation should be used, since any difference (i.e., error) would be associated spatial uncertainty. However, with the exception of large non-redundant drilled shafts, most deep foundations (e.g., driven piles) have borings that vary in number and distance from the foundation. Recently, however, FDOT BDK-75-977-23 has shown that running pile/shaft software over multiple borings on a site allows the evaluation of spatial uncertainty component of CV_R. Therefore the GP algorithm will be used on all sites, with multiple borings on each site with the focus of minimizing the total CV_R for all sites (includes spatial and method uncertainty). Then, the error between predictions and load test, σ_{ε}^2, as well prediction error between borings, $\sigma_{\varepsilon\prime}^2$, will be found from which the method error, σ_m^2, for the GP developed curves based on distance (e.g., 100ft, 500ft and 1000ft) may be obtained.

1.2.4 Task 4 – Development and Evaluation of Pile Capacity Equations from In situ Data

Using the pile and shaft data recorded in Task 1, the Genetic Program will be run on the insitu data set (Task 3) using all borings with specified distances from the load tests (e.g., 100, 200ft, etc.). The predicted set of equations to describe skin and tip resistance of piles at Davisson and Ultimate capacities, 5% diameter (FHWA) for drilled shafts will be used. As identified earlier, Genetic Programming allows the use of constraints and complex functions (e.g., averaging rules, etc.). The work will focus on using a consistent set of relationship based on soil type, pile size, etc. In the analysis, the Unified Soil Classification System (USCS) will be used to separate all soils/rock into one of the four general soil descriptions. The criterion used to develop the equations will be the reduction of the mean square error, bias (measured/predicted), as well as total CV_R for all borings and sites analyzed.

After developing the relationships for skin friction and end bearing for piles and drilled shafts, the equations will be used on each site to evaluate spatial uncertainty, which will be subtracted from total uncertainty, CV_R, to obtain assessment of method error. Note, each site will have anywhere from 10 to 15 borings to evaluate spatial uncertainty.

1.2.5 Task 5 – Final Report and Database Update

This task involves reporting the final recommended skin and tip resistance equations for the design of driven piles and drilled shafts using in situ SPT data. The equations may be expressed analytical or shown through plots (e.g., SPT N vs. unit skin friction based on soil type). The equations will consider both Davisson and FHWA (settlement equal to 5% diameter) for drilled shafts. Expression for critical depths, averaging, etc. will also be presented.

Finally, all the in situ data and pile data (i.e., dimension, static load test and driving information) used in the project will be uploaded into the new FDOT internet database. Since the sites will include significant boring data (i.e., section 1.2.1), this data will be of great use to the FDOT on any planned bridge widening, or new bridge construction. Consequently, the data physical location (i.e., station numbers) with soil description (Unified Soil Classification, Soils and Foundations Handbook) meets standard FDOT practices.

CHAPTER 2
FDOT'S DATATBASE ON SITE BORINGS AND PILE STATIC LOAD TESTS

2.1 Background

Prior research for FDOT and NCHRP by UF resulted in PC based Microsoft Access database for piles and drilled shafts, Figure 2.1. The database consists of approximately

Figure 2.1 FDOT/NCHRP Microsoft Access Database of Pile/Shafts

395 piles (concrete, steel, circular, etc.) and 232 drilled shafts from multiple states: Florida, Louisiana, California, and North Carolina, etc. Each record consists of site load test (Figure 2.2), in situ data (nearest boring), lab data, and pile/shaft dimensions, etc. Unfortunately, the in situ test data, Figure 2.3, associated with the load test only provides one boring, which may be within 10ft or as far away as 200ft.

A single boring provides minimal information on uncertainty of in situ mean, site variability, and spatial correlation. For instance, if the boring is outside the spatial correlation length, the use of mean site/zone boring data, instead of the single boring, may result in a better prediction of the pile load test response. The boring information is very important for

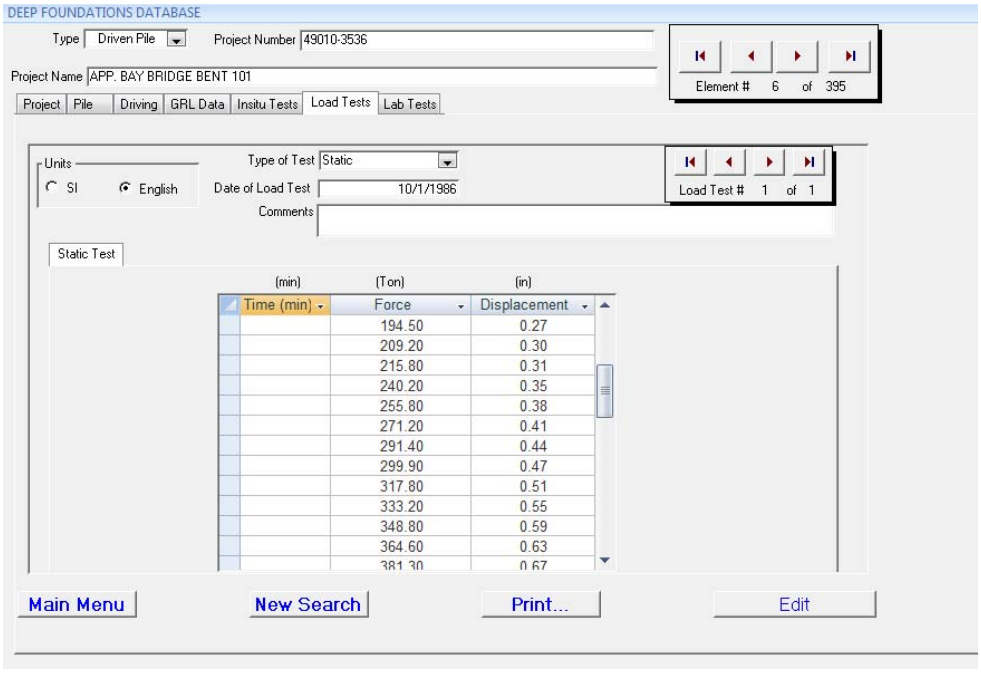

Figure 2.2 Typical Pile Load Test Data in the Database

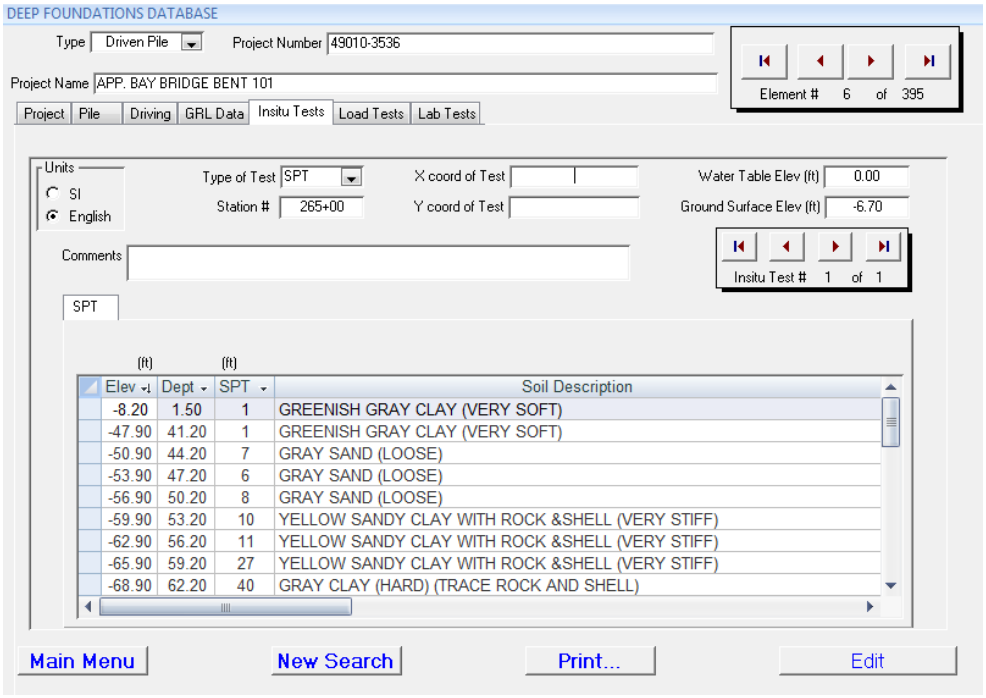

Figure 2.3 Typical SPT Boring Log for Load Test Pile

both improving the design approaches, and identifying uncertainty. Similarly, the predictions of all borings on the site may help assess the spatial variability on the site from which the method error (uncertainty of prediction methods) may be reduced by improving the design equations with the ANN or Genetic programming predictions on all of the sites.

Since this work involves both prestressed concrete piles and drilled shafts in Florida soils and limestone, the Access database had to be reviewed for piles and shafts, which met the criterion. In addition, since the database had only one boring, both the plans and Geotechnical Reports for the sites had to be located and mined for in situ data. Also, since the Access database did not contain any information on separation of skin friction and end bearing, the Load Test report for each piles/shaft had to be found and this information recovered. This chapter discusses the data collected for both prestressed concrete piles and drilled shafts. All data collected was subsequently uploaded to the FDOT online database.

2.2 Microsoft Access Prestressed Concrete Database

The Microsoft database was carefully searched by pile type and site location. Shown in Figures 2.4 (a) and (b) are the prestressed concrete piles. The figures identify the FDOT bridge site, pile dimensions (width, length, and embedment), and pier location. Evident some of the sites have almost ten load tests (e.g., Sunshine, Choctawhatchee, etc.). There are approximately 75 piles in the database, however, it is not known from the database how many had measured side and tip resistance that reached Davisson capacity. The effort next focused on obtaining the load settlement response of each pile from the database.

Site	Proj Num	Engineeer	database #	Pile Width(in	Length(FT)	Embed Len(ft)
49th st bridge TP38	9391121	Williams and Assoc	1	24	59	23.6
Appachicola River Pier 3	49010-3533	Schmert & Crapps	85	24	93.2	90.6
Appachicola River Pier 14	49010-3533	Schmert & Crapps	96	30	83.9	58.8
Appachicola River Pier 25	49010-3533	Schmert & Crapps	107	24	66.3	55.5
Appachicola River FSB16	49010-3533	Schmert & Crapps	118	18	65.2	61
Applac Bay Bent 101	49010-3536	Schmert & Crapps	6	24	80.5	62.1
Applac Bay Bent 133	49010-3536	Schmert & Crapps	7	24	123.7	104.9
Applac Bay Bent 41	49010-3536	Schmert & Crapps	129	24	69.2	52.3
Applac Bay Bent 145	49010-3536	Schmert & Crapps	18	24	121.5	103
Applac Bay FSB22	49010-3536	Schmert & Crapps	29	18	68.2	64
Blount Island Site 215			13	10	70	68
Blount Island Site 316			14	14	52	52
Blount Island Site 348			15	18	49	49
I-95 West Palm Beach #1			11	18	35	26.5
I-95 West Palm Beach #2			12	18	45	37.2
I-275 34th St Pinellas			16	18	70	69
Sunshine Skyway Site 1A		Williams and Assoc	24	24	68.8	49.2
Sunshine Skyway Site 1B		Williams and Assoc	25	20	68	47.3
Sunshine Skyway Site 3		Williams and Assoc	26	24	79.6	48
Sunshine Skyway Site 10		Williams and Assoc	27	24	60.5	27.9
Sunshine Skyway Site 13A		Williams and Assoc	28	20	38.2	20.5
Sunshine Skyway Site 13B		Williams and Assoc	140	24	43.5	26.9
Sunshine Skyway Site 15		Williams and Assoc	141	20	49.7	32
Talmadge memorial bridge		Dames & Moore	34	14	75	73
Fort Myers		Ardaman & Assoc	37	14	67	67
Port Orange Bent 2 Pile 6	79180-3514/3502	Schmert & Crapps	44	18	34.3	30.9
Port Orange Bent 19 Pile 10	79180-3514/3503	Schmert & Crapps	45	18	32.8	30.1
Dodge Island 3 E-18		Law Engineers	49	30	65	49.4
Dodge Island 4 E-18		Law Engineers	50	30	75	52.8
Dodge Island 6 E-20		Law Engineers	51	30	97.2	51.56
Dodge Island 8 E-20		Law Engineers	53	30	110	39.8
Dodge Island 9 E-20		Law Engineers	54	30	65	29
Dodge Island LTP (static)		Law Engineers	55	30	110	39.8
Howard Franklin LS3	15190-3479	Williams and Assoc	52	30	67.7	39.6
Howard Franklin LS4 short	15190-3479	Williams and Assoc	63	30	52.9	24.6
Howard Franklin LS4 Long	15190-3479	Williams and Assoc	74	30	101.8	73.5
Choctawhatchee FSB-3	60040-3527(bay)	Schmert & Crapps	56	24	83.9	77.7
Choctawhatchee FSB-26	60040-3527(bay)	Schmert & Crapps	65	24	69	64.8
Choctawhatchee FSB-26?	60040-3527(bay)	Schmert & Crapps	66	24	125	87.2
Choctawhatchee P-5	60040-3527(bay)	Schmert & Crapps	57	30	71.1	53.9
Choctawhatchee P-11	60040-3527(bay)	Schmert & Crapps	58	30	106	85.5
Choctawhatchee P-17	60040-3527(bay)	Schmert & Crapps	59	30	102	77.8
Choctawhatchee P-23	60040-3527(bay)	Schmert & Crapps	60	30	101	82.5
Choctawhatchee P-29	60040-3527(bay)	Schmert & Crapps	61	30	103.6	84.4
Choctawhatchee P-35	60040-3527(bay)	Schmert & Crapps	62	30	98.5	79
Choctawhatchee P-41	60040-3527(bay)	Schmert & Crapps	64	30	85	65.2

Figure 2.4(a) Prestressed Concrete Pile in Access Database

White City Bridge TP1	51020-3514	Dames & Moore	71	24	125.6	50.1
White City Bridge TP2	51020-3514	Dames & Moore	72	24	51.3	40
White City Bridge TP3	51020-3514	Dames & Moore	73	24	40.3	37.2
White City Bridge TP4	51020-3514	Dames & Moore	75	24	34.8	29.5
White City Bridge TP5	51020-3514	Dames & Moore	76	24	37.8	29.3
White City Bridge TP6	51020-3514	Dames & Moore	77	24	31	28.5
Acosta Bridge Pier F6	89-783	Schmert & Crapps	80	24	67	58.5
Acosta Bridge Pier G13	89-783	Schmert & Crapps	81	24	62	46.1
Acosta Bridge Pier H2	89-783	Schmert & Crapps	82	24	39	35.9
West Bay Bridge TP9		Dames & Moore	83	30	130	128.4
West Bay Bridge TP15		Dames & Moore	84	30	105	103.6
Escambia River Bent 5	91-861	Schmert & Crapps	86	24	92	85.7
Escambia River Bent 77	91-861	Schmert & Crapps	87	24	65	61.3
Roosevelt Bridge A-30	448-00903-01	Law Engineers	88	30	72	53.4
Roosevelt Bridge B-30W	448-00903-01	Law Engineers	89	30	62.5	43.8
Buckman Bridge TS-13	92-884	Schmert & Crapps	90	30	121	94.5
Buckman Bridge TS-19	92-884	Schmert & Crapps	91	30	116.9	89.3
Buckman Bridge TS-24	92-884	Schmert & Crapps	92	30	110.6	80.8
Buckman Bridge TS-29	92-884	Schmert & Crapps	93	30	104.5	80
Jul. Creek Bent 55-p4 10F2		Ardaman & Assoc	94	24	80	51
Jul. Creek Bent 55-p4 20F2		Ardaman & Assoc	95	24	80	72
Jul. Creek Bent 47-p4#1		Ardaman & Assoc	97	24	95	74
SR 580 Oldsmar			133	20	50	47
Dixie Highway Bent 1		Applied Foundations		24	50	45
Dixie Highway Pier 8		Applied Foundations		24	50	45
Dixie Highway Pier 4		Applied Foundations		24	50	45
Caminida Bent 1		Applied Foundations		30	60	68.9
Caminida Bent 7		Applied Foundations		30	60	65
5th St Bascule Br Pier 2 p37		Applied Foundations		18	55	45
5th St Bascule Br Pier 2 p53		Applied Foundations		18	55	45
5th St Bascule Br Pier3 p9		Applied Foundations		18	55	45
5th St Bascule Br Pier 3 p42		Applied Foundations		18	55	45

Figure 2.4(b) Prestressed Concrete Pile in Access Database

2.2.1 Retrieving Pile Load Test Data from FDOT Access Database

To retrieve data from the Access program, the database has to be unlocked and opened, Figure 2.5. All of Microsoft's Access information is available in Excel spreadsheet format. For instance, Figure 2.5 show the Load Test Static information (highlighted). The first column identifies the load test number (e.g., 30, 31, etc.) and the other columns show: load (kips), displacement (in.), Load (kN), and displacement (mm) in sequential order. The data, e.g., for

load test 31, of the load began at zero and increase to 300 kips with 0.65 in of displacement and then unloaded. For this work, the load, displacement data was copied from the Access database to an XML format (discussed later) and subsequently uploaded to the FDOT internet online database.

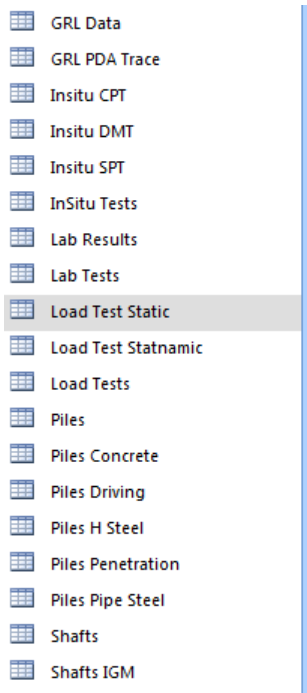

30	347.00	1.65	3,087.05	41.91
30	277.00	1.58	2,464.30	40.23
30	208.00	1.52	1,850.45	38.56
30	139.00	1.44	1,236.60	36.50
30	70.00	1.34	622.75	34.14
30	14.00	1.27	124.55	32.38
30	0.00	1.18	0.00	30.00
30	0.00	1.16	0.00	29.44
30	0.00	0.00	0.00	0.00
30	25.00	0.02	222.41	0.46
30	50.00	0.03	444.82	0.84
30	75.00	0.06	667.23	1.42
31	0.00	0.00	0.00	0.00
31	12.50	0.02	111.21	0.51
31	25.00	0.04	222.41	1.12
31	37.50	0.06	333.61	1.57
31	50.00	0.08	444.82	2.03
31	62.50	0.09	556.03	2.41
31	75.00	0.12	667.23	2.95
31	87.50	0.13	778.43	3.30
31	100.00	0.14	889.64	3.63
31	125.00	0.18	1,112.05	4.47
31	150.00	0.22	1,334.46	5.49
31	175.00	0.26	1,556.87	6.50
31	200.00	0.31	1,779.28	7.82
31	224.00	0.37	1,992.79	9.35
31	237.50	0.39	2,112.90	9.91
31	262.50	0.47	2,335.30	11.84
31	287.50	0.55	2,557.72	13.87
31	300.00	0.59	2,668.92	15.04
31	300.00	0.65	2,668.92	16.46
31	233.00	0.64	2,072.86	16.21
31	204.00	0.61	1,814.87	15.54
31	177.00	0.58	1,574.66	14.68
31	142.00	0.53	1,263.29	13.54
31	104.00	0.47	925.23	11.99
31	73.00	0.42	649.44	10.77
31	38.00	0.36	338.06	9.25

Figure 2.5 Load Test Information in FDOT Access Database

2.3 Onsite Geotechnical and Load Test Reports for Prestressed Concrete Piles

All of the UF file cabinets, which contained FDOT Geotechnical Reports, Load Tests and Plans were reviewed for this effort. Shown in Table 2.1 are the projects, which had the plans, reports, etc., for the pile load tests reported in the FDOT Access database.

Table 2.1 Collected and XML Formatted Project Plans

Project Site	Project Number	Engineer	No. Borings	No. Load Tests	Foundation		
					Dimension (in.)	Pile (Concrete/Steel)	Length (ft)
Apalachicola River (S.R.20)	47010-3519/56010-3520	Schmertmann & Crapps	64	4	30	Concrete	60-90
Buckman Bridge	72001-3462	Schmertmann & Crapps	40	8*	30	Concrete	104.5-121
Dixie Highway	230656-1-52-01	Applied Foundations	22	3*	24	Concrete	50
West Bay Bridge	217911-5-52-01	Dames & Moore	19	2	30	Concrete	105-130
White City Bridge	51020-3514	Dames & Moore	16	2	24	Concrete	31-125.6

* = includes tension tests

All of data in Table 2.1, i.e., the borings and load tests, with their respective project, pier, and pile numbers were used in the research. The asterisk (*) variable represents tension load tests in the overall summation of that project's load tests. Note, a total of 75 concrete load tests were located from the database, which consists of 70 compression and 5 tension load tests. A discussion of the onsite piles and predominate soil conditions follows.

Apalachicola River Bridge (S.R. 20) has a total of 64 catalogued borings and 4 known load tests on driven piles. The bridge runs between Calhoun and Liberty Counties, which accounts for the two project numbers listed. The driven pile tests range in depths from 60 to 90 feet. The general overview of subsoil at the Apalachicola River Bridge project site is a silty-clay layer underlain by sands followed by limestone at variable depths.

West Bay Bridge has a total of 19 SPT borings and 2 load tests. The foundation consist of 30" square concrete piles ranging in lengths from 105 to 130 feet. The general overview of subsoil at the West Bay Bridge project site is primarily silty-sand to sand overlying limestone.

White City Bridge had 16 SPT borings with a total of 2 load tests. The foundation consist of 24 square inch concrete piles ranging in length from 31 to 125.6 feet. The general stratigraphy of subsoil at the White City Bridge site is sandy-clay to sand overlying a dense shelly sand bearing layer.

Buckman Bridge has 40 borings and 8 load tests (4 compression load tests and 4 tension load tests). The foundation consists of 30" square concrete piles ranging in length from 104.5 to 121 feet. The subsoil stratigraphy of Buckman Bridge site is a sand to shelly-clay overlying strong limestone at variable depths.

Dixie Highway has a total of 22 borings and 3 load tests (2 compression load tests and 1 tension load test). The foundation consists of 24" square concrete piles of approximately 50 feet long. The general subsoil stratigraphy of the site is sand overlying weathered limestone.

2.4 Request to FDOT Districts for Missing Pile Data

Important for the research was not only multiple boring data, but the location of the borings relative to one another and the load test. Table 2.2 identifies the projects that had geotechnical and load test reports, but plans were missing (i.e., location of borings and load test). Shown in Table 2.3 are projects, which were missing plans, and load test reports. The various FDOT districts that the projects were located at were contacted and the missing information was obtained.

Table 2.2 Projects with Missing Plans

Project Site	Project Number	Engineer	No. Borings	No. Load Tests	Foundation		
					Dimension (in.)	Pile (Concrete/Steel)	Length (ft)
I-95 West Palm Beach	93220-3473	Williams and Associates	20	2	18	Concrete	35-45
Acosta Bridge	72160-3506	Schmertmann & Crapps	33	3	24	Concrete	39-67
Appalachicola Bay	49010-3536	Schmertmann & Crapps	28	5	18-24	Concrete	68.2-123.7
Appalachicola River	49010-3533	Schmertmann & Crapps	33	4	18-30	Concrete	65.2-93.2
Choctawhatchee	60040-3527	Schmertmann & Crapps	21	10	24-30	Concrete	69-125
Dodge Island	87000-3675	Law Engineers	6	1	30	Concrete	65-110
Escambia River	48140-3509/58080-3516	Schmertmann & Crapps	53	2	24	Concrete	65-92
Howard Frankland	15190-3479	Williams and Associates	6	3	30	Concrete	52.9-101.8
Julington Creek	78070-3517/72160-3571	Ardaman & Associates	24	7	20-24	Concrete/Steel	38.2-79.6
Sunshine Skyway	15170-3421	Schmertmann & Crapps	24	7	20-24	Concrete/Steel	38.2-79.6

Table 2.3 Projects with Missing Plans and Load Test Reports

Project Site	Project Number	Engineer	No. Load Tests	Foundation		
				Dimension (in.)	Pile (Concrete/Steel)	Length (ft)
49th St. Bridge	9391121	Williams and Associates	1	24	Concrete	59
5th St. Bascule Bridge	412808-1-52-01	Mactec	4	18	Concrete	55
Blount Island	X	X	3	10-18	Concrete	49-70
Caminida	061-01-0040	Applied Foundations	2	30	Concrete	55-60
Fort Myers	X	Ardaman & Associates	1	14	Concrete	34.3
I-275 34th St Pinellas	X	X	1	18	Concrete	75
Julington Creek	78070-3517/72160-3571	Ardaman & Associates	3	24	Concrete	80-95
Port Orange	79180-3514	Schmertmann & Crapps	1	18	Concrete	32.8-34.3
Roosevelt Bridge	448-00903-01	Law Engineers	2	30	Concrete	62.5-70
SR 580 Oldsmar	X	X	X	20	Concrete	50

X = unknown presently

2.5 Static Pile Capacities and Distribution of Side and Tip Resistance

The original Access database did not identify the Davisson capacity or the skin and tip resistance for each pile. Consequently, each load test report was investigated to identify the reported capacities as well as skin and tip resistance. Unfortunately some of the reports were missing some of the latter information. In the case of Davisson capacity, each digitized load test was plotted along with the elastic shortening (PL/AE) plus an offset 0.15 + B/120 (B<30) or + B/30 (B≥30). The intersection of the elastic offset and the digitized pile load-settlement

response was used to assess the Davisson Capacity of the pile. In the case of reports not identifying skin and tip resistance, the provided instrumentation data (e.g., strain gages and telltales) was used. For instance, a number of reports identified telltale information at the bottom of the pile. For the latter cases, the pile's bottom force was computed from

$$P_{bot} = 2EA\left(\frac{\Delta}{L}\right) - P_{top} \quad \text{Eq. 2.1}$$

where, E = Young's Modulus, A = cross-sectional area, L= pile length, Δ = recorded telltale, and P_{top} = applied force at top of pile. Values of P_{top} and Δ at the Davisson load were used, with estimated skin friction at Davisson Capacity equal to $P_{top} - P_{bot}$ (Eq. 2.1). Similarly, for the case of piles with installed strain gages, the tip resistance was assessed from the strain values times the cross-sectional area, A, and Young's Modulus, E, of the pile. Skin friction was obtained by subtracting the tip resistance from the applied top load on the pile. In the case of piles, which did not have any instrumentation (strain gages or telltales), the load vs. settlement of the pile was plotted on a log – log plot, and the break in the slope (i.e., Debeer) was used to separate skin from tip resistance. All piles had their load test results separated into Davisson Capacity and Ultimate Capacity as well as side and tip resistance for each. Note, in the case of ultimate pile skin resistance, the ultimate pile tip resistance was subtracted from the ultimate applied top load. Table 2.4 shows an example for two sites, Apalachicola River and Bay and associated capacities, as well as distributions (skin and tip).

Table 2.4 Pile Capacities and Distribution of Resistance

Apalachicola River					
Pile	P_{ult} (kips)	P_{dav} (kips)	P_{tip_dav} (kips)	P_{skin} (kips)	P_{tip_ult} (kips)
7	1035	958	294	664	371
1	1100	952	369	583	517
2	925	714	270	444	481
3	330	330	108	222	108
Apalachicola Bay					
Pile	P_{ult} (kips)	P_{dav} (kips)	P_{tip_dav} (kips)	P_{skin} (kips)	P_{tip_ult} (kips)
(B101) 3	910	812	457	355	555
(B133) 3	951	808	258	523	428
(B145) 3	1041	976	456	520	521
4	472	426	84.72	341.28	132.72
(B41) 3	544	524	24	500	44

2.6 Uploading Load vs. Settlement, Pile Capacities, and Distributions into FDOT Database

Prior to this research, there was no means to upload pile or shaft load test results into the FDOT online database, which predominately in situ (SPT and CPT) and laboratory (i.e., Unified soil classification, and rock strengths). For this work, a graphical user interface, GUI was written to convert pile load results into XML hierarchy, which could then be upload to the FDOT's online database. The GUI accounts for all inputs available in the Microsoft's Access database for top down load test of driven piles only. Table 2.5 shows all the Access database fields and their corresponding FDOT Database/GUI input fields.

Table 2.5 Corresponding Microsoft Access to FDOT's Online Database Fields

Access Database Field	FDOT Database Field
Pile elastic modulus (psi)	Pile_E (ksi)
Capwap elastic modulus (psi)	x
Pile wave speed (ft/s)	x
Pile Impedance (lb-s/ft)	x
Pile description (square/round)	Description
Void diameter (in.)	Void (in.)
Width or diameter (in.)	Dia_or_B (in.)
Cross-sectional area (in^2)	Pile_Cross_Area (in^2)
Total length (ft)	T_Length (ft)
Embedment length (ft)	Embed_Length (ft)
Total weight (tons)	Material_Weight (kip)
Concrete strength (psi)	Concrete_str (ksi)
Station and offset	Station, Offset *Separate Fields
Force (tons)	Load (kip)
Displacement (in.)	Disp2, Disp4 (in.)

Figure 2.6 shows the GUI with data entered for the Apalachicola River Project (49010-3533). Note also, the data may be inputted manually or copy and pasted from an existing Excel sheet (e.g., Figure 2.5). For visual check, Figure 2.6, the GUI plots the load vs. settlement curve for identification of outliers.

The interface also allows the user to input multiple sets of load test data for a given project as shown in the drop down menu (red box) in Figure 2.6. For this case, the Apalachicola River Project (49010-3533), four (4) separate load tests were available, and the interface was used to record the information for each load test. Next, clicking the "Save as XML" button in the GUI, Figure 2.6, was used to convert the measured data into XML formatted file, shown in Figure 2.7. The resulting XML file was used with database loader DLL to upload the XML file to the FDOT's online database. As shown in Figure 2.7, all load tests are located by Project, followed by Bridge, and Pier in the online database.

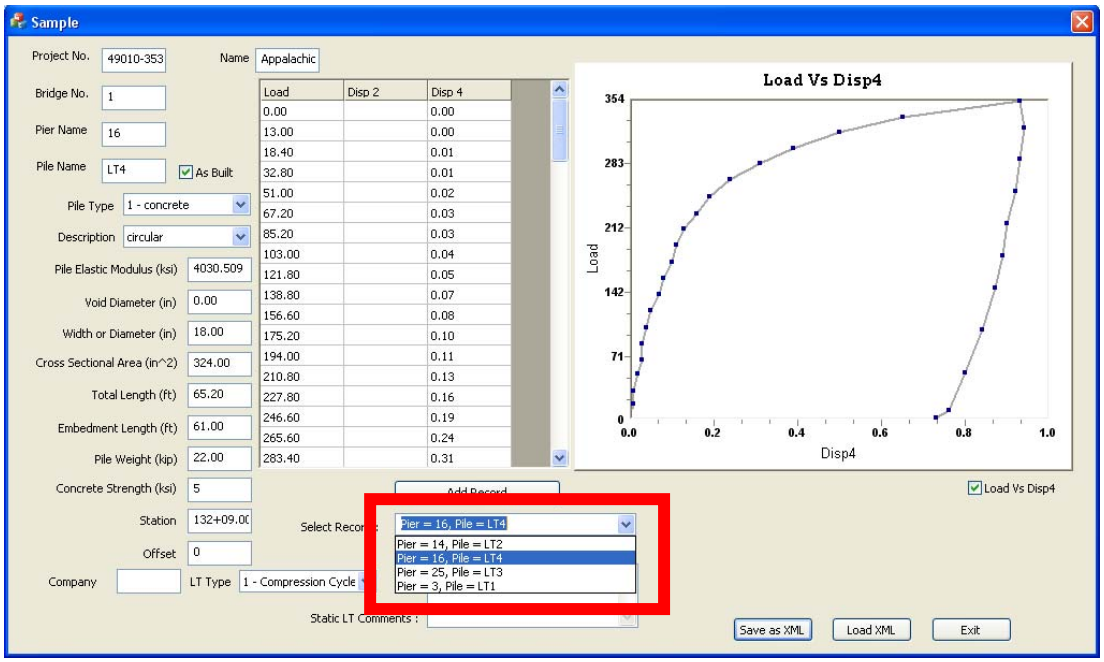

Figure 2.6 Screen Shot of Pile Load Test Data Required for XML GUI

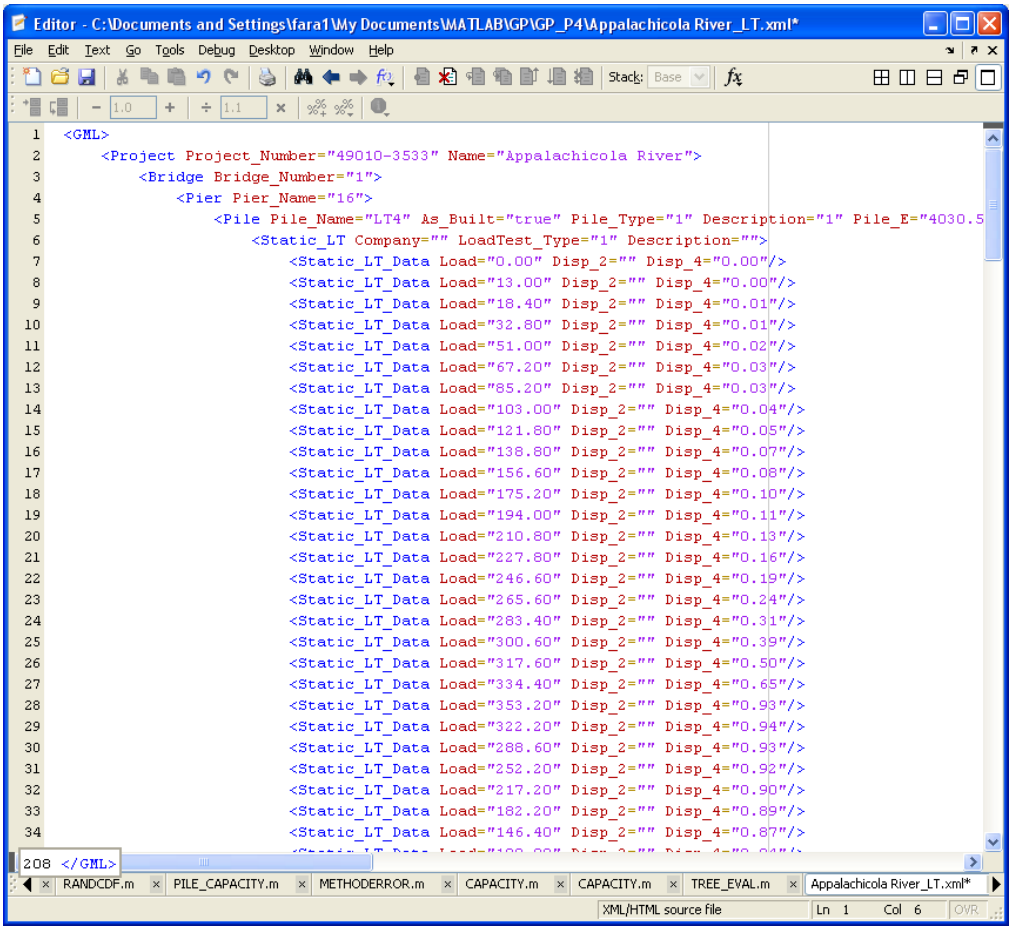

Figure 2.7 Corresponding XML File Generated by GUI for Apalachicola River Project

2.7 Complete Boring and Pile Load Test Data Uploaded to FDOT Online Database

Shown in Table 2.6 is the final list of bridge sites, load tests and borings uploaded into

Table 2.6 Final Bridge Sites, Load Tests and Borings in FDOT Online Database

Project Site	Project Number	Borings (Firm)	Load Test (Firm)	No. Borings	No. Load Tests
Acosta Bridge	72160-3506	Law Engineers	Schmertmann & Crapps	53	3
Apalachicola Bay	49010-3536	FDOT	Schmertmann & Crapps	28	5
Apalachicola River	49010-3533	FDOT	Schmertmann & Crapps	33	4
Blackwater Bridge (I-10)	58002-3449	Williams Earth Sciences	William Earth Sciences	4	2
Buckman Bridge	72001-3462	Ardaman & Associates	Schmertmann & Crapps	40	4
Caminida Bay	061-01-0040	Applied Foundations	LADOT	4	2
Choctawhatchee	60040-3527	FDOT	Schmertmann & Crapps	35	9
Dixie Highway	230656-1-52-01	PSI	Applied Foundations	22	3
Dodge Island	87000-3675	Law Engineers	Law Engineers	6	1
Escambia River	48140-3509/58080-3516	FDOT	Schmertmann & Crapps	53	2
Howard Frankland	15190-3479	Williams and Associates	HDR	49	4
Port Orange	79180-3514	Franco/Williams & Dawson	Schmertmann & Crapps	11	2
Roosevelt Bridge	89010-3541	Law Engineers	Law Engineers	41	2
Sunshine Skyway	15170-3421	Williams and Associates	Schmertmann & Crapps	22	7
West Bay Bridge	217911-5-52-01	FDOT	Dames & Moore	19	3
White City Bridge	51020-3514	FDOT	Applied Foundations	16	2
5th St. Bascule Bridge	412808-1-52-01	Mactec	Applied Foundations	7	4
Bayou Chico	48050-3536	FDOT	Williams Earth Sciences	7	3
Matanzas River (SR 312)	78002-3509	FDOT	Williams Earth Sciences	8	2
			Totals:	**458**	**64**

the FDOT online database. The total number of prestressed concrete piles was reduced from 75 (section 2.2) to 64 (Table 2.6) because a number of piles did not reach the Davisson Failure Capacity. Note, a number of the remaining piles did not exhibit full mobilization of skin friction; however, the piles were left in the analysis for subsequent comparison with Davisson capacity.

For the soil borings, besides the physical descriptors (e.g. silty-sand, sand w/ trace of limestone, etc.), all SPT N values are accompanied with their Unified Soil Classification System Symbols: CL, ML, CL-ML, CH, MH, OL, OH, Pt, SM, SC, SW-SC, SP-SC, SM-SC, SW-SM, SP-SM, SW, SP, GW, GP, GM, GC, GC-GM, GW-GM, GW-GC, GP-GM, and GP-GC. The USCS classification will be used in delineating the four possible soil/rock skin and tip resistance curves to assess pile capacity.

2.8 Drilled Shaft Boring and Load Test Data uploaded to FDOT Online Database

The drilled shaft research initiated with a review of the FDOT Microsoft Access Database for drilled shafts with load test information in Florida. Since the database had both commercial (e.g. buildings) and FDOT bridge data, the information was separated into two categories: 1) FDOT projects and 2) Non-FDOT projects, which was not possible to obtain more information. Shown in Table 2.7 are all Non-FDOT projects. After review of the data, only one site (Barnett Tower) had more than 2 borings (but >100ft from load test), which was needed for spatial uncertainty assessment. In addition, one of the load test of the Barnett site did not achieve the nominal resistance (settlement equal to 5% of diameter).

Shown in Table 2.8 is the final FDOT Bridge projects, which were collect from: 1) Access database, 2) onsite project reports and 3) requested plans, reports, etc. from the FDOT districts. This includes a total of 815 individual borings and 63 individual load tests (33 Osterberg, 15 Statnamic and 15 top down). Note, because each of the load tests has multiple sets of strain gages along its lengths, individual assessment of unit skin friction vs. SPT N for specific

soil layers were considered. Again, the Unified Soil Classification System (USCS), Symbols: CL, ML, CL-ML, CH, MH, OL, OH, Pt, SM, SC, SW-SC, SP-SC, SM-SC, SW-SM, SP-SM, SW, SP, GW, GP, GM, GC, GC-GM, GW-GM, GW-GC, GP-GM, and GP-GC was used in delineating the four possible soil/rock skin and tip resistance curves.

Table 2.7 Non-FDOT Drilled Shaft Projects

UF Access Database Projects	Project Number	Borings (Firm)	Load Tests (Firm)	No. Borings	Static	Foundation	
						Dimension (in.)	Length (ft)
AMERICANA HOTEL - TAMPA #1, #2	X	Law Engineering	X	2	2	14	20.17-37.5
BARNETT CENTER, JACKSONVILLE	J-5272	Law Engineering	ATLANTA TESTING ENGINEERING	15	1	36	58.3
BARNETT TOWER, CLEARWATER	X	Driggers Engineering Services, Inc.	X	1	1	28	90
BAY ST. PARKING GARAGE, JAX.	X	Law Engineering	X	1	1	24	60.8
BAYSHORE PLACE, TAMPA, FL	X	Jammal & Associates, Inc.	X	1	1	24	34
CEMENT STORAGE SILOS, DADE CO.	X	K.B.C. Consultants, Inc.	X	X	1	30	20
COCOA BEACH, BREVARD, FL	X	X	X	X	1	15	23
DEPT. OF ED. BUILD. TALLAHASSEE	X	Ardaman & Associates, Inc.	X	1	1	28	56
ENTERPRISE CENTER JAX. FL	X	Law Engineering	X	1	1	30	62.1
ISLAMORADA, FL SHAFT 1, SHAFT 2	X	Lymon C. Reese, Texas University	X	X	2	36	24.5-60.43
JACKSONVILLE CENTER, FLORIDA	X	Law Engineering	X	1	1	28.5	22
LEWIS STATE BANK-TALLAHASSEE #1, #2	X	David L. Federer & Associates, Inc.	X	2	2	36	51
MARRIOT HOTEL, MIAMI-FLORIDA	X	Dames & Moore	X	X	1	36	49
MEMORIAL HOSPITAL, TAMPA, FL	X	Atlanta Testing & Engineering	X	1	1	30	35
MIAMI CENTER PHASE II CONDO	X	Dames & Moore	X	X	1	30	60
PALM BEACH - HAMPTONS, FL	X	Dames & Moore	X	X	1	30	10.5
REGISTRY HOTEL, NAPLES, FL	14285-001-26	Dames & Moore	Dames & Moore	X	1	30	70.4

Table 2.7 (-Cont.-) Non-FDOT Drilled Shaft Projects

UF Access Database Projects	Project Number	Borings (Firm)	Load Tests (Firm)	No. Borings	Static	Foundation	
						Dimension (in.)	Length (ft)
S. E. FINANCIAL CENTER, MIAMI	X	Dames & Moore	X	X	1	30	75
S. E. BANK BUILDING, JAX. TEST 1, TEST 2	X	Ellis & Associates, Inc.	X	1	1	24	35.79-35.97
SINGER ISLAND, RIVIERA BEACH	X	Dames & Moore	X	1	1	30	30.7
SUWANNEE RIVER BRIDGE, DIXIE CO.	N/A	N/A	Schmertmann & Crapps	1	1	42	82.5
TAMPA INTERNATIONAL AIRPORT,	X	CH2M Hill Southeast, Inc.	X	3	3	28-30	29.5-34.5
WEST PALM BEACH ADMIN. OFF. #1, #2	X	X	X	2	2	30	34.1-34.5

X=unknown field

Totals	34	29

Table 2.8 FDOT Drilled Shaft Projects Uploaded into Online Database

Project Site	Project Number	Borings (Firm)	Load Tests (Firm)	No. Borings	Osterberg Tests	Statnamic	Static	Foundation	
								Dimension (in.)	Length (ft)
17th St. Causeway	86180-1522	Williams and Associates	LOADTEST / Applied Foundation	165	4	6	0	48	40-100
Acosta Bridge	72160-3528	Law Engineers	Schmertmann & Crapps	53	4	0	2	36	64.19-113.92
Appalachicola River (S.R.20)	47010-3519/ 56010-3520	Ardaman and Associates	Schmertmann & Crapps	64	6	0	0	108	60-90
Fuller Warren	72020-1485	Law Engineering	Williams and Associates	26	4	0	0	36-72	74.5-201.5
Gandy Bridge	10130-1544	Beiswenger, Hoch & Assoc.	Williams and Associates	98	3	3	0	48	43.1-83
Hillsborough Ave.	10150-3543/ 10150-3546	Williams and Associates	Williams and Associates	34	1	2	0	30-48	63.5
Howard Frankland	15190-3479	HDR	Williams and Associates	49	0	0	5	36	50-70
I-4 Widening	418760-2-52-01	Ardaman and Associates	LOADTEST	14	1	0	0	60	84-125
I-595 Fort Lauderdale	86095-3406	Schmertmann & Crapps	Schmertmann & Crapps	2	0	0	2	36	65.5-75.5
Jewfish_Creek	250445-1-52-01	MACTEC	MACTEC	98	0	2	0	48-60	44.9-67.4
Macarthur Causeway	87060-1549	Law Engineering	Law Engineering	44	0	0	1	42	30.5-150
Miami Intermodal Center	406800-2-32-01	MACTEC	MACTEC	17	0	1	0	54	67
MIC/MIA Elevated People Mover	408320-1-52-01	PSI	LOADTEST	24	1	0	0	84	89
Port Orange Bridge	79180-3502	Schmertmann & Crapps	Schmertmann & Crapps	2	2	0	1	36-54	95.4-98.4
SR 686	256994-1-52-01	Ardaman and Associates	Ardaman and Associates	58	2	0	0	60	98-114.2
Sunshine Skyway	15170-3421	Williams and Associates	Schmertmann & Crapps	22	0	0	4	24-48	38.2-79.6
Venetian Causeway	87000-1601	Dames & Moore	Florida Testing & Engineering, Inc	17	0	0	0	48	50-82
Victory Bridge	53020-3540	Schmertmann & Crapps	Schmertmann & Crapps	28	5	1	0	48	69-100
			Totals	815	33	15	15		

CHAPTER 3
DEVELOPMENT OF GENETIC PROGRAM TO ASSESS SKIN AND TIP RESISTANCE

3.1 Background

The use of artificial neural networks (ANN) to predict lateral and axial pile capacity from in situ data is seeing increased use. For instance, Nawari et al. (1999) developed an ANN code for estimating axial and lateral capacities/movements of driven piles (concrete, pipe, etc.) for SPT data. Using a database of 60 piles loaded axially and 25 piles loaded laterally, Nawari et al. (1999) showed ANN comparisons with traditional methods (SPT 91, Coyle & Costello, Reese p-y). Generally, the ANN had correlation coefficients between 0.88 (axial) and 0.94 (lateral) vs. 0.65 (Coyle) and 0.78 (SPT 91). More recently, Rezania and Javadi (2007) improved Artificial Neural Networks (ANN) approach with Genetic Programming (GP). In the latter case, the neural network of weighting values (ANN) was replaced with a genetic program (variables, and function statements – sqrt, log, division, etc.), which was trained through genetic evolution (i.e., cross-over, mutation) on a database to evolve an analytical model (i.e., equation) to predict shallow foundation settlements. Of interest is the development of improved unit skin friction and tip resistance functions from in situ SPT and laboratory data (e.g., rock strength) for prestressed concrete piles and drilled shafts in Florida soil/rock conditions using genetic programming. A discussion of the genetic process is presented first, followed a detailed description of the program development for estimating axial pile and drilled shaft response.

3.2 Genetic Program (GP) Overview

Genetic programming (GP) is an algorithm that seeks an optimal model/solution (i.e., set of equations) based on known inputs (in situ measurements) and corresponding measured outputs (unit skin friction and tip resistance). Implementation of GP begins with creating a population of possible models (i.e., solutions) that use the known inputs along with random functions and

constants to predict the measured output. Models used in the GP are represented in a tree structure composed of multiple nodes. Shown in Figure 3.1 is an example of the representation of the equation $[2/X_1 + X_2]^2$ in a tree structure. Each node (i.e., circle in drawing) on the tree is either a function set or terminal set. The function set can be arithmetic operators (+, -, x, /), or mathematical operators (e.g., sin(·), cos(·), ln(·), exp(·), etc.). Each node in a function set requires arguments (branches) beneath to describe the function. These can be either binary requiring two arguments (e.g., +) or unary requiring one argument (e.g., sin(·)). The other type of node is called a terminal set. These are represented as constants, such as input parameters (e.g., insitu measurements, foundation dimensions, etc.). These nodes are called terminal because the tree structure (i.e., branch) ends at these nodes. All tree structures are read (i.e., written) from the bottom up. For instance, for Figure 3.1, two is divided by X_1, which is then added to X_2 and the whole term is then squared, or $[2/ X_1 + X_2]^2$.

For any analysis, the program must begin with an initial population (e.g., 100 to 200) of models, which are generated randomly at the beginning. Next, the program optimizes the initial models in future generations (i.e., iterations) of the population to match the measured outputs (e.g., measured unit skin and tip resistance). This optimization process occurs through a process called Cross Over, Mutation and Reproduction.

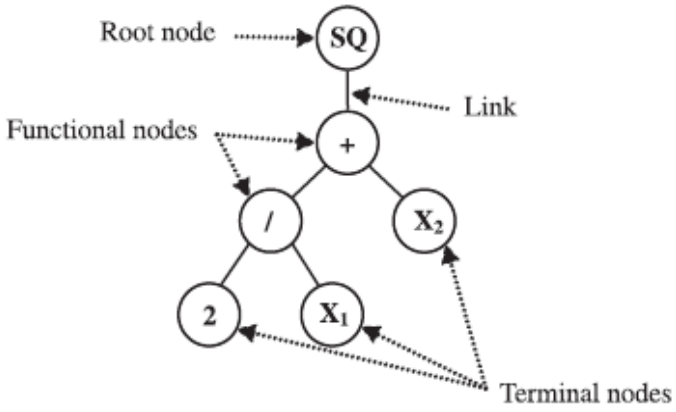

Figure 3.1 Tree Structure, $[2/X_1 + X_2]^2$ (Rezania and Javadi, 2007)

This process begins with a selection of one of the models (100 to 200 initially created) selected using a method called the Roulette Wheel. This method allows models to be selected at random but is biased by their level of fitness. That is, models have higher level of fitness [e.g., lower RMSE (root mean squared error) – see section 1.3] have a higher probability of being selected for use in a given iteration of the GP analysis.

Once a particular set of models are selected, one of three possible genetic operations may occur: 1) Cross Over; 2) Mutation; and 3) Reproduction. The first process, Cross Over is used to introduce new tree structures to the population. Specifically, from each model's trees, Figure 3.2, a node is randomly selected from each. Note, all nodes in each tree have an equal probable chance of being selected. Once a node is selected on each tree, the nodes associated with it, i.e., sub-tree, branch, are gathered and swapped between each model. This results in two new models, which are then used in the next generation. An example of the cross over process is shown in Figure 3.2 (a), where the log node is selected in model 1 and the multiplication node is selected from model 2. The branches of each model [$g(X_1)$ and $X_1^2 X_2$] are then swapped to give the two models shown in Figure 3.2 (b), creating new models for the next generation.

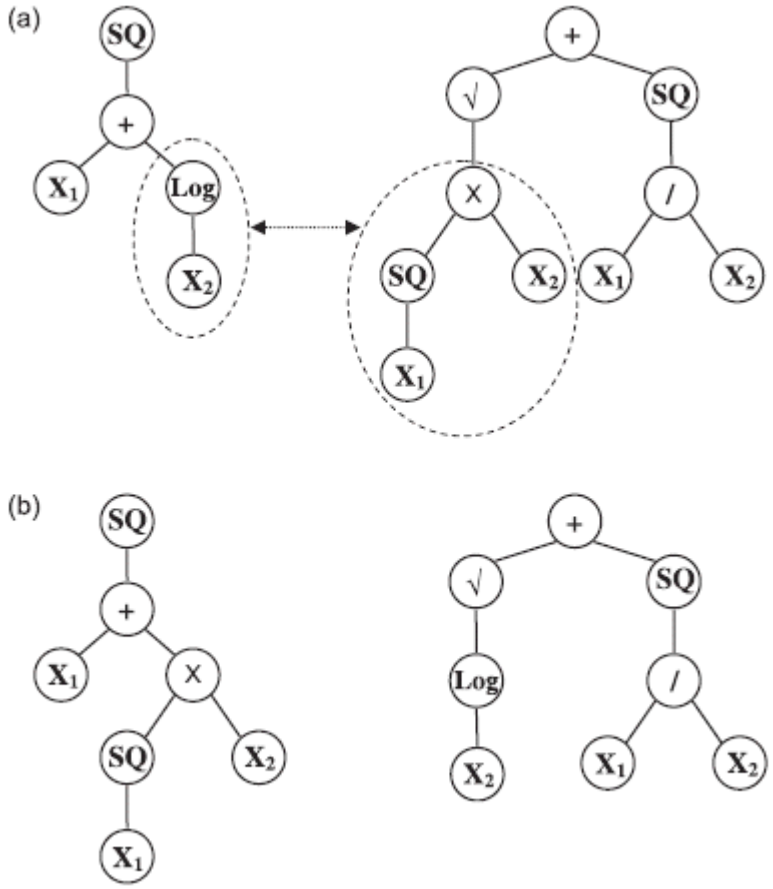

Figure 3.2 Cross-Over Operation in Genetic Programming Showing (a) Parents and (b) Children (Rezania and Javadi, 2007)

The second genetic process/operation that the GP employs is mutation. The process begins with the selection of only one model with the roulette wheel. Subsequently, one node is then selected at random from the model's tree; note each node has an equal probable chance of being selected. The selected node is then replaced with a new node of the same function set or terminal set. An example of the process is shown in Figure 3.3. In Figure 3.3 (a), a multiplication node was randomly selected and changed into a division node, Figure 3.3 (b).

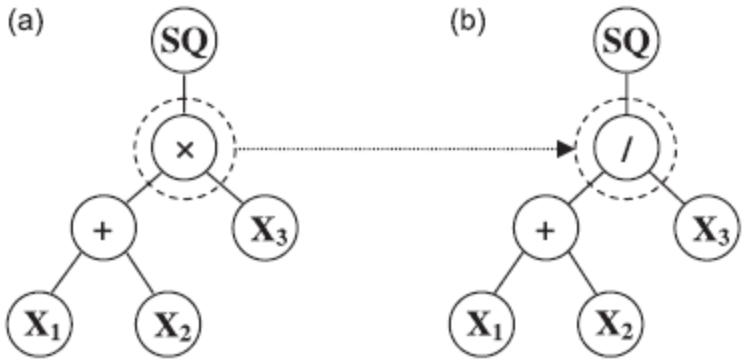

Figure 3.3 Mutation Operations in Genetic Programming (a) before Mutation and (b) after Mutation (Rezania and Javadi, 2007)

The third and final genetic process/operation is simple reproduction without any changes. This process involves the random selection of a model that is then copied, with no modification, into the next generation. With the three genetic operators (cross over, mutation, and reproduction), all successive generations are created. In the creation process, the selection of any genetic operator is based on specified probabilities. For this work, GP code used the following probabilities: Cross Over = 90%, Mutation = 2% and Reproduction 8%, (Rezania and Javadi, 2007), for successive generations, i.e., iterations. For instance, for 100 model generations, 90 would include Cross Over, 8 would be straight reproduction (i.e., no changes), and 2 would involve mutations. A general flow chart of the genetic program (GP) is shown in Figure 3.4. The next section describes the evaluation of the fitness of the models in the population (i.e., selection of models, which remain in the population).

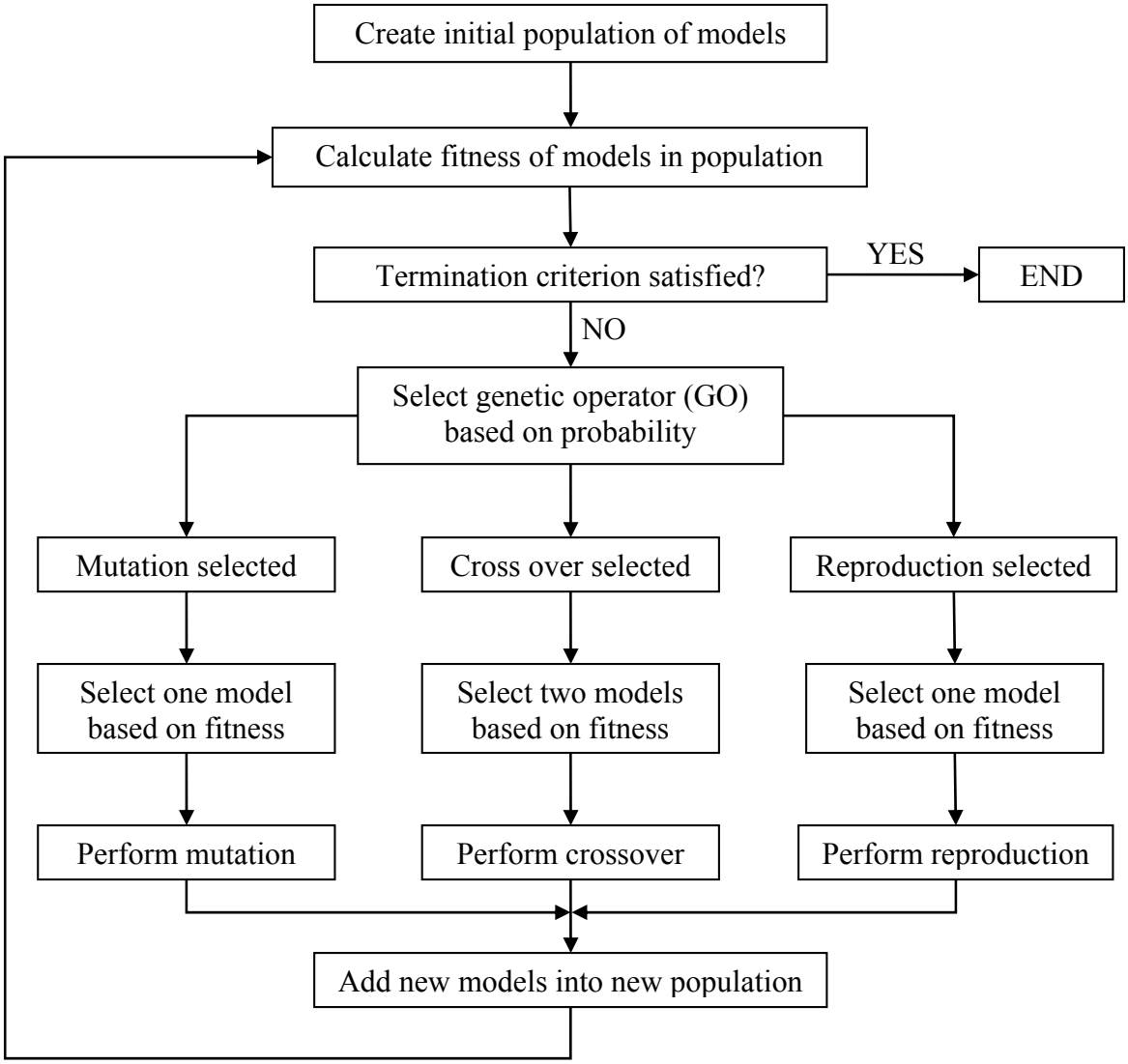

Figure 3.4 Program Diagram of Genetic Program

3.3 Fitness Test of a Genetic Program Model

Testing to measure the fitness of any model (section 3.2) versus another model in the genetic program (GP) was performed using the root mean squared error (RMSE), defined as the square root of the mean square error,

$$MSE = \frac{1}{n}\sum_{i}^{n}(P_i - M_i)^2 \qquad \text{Eq. 3.1}$$

where P_i is the predicted result of the model (e.g., predicted skin/tip resistance based on blow counts); and M_i is the measured output for the corresponding specified inputs (e.g., known/measured skin friction or tip resistance) for a given pile.

Note, it can be shown that the MSE is equal to

$$MSE = \frac{1}{n}\sum_{i}^{n}\left[(P_i - M_i) - \frac{1}{n}\sum_{i}^{n}(P_i - M_i)\right]^2 \mp \left[\frac{1}{n}\sum_{i}^{n}(P_i - M_i)\right]^2 \quad \text{Eq. 3.2}$$

where the first squared term on the right is the variance (standard deviation squared) of the residual, ($P_i - M_i$), and the second squared term on the right is referred to as the mean of the residual/error. Evidently, if the MSE approaches zero (i.e., $P_i \propto M_i$) then both the mean of the residual/error as well as its standard deviation (i.e., distribution about the mean) will also approach zero, or the predicted and measured response should match. The program uses the RMSE, which is the square root of the mean square error (MSE), and it will have the same units as the measured output, (M_i , e.g., unit skin/tip stress). Also note, both MSE and RMSE will always be positive because of the square in Eq. 3.1.

Controlling the model to be used by the genetic operator is the roulette wheel which considers selection probabilities for each model. To ensure that models with the best fit, i.e., the lowest RMSE, are preferably selected, their assigned probability of selection is computed from its inverse RMSE divided by the sum of all the models' inverse RMSE summed.

To test the GP, and RMSE concept, a range of inputs, X (1 to 50) with a known function, M=F(X), was used to see if the GP program could create a function that has a RMSE = 0. An outline of the process was (a) specify range of inputs and function F(X) (e.g., polynomial, exp, etc.) to determine corresponding outputs, M [i.e., substitute X values in F(X)], (b) generate initial population of models, c) evaluate fitness of each model in the population, (d) perform genetic

operations, Figure 3.4, until population of the new generation was met, (e) repeat steps b and c for specified number of generations, and finally, (f) select model from final generation with smallest RMSE and compare to the specified *M* function.

For the test, a simple 2nd order polynomial, $M = 5X^2 + 2X + 15$ was used to generate the M_i values (X_i varied 1 to 50). Next, the Genetic Program was setup with an initial population of 100 random functions (Table 3.1) from which could select mathematical operators from the function set of (+, -, x, /, exp) and constants of 2, 3, 5 and variable X. . Then the program underwent 100 iterations or genetic evolutions; for each iteration, the RMSE for each model was computed for each X_i (1 to 50), with P_i value compared to M_i (Eq. 3.1), and successive selections based on RMSE. The results of the GP evolution are shown in Figure 3.5 for minimum RMSE value for the entire population in each iteration or generation. It can be seen that the GP converges on a solution after 29 generations with a very low (≈ 0) RMSE. The resulting model, Table 3.1, that the GP predicts is an exact match to the function originally specified.

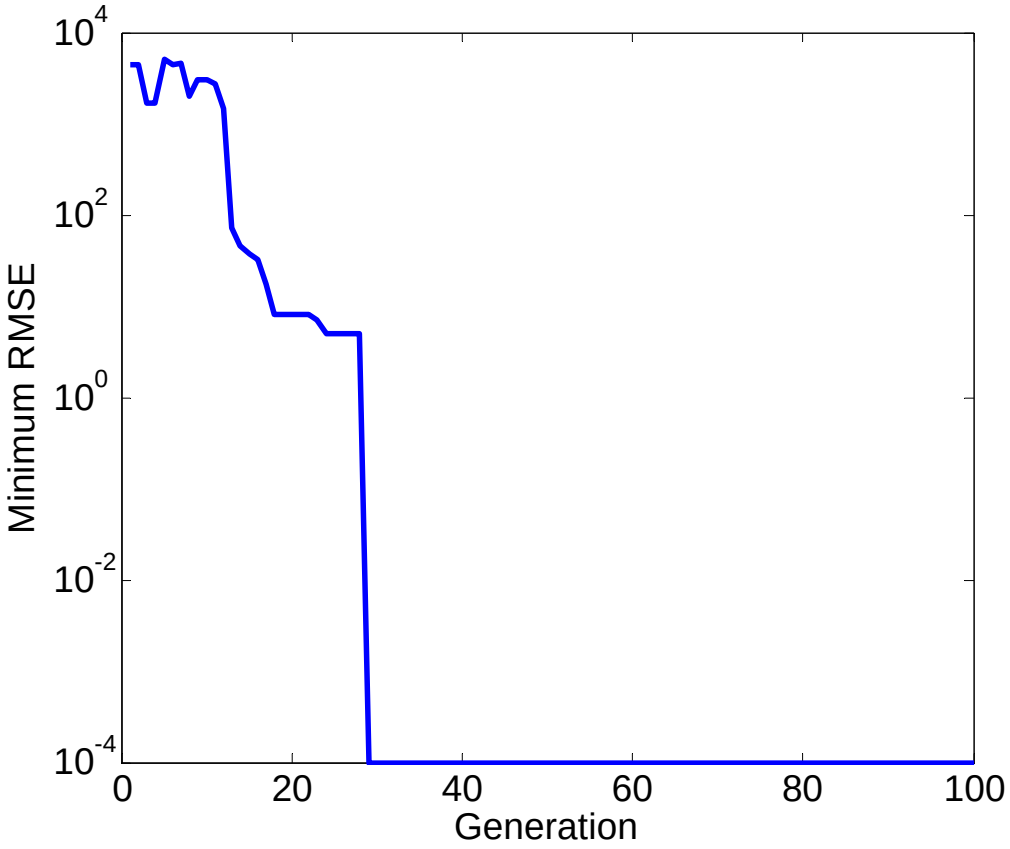

Figure 3.5 Minimum RMSE of Population by Generation for Test 1

Table 3.1 GP Parameters for Polynomial Test

Terminal Set: [X=1:50, 2, 3, 5]
Function Set: [+, -, x, /, exp]
Output Function; $P = 5X^2 + 2X + 15$
Fitness Evaluation: RMSE
GO Selection: Cross Over = 0.90, Mutation = 0.02. Reproduction = 0.08.
Population Size = 100
Total Number of Generation = 100

3.4 Modeling Pile's Skin Friction with Genetic Program

Required to model a pile's unit skin friction would include SPT-N borings log, and pile dimensions (length and width) with the corresponding output being ultimate side friction. A number of evolutions (i.e., iterations) occurred in the development.

In the first iteration, the GP tree structure was setup to replicate the FB-DEEP program, as shown in Figure 3.6. In this process,FB-DEEP converts an array of SPT-N blow counts to an array of unit side friction values (Figure 3.7) by an equation depending on the SPT-N's soil type. This array of unit side friction is then converted to one unit side friction value for the entire pile using area averaging, Figure 3.7, where each individual USF_i is multiplied by its attributed length, L_i, then the array is summed and divided by the total length of the pile, L. Finally, the average unit skin friction is multiplied by the total surface area of the pile, A_s, Figure 3.6 of the pile to calculate the pile side resistance, force.

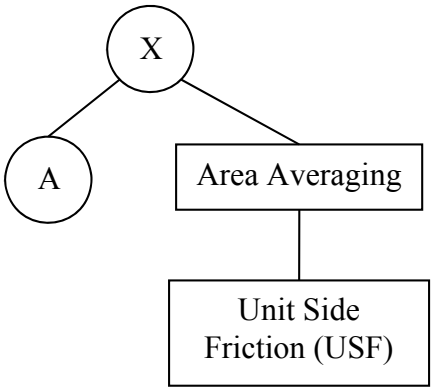

Figure 3.6 Simplified Tree Structure of FB-DEEP

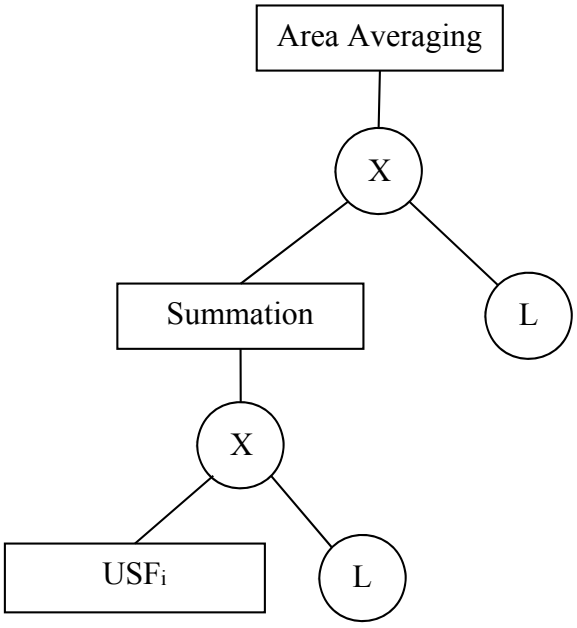

Figure 3.7 Detailed Tree Structure of FB-DEEP's Area Averaging Subroutine

Note, for this rendition, the unit skin friction, Figure 3.6 must be obtained for any SPT-N values contained in different soil types alongside a pile. To characterize the different soil types, the use of program nodes involving logical (e.g., loops, etc.) and Booleans (if, >,<, etc.) have to be employed. One rendition is shown in Figure 3.8. In this characterization, a node would incorporate a Boolean operator (e.g., if soil type, ST = 1, etc.), representing a different branch of soil type and analysis (e.g., linear relationship to unit skin friction, f_{ST}, and SPT N) that would be undertaken to evaluate unit skin friction. However, this approach (Figures 3.6 to 3.8) was considered too complex, and did not allow other averaging techniques, such as harmonic, geometric, etc.

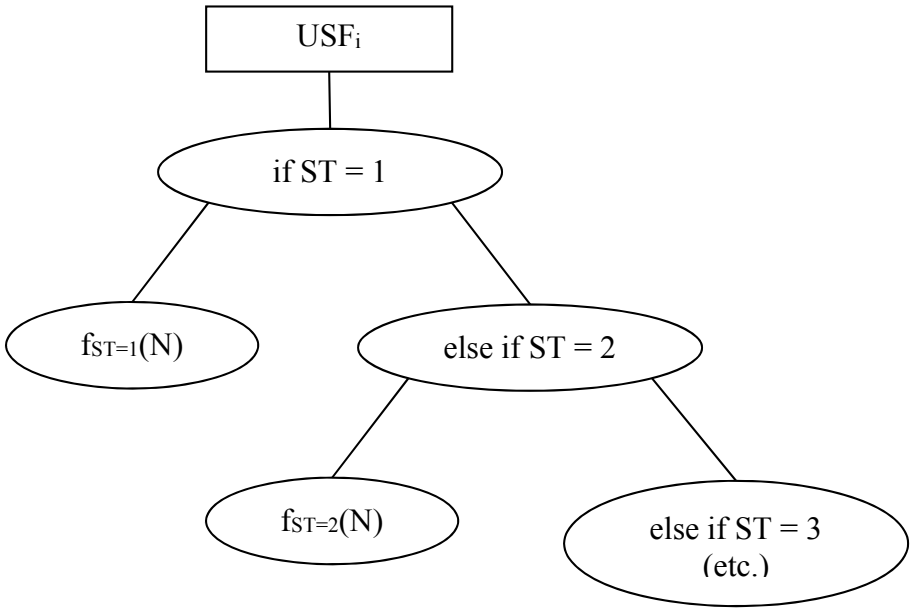

Figure 3.8 Detailed Tree Structure of FB-DEEP's Unit Side Friction Subroutine.

The second or final iteration to evaluate total side resistance of a pile, focuses on the layers of different soil types that are found when computing skin friction. The GP's analysis of multiple soil models begins with the determination of length segments, L_i, for each N_{SPT} soil type that are located alongside that pile length. An example is shown in Figure 3.9 where Li values are centered at their respective N_{SPT} and span from the midpoint between N_{SPT} measurements above and below. For the case of N_{SPT} points located near the surface, Li, are assessed from ground surface elevation to the middle of first and second N value (i.e., L_1) and in the case of the bottom (i.e., L_n), the length upward from the tip to middle of the last 2 N values along the pile are used.

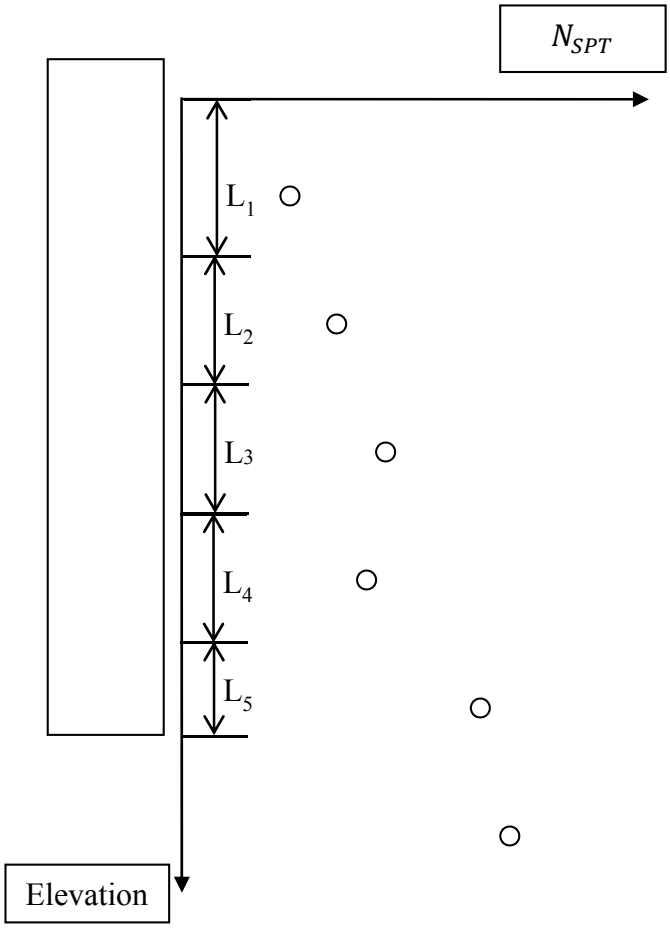

Figure 3.9 Determination of L_i along Pile Side for Each N_{SPT}

Next, with the individual Li values, an average unit side resistance $\bar{f}_{ST}$ can be computed based on each soil type, ST, and SPT N value. This process is shown in Eq. 3.3, where L_{ST_i} is the Li value for the soil type ST, and f_{ST_i} is the unit side resistance predicted by the GP's model for ST at the corresponding N_{SPT}. The value k in Eq. 3.3 is the averaging process (Renard and de Marsily, 1997), ranging from -1 to +1; in the case where k = -1, harmonic averaging is occurring (i.e., reciprocal of unit skin frictions), k = 0 is geometric averaging (which can be shown through limit analysis) and k = 1 is arithmetic averaging (currently used in FB-DEEP). The single parameter k is evaluated by the GP algorithm, i.e., the flexibility of considering

different averaging techniques when evaluating side friction curves (i.e., reducing MSE). The total side friction, USF, alongside the pile, is found from Eq. 3.4, where *Prm* is the pile's perimeter (units of length), and L_{STi} is summed along the total pile length and multiplied by the average unit skin friction, f_{ST}

$$\bar{f}_{ST} = \frac{1}{\sum L_{ST_i}} \left(\sum L_{ST_i} f_{ST_i}^{k} \right)^{\frac{1}{k}} \quad \text{Eq. 3.3}$$

$$USF = Prm \sum_{ST=1:n} \bar{f}_{ST} \sum L_{ST_i} \quad \text{Eq. 3.4}$$

To validate the proposed process for assessing unit side friction with the GP, a case study of two FB-DEEP models was undertaken; a 24 inch square pile that is embedded 50 feet into a clay layer overlying a sand layer. To ensure a wide variety of soil profiles, the depth of an individual clay or sand layer was randomly selected from a range of 5 to 90 feet. Next, each layer's N_{SPT} was randomly drawn from uniform distribution ranging for 5 to 60. This was repeated 100 times, representing different borings from which FB-DEEP computed ultimate side resistance was found. This model is expected to represent the database, i.e., a data set that has piles whose capacities vary dependent on each soil layer thickness and model type with the FB-DEEP file representing a boring and corresponding FB-DEEP calculated resistance as a synthetic load test, which the GP algorithm will use as M_i in equation 3.4. Note, this data set is less likely to be dominated by one soil model (e.g., Clay model contributes to most of side friction resistance, thus causing the GP to just converge on only the clay model and neglect the sand model). Next, using the generated FB-DEEP data set, the GP algorithm was run to determine both the clay and sand friction models. For the analysis, a population of 500 models and genetic

evolutions (i.e., iterations) were limited to 50 generations, with MSE (section 3.2) used in testing the models. Note, RMSE could also be used as a criterion to converge on a solution.

Table 3.2 shows the predicted models from multiple GP runs, using Eqs 3.3 and 3.4. It can be seen that the GP models predict FB-DEEP curves reasonably well (MSE given on the right). Evident, some of these models have extra terms (e.g., GP run 3, ST1 $\sin(\sin(14.3 - N_{SPT}))$) but these terms have little impact on the predicted fs value for N_{SPT} ranges of 5 to 60. Also when comparing the different GP results, it is evident that some of the model prediction (e.g., run 2, Table 3.2) has higher MSE values. This is likely due to the difficulty of optimizing two models with less direct information on the resistance contribution for each model. Interestingly, even though the MSE values are higher, looking at the plots of the analysis for GP vs. SPT N values (Figure 3.10), multiple models exhibit reasonable matches. Also evident, the rate of convergence (12 iterations, Figure 3.10) was quite reasonable given the number of unknowns, and variability of soil layering, SPT N values, etc. The final issue evaluated was the convergence of model constants, e.g., 38 vs. 31.3 in Table 3.2 used in the models.

Table 3.2 Results for Multiple GP Runs

GP Run	ST 1 Model $f_s = 109.8N_{SPT} - N_{SPT}^2 \ (psf)$	ST 3 Model $f_s = 38N_{SPT}(psf)$	MSE (lbs^2)
1	$109.8N_{SPT} - N_{SPT}^2 + 5.28$	$31.3N_{SPT} - \sin(N_{SPT} + 65.5) + 65.1$	1.14e+08
2	$65.9N_{SPT}$	$38.1N_{SPT} - 3.6/\ln(N_{SPT}) + 26.6$	2.07e+10
3	$109.6N_{SPT} - \sin(\sin(14.3 - N_{SPT})) - N_{SPT}^2$	$33.2N_{SPT}$	1.25e+08

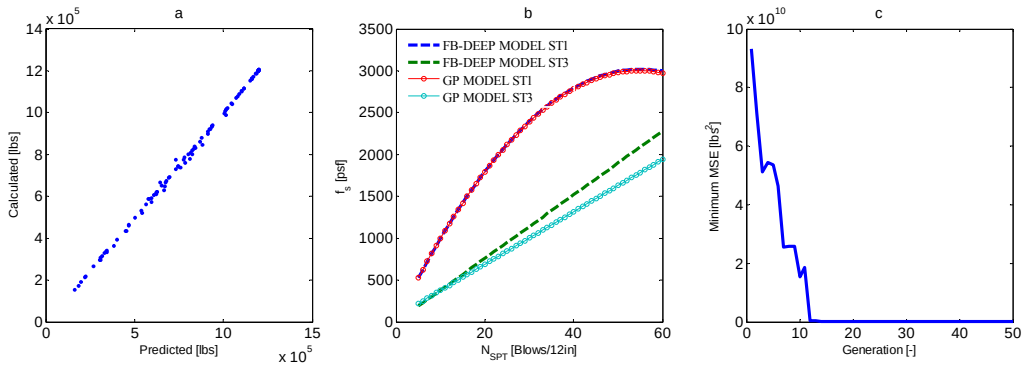

(a) (b) (c)

Figure 3.10 GP Runs, Prediction of FB-DEEP for Soil Types 1 and 3: (a) FB-DEEP Calculated Capacity vs. GP Predicted, (b) Resistance Models, and (c) Minimum Error of Generation

3.5 Evaluating Constants in the GP Algorithm

As identified in multiple sections (3.2 and 3.4), the GP algorithm must solve various complex equations for each soil type model. In a few of the examples, it was identified that not all runs of the GP code would exactly replicate (Table 3.2) the equation used to generate the data. In some cases, the GP solution would either simplify or match exactly (e.g., Table 3.1 reduction of terms) or a solution would be found with many terms (i.e., > 15), which did not exactly match the equations used in generating the data. This difference was attributed to the GP's search for the exact coefficients used in the test equation without them initially being specified in the terminal set.

A literature review was conducted to find a solution to improve the ability of the GP algorithm to find unknown coefficients in an equation. It was found that in simpler versions of GP, presented in section 3.2, that it is a poor tool when trying to determine unknown coefficients. It was found for these cases that the GP would find a model with a minimal error, but created an equation that would fill up a few pages. To fix this, Koza (1992) suggested the using a random

constant, $\mathbb{R}$, referred to in the literature as the ephemeral random constant. In this implementation, $\mathbb{R}$ is added to the terminal set for the GP to use. When $\mathbb{R}$ is selected by a node in the generation of a tree for the initial population, it should be given a random constant value from a specified range (selected from a random uniform distribution). Note, these random constants, $\mathbb{R}$, should be treated as unknown in the evolution process. This process was found to be the easiest to implement; however, this approach was found to be not very efficient when determining unknown coefficients. Moreover models with significant amount of terms were still observed with this approach.

Another approach used to find unknown coefficients, $\mathbb{R}$, is the use of a technique called numerical mutation during the evolutionary process, Evett and Fernandez (1998). In the evolutionary process, a portion of the population is selected and all of its' numerical constants are changed randomly. The constants to be changed are selected from a uniform random distribution whose range is determined by the old constant's value and a specified range factor. The range factor is based on the fitness of model whose constants are being changed. Generally, this results in models with good fits having little changes and models with poor fits have larger changes in the values of the constants.

A third option for dealing with unknown coefficients is the use of an optimization tool during the evolutionary process. In this implementation, a tool like the genetic algorithm is used to minimize the error associated with the coefficients as it proceeds. This requires the addition of an optimization tool within the evolutionary process (finds the unknown coefficients in an equation). Additionally this process may add significant computing time and difficulty in coding, as well as reduce the flexibility of the GP optimization process.

All three methods were investigated in the GP algorithm, with method proposed by Evett and Fernandez (1998) showing the best convergence. Again, for this approach, the models' coefficients, R – random variables, are changed by selecting a new value from a uniform random distribution whose range is determined by the old R's value and a specified range factor. The range factor is determined by the best raw fitness score (i.e., method error) multiplied by a reduction factor (a recommended value of 0.2). Consequently, if the population of models has poor fit, large changes are made to the $\mathbb{R}$ values. However, as population models improve their fitting, smaller changes are made to the $\mathbb{R}$ values. For each generation the numerical mutation algorithm is only applied to the top 20% of the population with the best fitting models.

3.6 Modeling Pile's Tip Resistance with Genetic Program

Besides skin friction, GP will be used to assess unit tip resistance, q_{ti}, vs. SPT N, where q_{ti} is a function (to be created by GP) of SPT-N and soil type, which will be averaged over the domain above and below the tip of the pile. For an initial model, Eq. 3.5 was programmed into the GP algorithm; note, for this analysis there is no depth correction and/or averaging was used, and all SPT N values were evenly spaced. Note, the depth correction was not coded in the GP algorithm, however arithmetic and harmonic averaging was considered along with different averaging domains. Using 100 generated FB-DEEP computed pile capacities (i.e., represents a synthetic load test to serve as a measured value in the GP algorithm), the GP algorithm was used to predict tip resistance models (i.e., q_{ti} vs. SPT N values) for the 3 FB-DEEP soil types (1, 2 and 3). Resulting models (i.e., with the lowest MSE, Eq. 3.1) from one of the analysis, using a population of 500 initial models and for 75 generations are shown in Figure 3.11 and Table 3.3. The GP converged on three reasonable models with MSE = 5.9×10^8 lbs^2. Note, the large MSE value shown results in a relativity small error when compared to the computed capacities. Also,

shown in Figure 3.11 are the original FB-DEEP curves that were used to generate the tip resistance.

$$q_{tip} = \frac{1}{2}\left[\frac{1}{n_{below}}\sum_{tip}^{tip+3.5D} q_{t_i} + \frac{1}{n_{above}}\sum_{tip-8D}^{tip} q_{t_i}\right] \quad \text{Eq. 3.5}$$

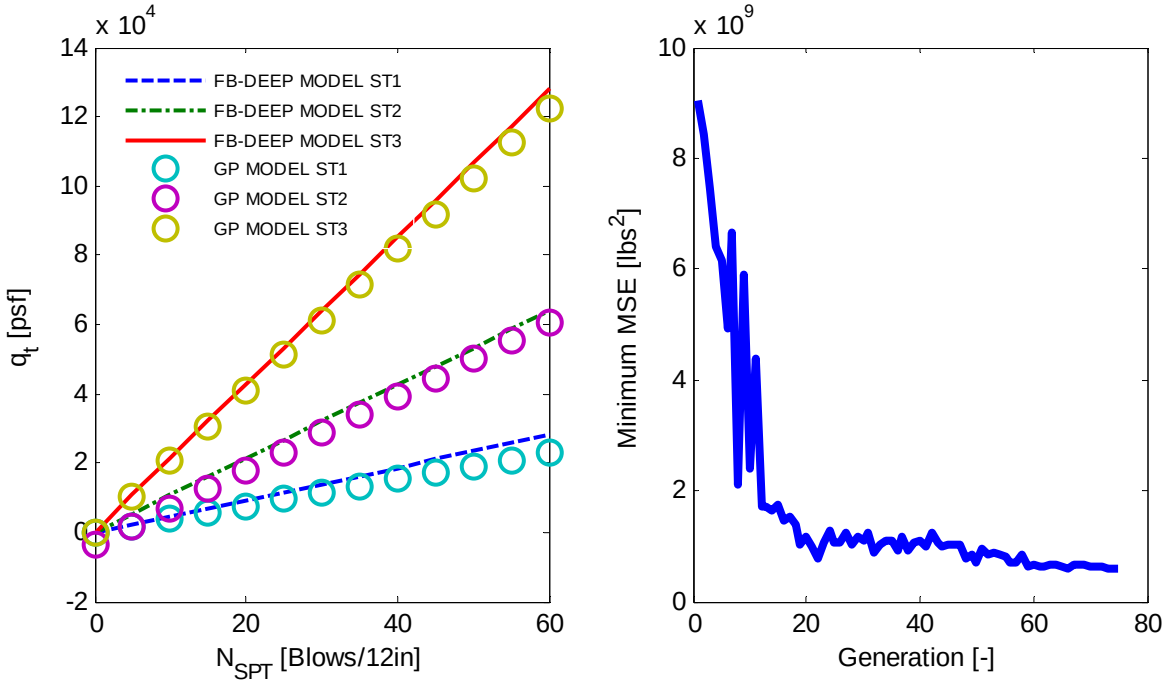

Figure 3.11 GP Predictions of FB-DEEP Tip Resistance for Soil Types 1, 2 and 3

Table 3.3 GP Predictions of FB-DEEP Tip Resistance for Soil Types 1, 2 and 3

Soil Type	FB-DEEP Equation [psf]	GP Predicted Equation [psf]
1	467 *SPTN*	382 *SPTN*
2	1067 *SPTN*	1076 *SPTN*-3742
3	2133 *SPTN*	2044 *SPTN*

To account for unevenly spaced SPT N values, as well as allow other types of averaging (e.g., harmonic, etc.), the approach identified in section 3.4 (Figure 3.9 – side friction) was used to characterize tip resistance. That is, for each SPT-N value located along the embedment length of the pile, individual length segments, L_i, are assigned. With individual L_i values determined,

the average unit tip resistance $\bar{q}_T$ was computed for each soil type, ST, found below and above the pile tip. This is given by Eq 3.6, where L_{qT_i} is the L_i for the soil type ST and q_{T_i} is the unit tip resistance predicted by the GP's model for ST at the corresponding SPT-N. The value k is the averaging parameter (Renard and de Marsily, 1997), ranging from -1 to +1, where k = -1 is harmonic averaging, k = 0 is geometric averaging (which can be shown by some limit properties) and k = 1 is arithmetic averaging. This gives the GP the flexibility of evaluating different averaging techniques. The q_{Ti} values are computed for each soil type around each pile, with the final average, q_T in Eqs. 3.6 & 3.8, is multiplied by A_{Tip} (pile's cross-sectional area), to give the total ultimate tip resistance, Q_{TIP}. W_i used in Eqs. 3.6 and 3.7 is length contribution of one blow count over total length (i.e., 3.5B below and 8B above), which is used with a given SPT N value.

$$\bar{q}_T = \left(\sum W_i \, q_{T_i}^k\right)^{\frac{1}{k}} \qquad \text{Eq. 3.6}$$

where

$$W_i = \frac{L_i}{L} \qquad \text{Eq. 3.7}$$

$$Q_{TIP} = A_{Tip} \, \bar{q}_T \qquad \text{Eq. 3.8}$$

The validity of the developed GP algorithm (coded in MATLAB) is evaluated extensively in Chapter 4, through comparison of all of FB-DEEP's unit skin and tip resistance curves based on random soil types, layering, and SPT N values.

CHAPTER 4
GP SIMULATION OF FB-DEEP OUTPUT AND ASSESSING METHOD UNCERTAINTY

4.1 Background

Prior to running the GP algorithm (chapter 3) on in situ data vs. the measured unit skin friction, and tip resistance (driven piles and drilled shafts, chapter 2), the program has to be verified/evaluated with known output. Since the focus of the research was to improve estimates of driven concrete pile and drilled shaft (founded in rock) resistances from in situ data, it was decided to perform the evaluation using FB-DEEP output from random soil/rock boring data.

Also, since all borings are generally not within the footprint of the pile/shaft, any boring prediction of axial capacity is composed of two general types of uncertainty: 1) spatial variability of capacity - from boring to boring; and 2) method error – uncertainty associated with given method's prediction approach, for example, difference between static load test resistance and predicted resistance using a boring in the footprint of the pile. Of great interest, is the separation of spatial and method uncertainties. If method uncertainty was evaluated separately (i.e., method specific), it could be added to the spatial uncertainty for a site (e.g., running FB-DEEP on many simulated boring data to find standard deviation of capacity), to assess the LRFD Φ on a site for given pile/shaft diameter and length. A discussion of the GP simulations using FB-DEEP output and assessing spatial variability follows.

4.2 GP Simulation of FB-DEEP's Side Friction for Concrete Piles

For this analysis, the properties of one hundred borings were randomly generated, which were composed of the four basic soil types: 1) plastic clays; 2) silts and other mixtures (e.g., clayey silt, sandy-silt, etc.); 3) clean sands and 4) limestone. Each boring was assumed to be 100 ft deep and was divided into four layers; the thickness of each soil layer was selected randomly; and the SPT N values, spaced every 2.5 ft were also selected randomly ($0 < N < 60$). For

instance, one 100 ft boring could have 15 ft of soil type 1, 25 ft of soil type 2, 40 ft of soil type 3 and 20 ft of rock (limestone), type 4, with 40 SPT N values randomly generated along its length.

FB-DEEP software was run for each of the 100 borings and the ultimate side friction, M_i, for each case was found. Note, the unit side friction for a specific layer was not analyzed or modeled, since the measured field data (i.e., load tests) is for the whole pile, not an individual layer. In the case of drilled shafts (discussed later), individual layering (e.g. in limestone) was characterized, since shaft instrumentation (i.e., strain gages) and laboratory data (e.g., qu, and qt) is available for individual layers.

Using the 100 borings composed of multiple soil layers and SPT N values, the GP algorithm was used to predict, P_i, the ultimate side resistance of each pile (total 100). Input for the analysis consisted of boring information, i.e., soil type (1 to 4) and SPT N value versus depth. For evaluation of error, as well as optimization, the GP algorithm used the natural log of MSE, or

$$MSE_{Ln} = \frac{1}{n}\sum [Ln(M_i) - Ln(P_i)]^2 \qquad \text{Eq. 4.1}$$

which is equal to

$$MSE_{Ln} = \frac{1}{n}\sum \left[Ln\left(\frac{M_i}{P_i}\right)\right]^2 \qquad \text{Eq. 4.2}$$

The use of the log removes the proportionality influence (i.e., normalized M_i with the magnitude of P_i) from the evaluation. That is, smaller total pile side frictions values have equal weight to higher (i.e., higher SPT N) values.

Shown in Figures 4.1 through 4.4 are the calculated, M_i (FB-DEEP) vs. predicted, P_i, (GP algorithm) unit skin friction, f_s, curves for each soil/rock type (1 through 4) for increasing SPT N values. Evident, the GP predictions match all linear models: sands, and limestone (Figures 4.3 and 4.4), quite closely. In the case of the nonlinear models: clays, and silts (Figures 4.1 and 4.2),

the GP predictions match FB-DEEP unit skin frictions quite well at the lower SPT N values, but slightly under predicts the clay (Figure 4.1), and over predicts the silts (Figure 4.2) at the higher SPT N values.

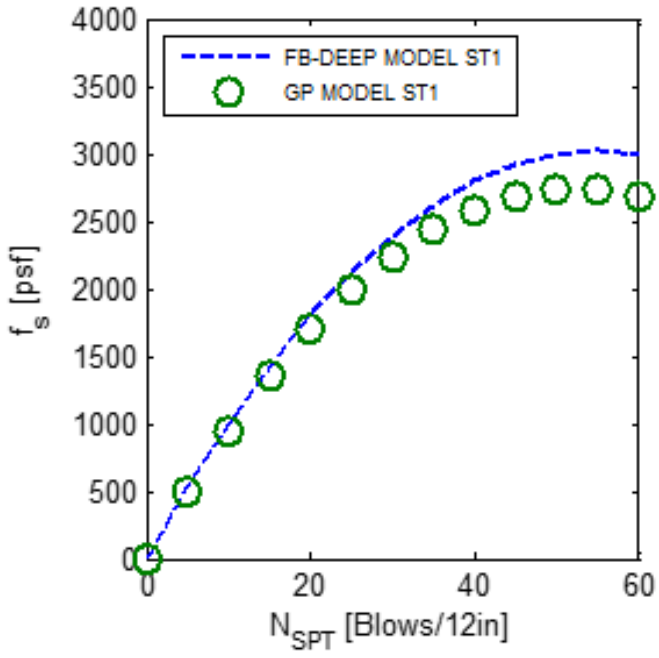

Figure 4.1 GP Unit Skin Friction vs. FB-DEEP for Soil Type 1 (Clay)

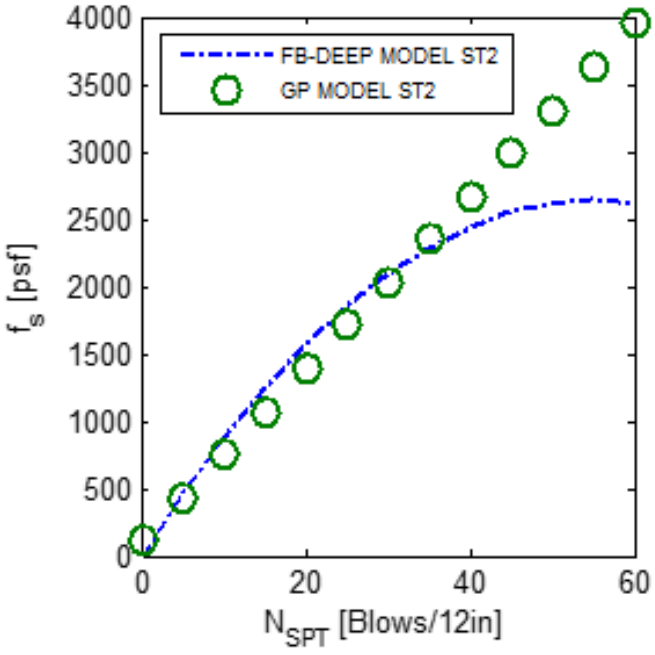

Figure 4.2 GP Unit Skin Friction vs. FB-DEEP for Soil Type 2 (Silt)

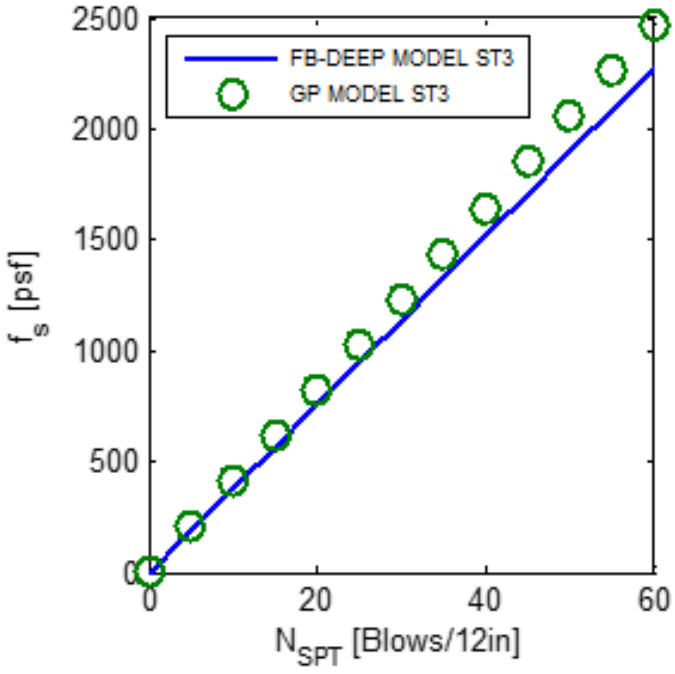

Figure 4.3 GP Unit Skin Friction vs. FB-DEEP for Soil Type 3 (Sand)

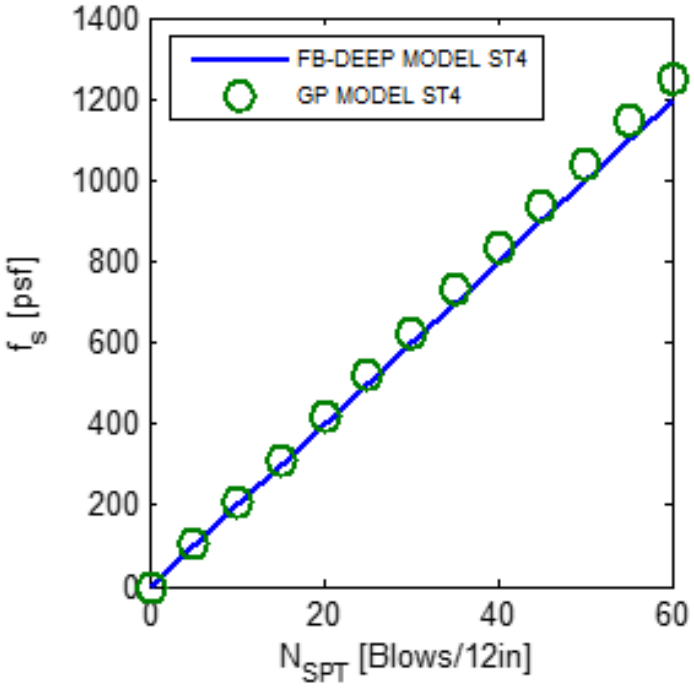

Figure 4.4 GP Unit Skin Friction vs. FB-DEEP for Soil Type 4 (Limestone)

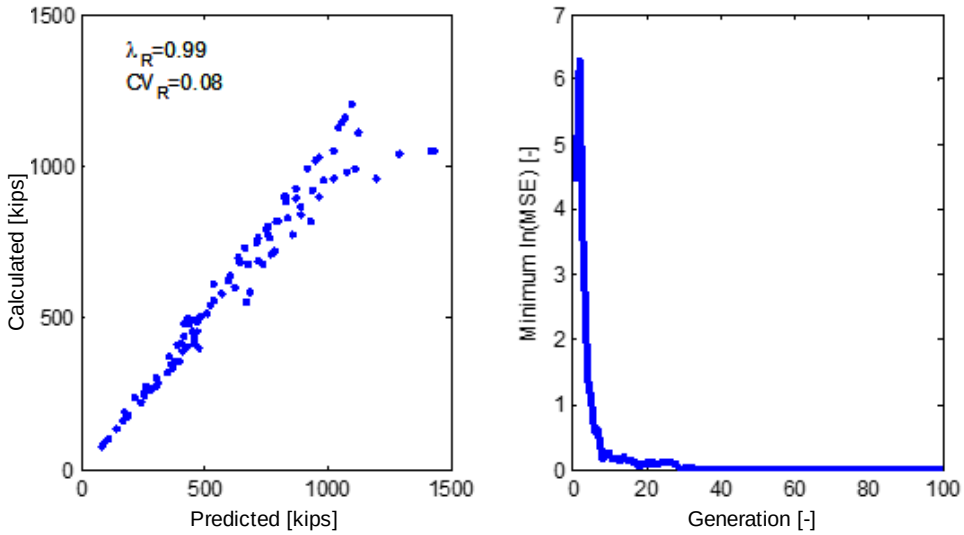

Figure 4.5 Calculated FB-DEEP vs. Predicted GP Side Resistance with Error

Presented in Figure 4.5 are the calculated and predicted total side friction (kips) for the 100 piles analyzed (left) and the natural log of MSE vs. the iteration number (right side). Also

shown in Figure 4.5 is the bias, λ_R, which is the mean ratio of measured (FB-DEEP) over predicted (GP), and the CV_R, coefficient of variation [standard deviation of λ, divided by the mean of λ (0.99)]. A mean λ (0.99), suggests that in general, the measured unit skin friction is 99% of the predicted side resistance, and a CV_R of 0.08 suggests that predicted side resistance has an approximate 8% error with the measured resistances.

4.3 GP Simulation of FB-DEEP's Unit Tip Resistance for Concrete Piles

Similar to the unit skin friction analysis, 100 borings composed of 4 soil types with random SPT N values were used by the GP algorithm to predict, P_i, unit tip resistance (psf) and compared to the measured, M_i, FB-DEEP calculation. Note, for the GP analysis, the SPT N values were average 8B (diameter) above and 3.5B below each pile tip, as identified in Eq. 3.5.

Evident from the comparisons (Figures 4.6 through 4.9), the GP algorithm matches each FB-DEEP unit soil tip resistance curves with reasonable accuracy as a function of SPT N values. Presented in Figure 4.10 are the FB-DEEP Calculation and GP predicted total tip resistance (kips) for the 100 piles analyzed (left), and the natural log of MSE vs. the iteration number (right side). Also shown in Figure 4.10 is the bias, λ_R, which is the mean ratio of measured (FB-DEEP) over predicted (GP), and the CV_R, coefficient of variation [standard deviation of λ, divided by the mean of λ (1.0)]. The figure reports a bias, λ, of 1.0 and a CV_R of 0.15, which are quite reasonable, considering that no predictions considered a correction for the bearing layer (i.e., layer tip of pile is located).

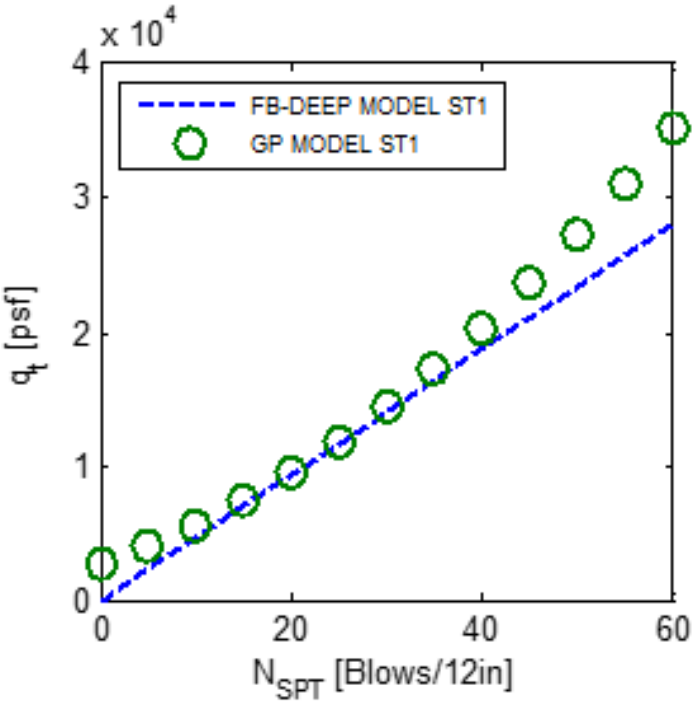

Figure 4.6 Unit Tip Resistance - GP vs. FB-DEEP for Soil Type 1 (Clay)

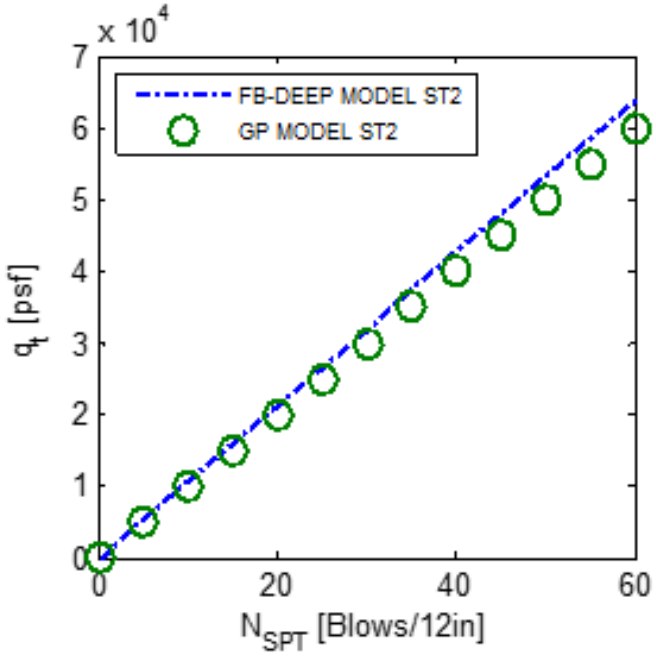

Figure 4.7 Unit Tip Resistance - GP vs. FB-DEEP for Soil Type 2 (Silt)

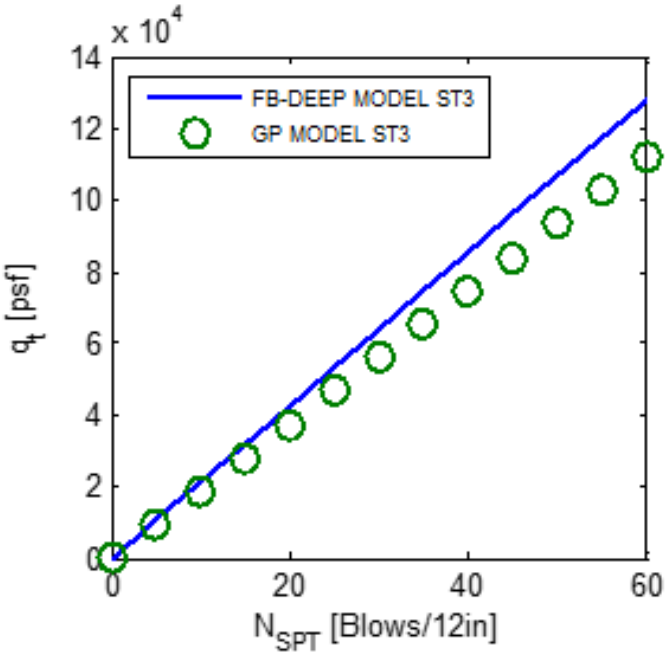

Figure 4.8 Unit Tip Resistance - GP vs. FB-DEEP for Soil Type 3 (Sand)

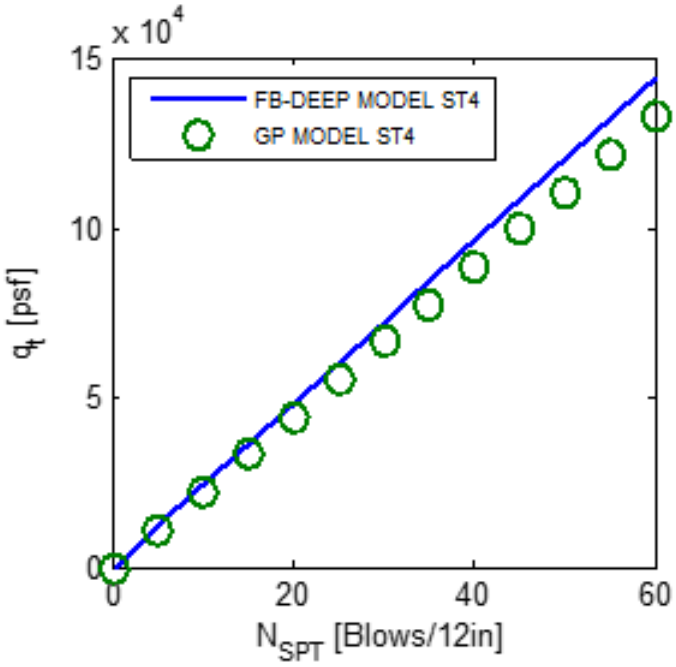

Figure 4.9 Unit Tip Resistance - GP vs. FB-DEEP for Soil Type 4 (Limestone)

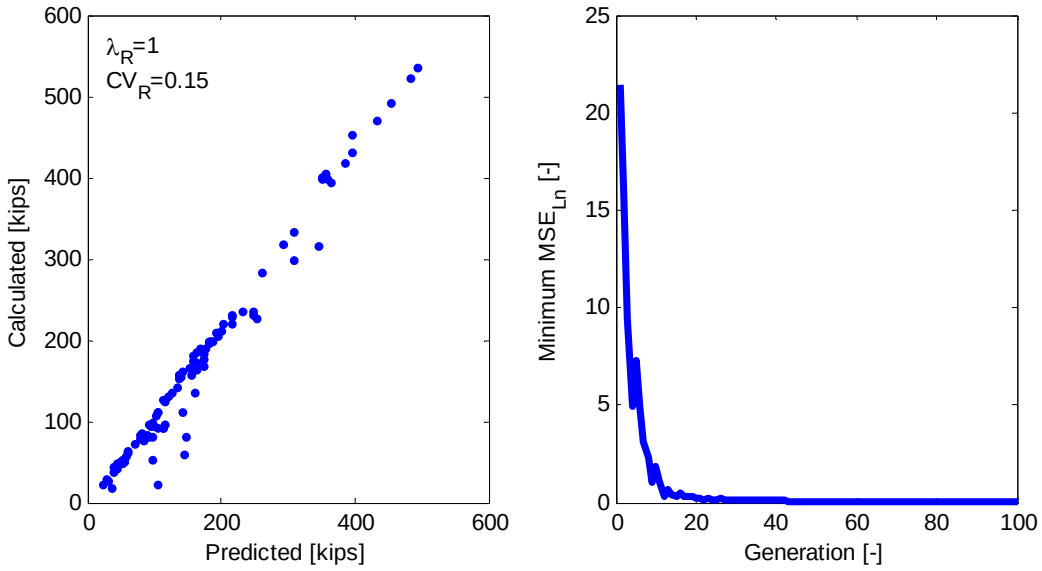

Figure 4.10 FB-DEEP Calculation vs. GP Predicted Tip Resistance with Error

4.4 GP Simulation of FB-DEEP's Unit Side Resistance for Drilled Shafts in Limestone

Of great interest was GP algorithm ability to characterize more complicated soil-structure interaction, such as unit skin friction of drilled shafts in Florida Limestone. For example FB-DEEP (FDOT) employs a three parameter model: unconfined compressive strength, q_u, split tensile strength, q_t, and rock recovery, REC for assessing unit skin friction along a shaft.

For the investigation, unit side friction values representative of measured results from strain gage data along a shaft recorder during static load test (e.g., Osterberg or conventional top down static tests) were employed. Note, the latter is representative of data in the database. The calculated, M_i, unit skin friction values were obtained from the standard FDOT equation:

$$f_s = \frac{1}{2}\sqrt{qu}\sqrt{qt}\ x\ Recovery \qquad \text{Eq. 4.3}$$

A total of 100 random unconfined compression, q_u, split tension, q_t, and recoveries were substituted into Eq. 4.3 and 100 calculated, M_i, unit skin friction values were generated. Next, 200 random GP models were generated using the three parameters: q_u, q_t, and recovery. Note, the models could be of any form, linear, quadratic, etc. Subsequently, the algorithm was allowed to perform 100 genetic (cross-over, mutation, and reproduction) evolutions to reduce MSE_{Ln}, Eq. 4.2 MSE_{Ln} is selected due to range of resistance values have an order of magnitude difference, thus accounting for proportionality affect when evaluation method error.

Shown in Figure 4.11 is the predicted unit skin friction for a range of q_u and q_t values with a recovery value of 50%. Presented in Figure 4.12 is the calculated unit skin friction

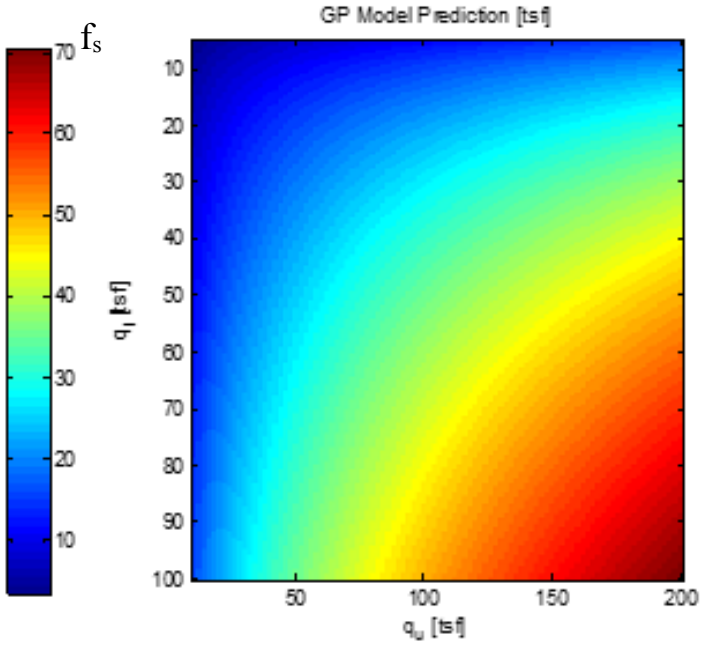

Figure 4.11 GP Predicted Unit Skin Friction for Range of q_u and q_t (Recovery =50%)

values, Eq. 4.3, that were used in the GP predictions, Figure 4.11. Shown in Figure 4.13 is the percent error (%) between the predicted GP results (Fig. 4.12) and the measured (Eq. 4.3) for

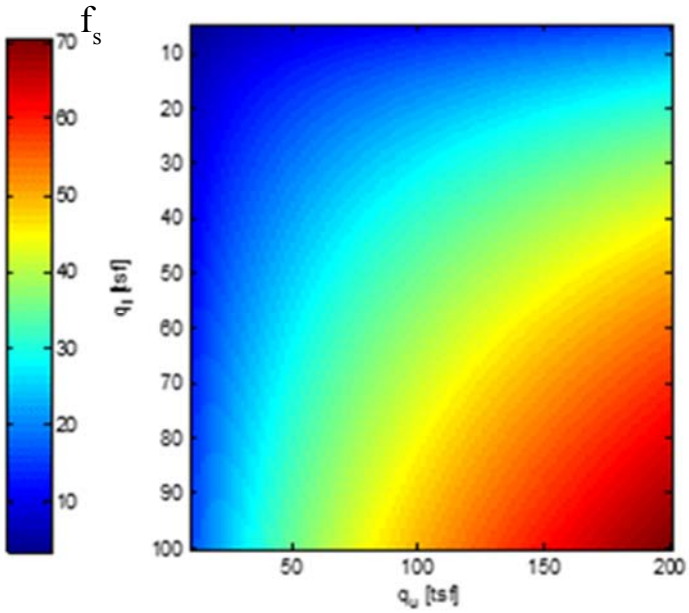

Figure 4.12 Calculated Unit Skin Friction, Eq.4.3 for Range of q_u and q_t (Recovery =50%)

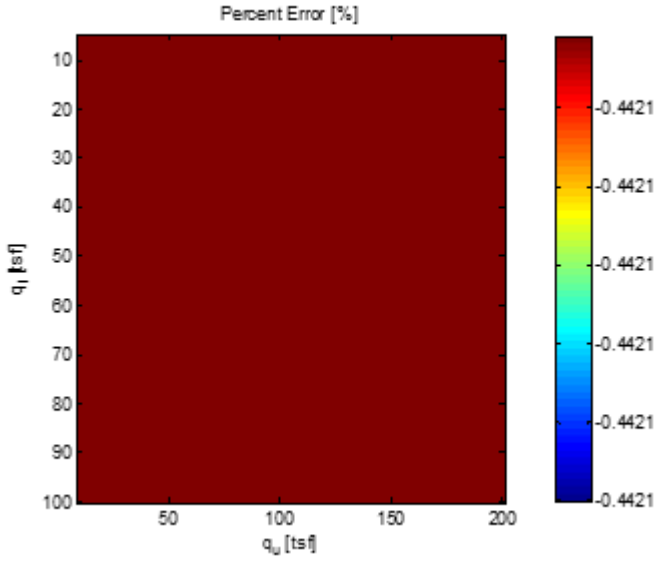

Figure 4.13 Percent Error (%) between Predicted (GP) and Calculated (FDOT)

all strength values (q_u and q_t) and one recovery (50%). Note, similar plots are available for other recoveries. Maximum error was 0.44% for any one value, which is relatively constant for all

combination of q_u, q_t and recovery, thus resulting in the constant color for Figure 4.13. The final predicted GP equation was given as,

$$P_s = 0.4976 \sqrt{q_u}\sqrt{q_t}\, x\, Recovery \qquad \text{Eq. 4.4}$$

Shown in Figure 4.14 is the Calculated and Predicted response, as well as the MSE_{Ln}, versus the iteration number. Evident, with a bias of one and a coefficient of variation of zero, the GP algorithm is capable of characterizing highly nonlinear data, if sufficient information is available.

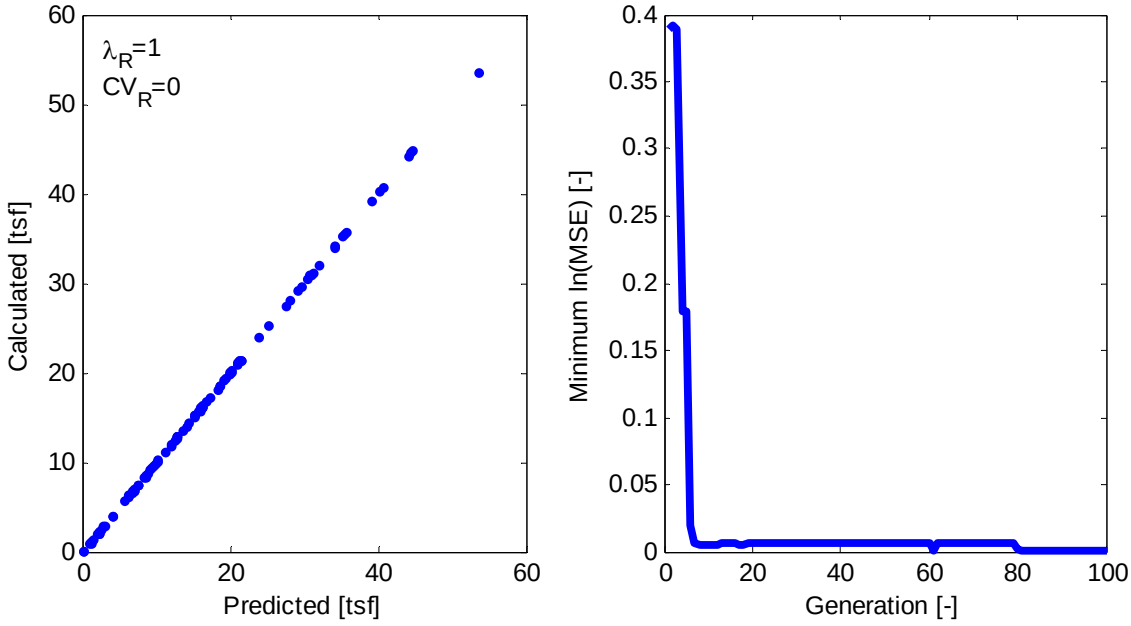

Figure 4.14 Calculated vs. Predicted GP Side Resistance with Error

4.5 Development of Equations to Assess Method Uncertainty

Critical to the development of any set of equations to predict pile/shaft capacity from boring data is ensuring the best fit and the minimization of prediction of uncertainty. Contributing to both the prediction, as well as the load test results are a number of uncertainties or variability. For instance, consider a number of sites, N_{site}, which each have $N_{lt,i}$ load tests

(subscript "i" refers to site, "lt" refers to load tests) and $N_{pred,i}$ prediction data (e.g., number of borings not within the load test footprint). Similarly, let t_{ij} be the jth load test value (true resistance) at the ith site and p_{ik} the kth prediction at the ith site. For any load test, t_{ij}, and prediction, p_{ik}, the pile/shaft's response may be influenced by sum of the following components:

$$t_{ij} = A + B + C_1 + D \quad \text{Eq. 4.5}$$

$$p_{ik} = A + E + C_2 + F \quad \text{Eq. 4.6}$$

Components A through F are random variables whose mean are zero, with the exception of A whose expectation is equal to the mean resistance over all site (equal for t_{ij} and p_{ik}, since bias correction is assumed). The variances are denoted by σ^2_A through σ^2_F, respectively, where all components are mutually independent and represent the following:

A - variability contained in both t_{ij} and p_{ik} (e.g., how well the mean prediction over all borings at a site estimates the mean load test resistance at the same site).B - Site to site variability not contained in p_{ik} (e.g., random construction issues / irregularities, which vary between sites, but not within sites, such as related to the choice of contractor / construction method for a site, if site is soil versus rock or any uniform ground property not accounted for in p_{ik}).

C - On site variability contained in t_{ij} and p_{ik}. Subscripts 1 and 2 are used to indicate that these components, although of equal variance σ^2_C, are not correlated between t_{ij} and p_{ik}, i.e., no spatial correlation between predictions and load tests within a site. This component represents the potential uncertainty reduction if predictions inside the footprint of load tests were used to estimate respective true resistances at the load test locations of a particular site.

D - Within site variability not contained in t_{ij} (e.g., random construction issues / irregularities, which vary within sites, such as drilled shaft geometry or any ground property not accounted for in p_{ik}).

E - Between site variability contained in p_{ij} (e.g., random measurement / prediction errors, which vary between sites, but not within sites, such as related to the choice of SPT rig for a site, if site is soil versus rock or any uniform ground property erroneously contained in p_{ik}).

F - Within site variability contained in p_{ik} (e.g., random measurement / prediction errors for same SPT rig – operator (safety hammer), which vary within sites, such as instrumentation / sample analysis errors or any ground property erroneously contained in p_{ik}).

The variances σ^2_t and σ^2_p of t_{ij} and p_{ik}, respectively, are then obtained from Equations 4.5 and 4.6 as

$$\sigma_t^2 = \sigma_A^2 + \sigma_B^2 + \sigma_C^2 + \sigma_D^2 \qquad \text{Eq. 4.7}$$

$$\sigma_p^2 = \sigma_A^2 + \sigma_E^2 + \sigma_C^2 + \sigma_F^2 \qquad \text{Eq. 4.8}$$

and the covariance $Cov(t_{ij},p_{ik})$ and $Cov(p_{ik},p_{im})$ for $k \neq m$ as

$$Cov(t_{ij}, p_{ik}) = \sigma_A^2 \qquad \text{Eq. 4.9}$$

$$Cov(p_{ik}, p_{im}) = \sigma_A^2 + \sigma_E^2 \qquad \text{Eq. 4.10}$$

Note that $Cov(t_{ij},p_{ik})$ is the covariance between all pairs of predictions and all load tested values at a specific site and $Cov(p_{ik},p_{im})$ is the covariance between all pairs of predictions for a specific site. With this, we can express an estimation error variance $\sigma^2_e = \sigma^2_t + \sigma^2_p - 2Cov(t_{ij},p_{ik})$ as

$$\sigma_e^2 = \sigma_B^2 + 2\sigma_C^2 + \sigma_D^2 + \sigma_E^2 + \sigma_F^2 = \frac{1}{N_{site}} \sum_{i=1}^{N_{site}} \frac{1}{N_{lt,i}} \sum_{j=1}^{N_{lt,i}} \frac{1}{N_{pred,ij}} \sum_{k=1}^{Npred,ij} \left(p_{ijk} - t_{ij}\right)^2 \qquad \text{Eq. 4.11}$$

where the final expression serves to numerically evaluate σ^2_e from pairing up all predictions with all load tested values at each site and computing a uniformly weighted error variance over all sites (rather than uniformly weighted over all load tests or predictions). That is, the estimation error variance $\sigma^2_{e,}$ which is the sum of uncertainties A through F minus 2 times the covariance, is equal to the right side of Eq. 4.11, which may be evaluate for every load test, t_{ij}, with predicted boring capacity, p_{ik}. The number of predictions available for the jth load test at the ith site is hereby denoted by $N_{pred,ij}$.

A different error variance, σ'^2_e, may be determined by using borings to predict other borings (instead of load tests) at same sites. Doing this for all sites, the boring site variances, σ'^2_e, is found from $\sigma'^2_e = 2\sigma^2_p - 2\text{Cov}(p_{ik},p_{im})$, and substituting in Eqs. 4.7 & 4.10, it may be expressed as

$$\sigma_e'^2 = 2\left(\sigma_c^2 + \sigma_F^2\right) = \frac{1}{N_{site}} \sum_{i=1}^{N_{site}} \frac{1}{N_{lt,i}} \sum_{j=1}^{N_{lt,i}} \frac{2}{N_{pred,ij}\left(N_{pred,ij} - 1\right)} \sum_{k=1}^{N_{pred,ij}} \sum_{m=k+1}^{N_{pred,ij}} \left(p_{ijk} - p_{ijm}\right)^2 \qquad \text{Eq. 4.12}$$

Which is readily found from the final expression on the right. Evidently, Eq. 4.12 gives the combined spatial variability, σ^2_C, and random measurement (e.g., SPT rig) variability, σ^2_F. It is expected that random measurement (e.g., SPT rig) variability, σ^2_F, may be found in the literature (e.g., Phoon and Kulhawy, 1999, FDOT, Davidson, 1995) or measured on a site by site basis (e.g., perform 3 SPT borings within 5 ft of one another). Knowing σ^2_F, the site variability, $\sigma^2_{C,}$ may be found from Eq. 4.12 for a particular site or as averages over all sites.

The other variability, σ^2_B (site-to-site variability for shaft installations by different contractors), σ^2_D (random within-site construction issues, such as geometry, method of installation), and σ^2_E (site-to-site measurements error, SPT rig, etc.) may be combined into one

variance, $\sigma^2_{BDE,}$ and may be found by summing variances, or $\sigma^2_{BDE} = \sigma^2_B + \sigma^2_D + \sigma^2_E$. Substituting in Equations 4.11 and 4.12 results in

$$\sigma^2_{BDE} = \sigma^2_e - \sigma'^2_e + \sigma^2_F \quad \text{Eq. 4.13}$$

which may also be evaluated if σ^2_F is known. Again, σ^2_F corresponds to random measurement / instrumentation errors, and may be readily found as the variance of predictions obtained at equal (or very close) locations. Both σ^2_e and σ'^2_e in Equations 4.11 and 4.12 will be determined from both the load test and boring data (to be collected over the sites).

Of interest is the quantification of method error due to prediction using SPT data and associated uncertainties within the footprint of load test. Here we consider that a prediction p_{ij} is available inside the footprint of a production shaft / pile which has true resistance t_{ij}, such that equations 3, 4 and 5 become

$$\sigma^2_{t,new} = \sigma^2_A + \sigma^2_B + \sigma^2_{C,new} + \sigma^2_D \quad \text{Eq. 4.14}$$

$$\sigma^2_{p,new} = \sigma^2_A + \sigma^2_E + \sigma^2_{C,new} + \sigma^2_F \quad \text{Eq. 4.15}$$

$$Cov(t_{new}, p_{new}) = \sigma^2_A + \sigma^2_{C,new} \quad \text{Eq. 4.16}$$

Note, the covariance in Eq. 4.16 now also contains $\sigma^2_{C,new}$, because there is no more spatial variability between prediction and foundation location (i.e., components C_1 and C_2 in equations 4.5 and 4.6 are now fully correlated). Defining the total estimation error variance, $\sigma^2_{e,foot}$, as sum of uncertainties, minus correlation, yields $\sigma^2_{e,foot} = \sigma^2_{t,new} + \sigma^2_{p,new} - 2Cov(t_{new}, p_{new})$, substituting in Eqs. 4.14, 4.15 and 4.16, result in

$$\sigma^2_{e,foot} = \sigma^2_{BDE} + \sigma^2_F \quad \text{Eq. 4.17}$$

Finally, substituting in Eq.4.13 for $\sigma^2_{BDE,}$ gives

$$\sigma^2_{e,foot} = \sigma^2_{BDE} + \sigma^2_F = \sigma^2_e - \sigma'^2_e + 2\sigma^2_F = \sigma^2_{m,foot} \quad \text{Eq. 4.18}$$

Eq. 4.18, represents the method error (i.e., prediction error in the absence of spatial uncertainty) and will simply be labeled as σ^2_m. It is readily found from σ^2_e (Eq 4.11) and σ'^2_e (Eq. 4.12), along with the measured/reported predicted in situ variability, σ^2_F.

Since typical predicted vs. measured pile capacity error has a strong proportional influence, it was decided to convert all measurements into natural logarithms in order to find the error variances (i.e., σ^2_m). For instance shown in Figure 4.15 is typical measured (i.e., load test) vs. FB-DEEP predicted prestressed concrete pile Davisson capacities. Evident, as the prediction capacity increases, the scatter (i.e., error) increases. However, if the natural log of the results is used, then any error assessment, (MSE_{LN}, (Eq. 4.2)) is normalized (i.e., division by Prediction), which generally results in more accurate error assessment over the full range of the data. This is demonstrated in Figure 4.16, which shows the measured and predicted pile response plotted on log scale. Note, the error (i.e., scatter about the mean, red line) is relatively constant over the whole range of data.

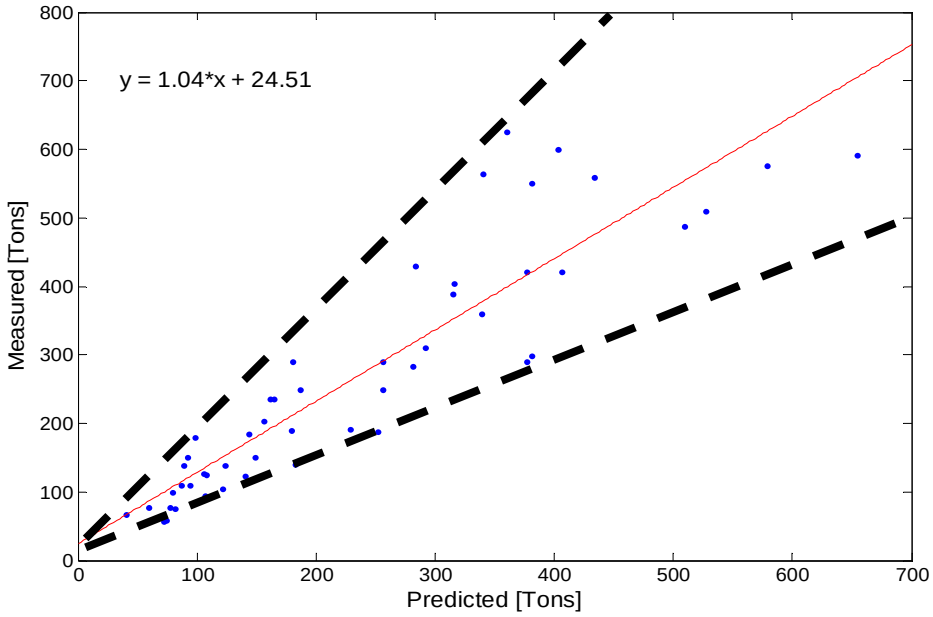

Figure 4.15 Measured and FB-DEEP Predicted Pile Davisson Capacities

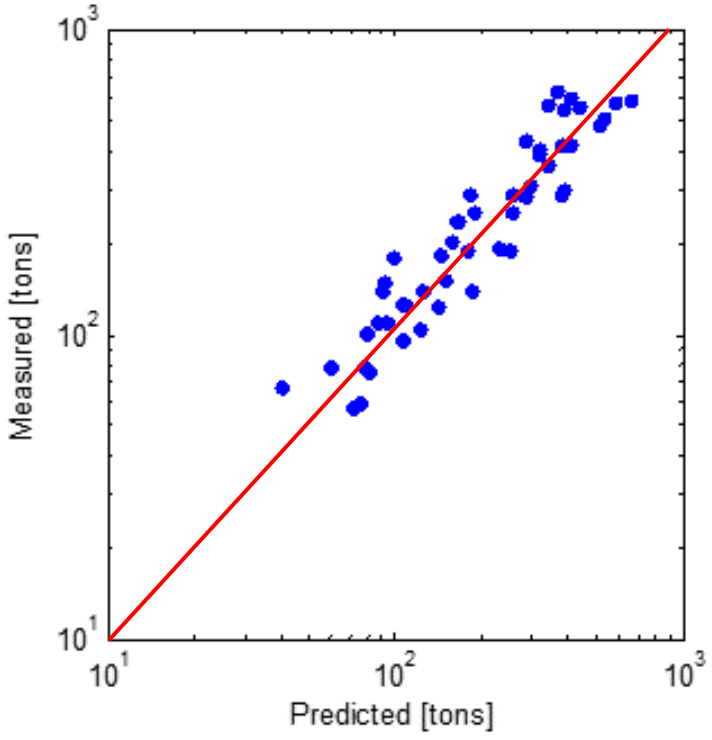

Figure 4.16 Measured and Predicted Pile Capacities Plotted with Log Scales

Consequently, the method error, σ_m^2 - Eq. 4.18, which is given in terms of σ^2_e (error between prediction and load test) and σ'^2_e (prediction error between borings) will be expressed in terms of natural logs as

$$\sigma_e^2 = \frac{1}{N_{site}} \sum_{i=1}^{N_{site}} \frac{1}{N_{lt,i}} \sum_{j=1}^{N_{lt,i}} \frac{1}{N_{pred,ij}} \sum_{k=1}^{Npred,ij} \left(\left[Ln\left(p_{ijk}\right) - Ln\left(t_{ij}\right) \right] \right)^2 \quad \text{Eq. 4.19}$$

and

$$\sigma_e'^2 = \frac{1}{N_{site}} \sum_{i=1}^{N_{site}} \frac{1}{N_{lt,i}} \sum_{j=1}^{N_{lt,i}} \frac{2}{N_{pred,ij}\left(N_{pred,ij} - 1\right)} \sum_{k=1}^{N_{pred,ij}} \sum_{m=k+1}^{N_{pred,ij}} \left(Ln\left(p_{ijk}\right) - Ln\left(p_{ijm}\right) \right)^2 \quad \text{Eq. 4.20}$$

Since, typical SPT data is log normally distributed, (e.g., Figure 4.17), the random measurement / prediction errors, associated with SPT rig – operator (safety hammer, etc.), σ_F^2, was assumed to be log normally distributed as well. Consequently, the log variance, σ_{LnF}^2 was expressed as

$$\sigma_{LnF}^2 = Ln\left(1 + CV_{SPT}^2\right) \quad \text{Eq. 4.21}$$

where, CV_{SPT}^2 is the associated uncertainty, i.e., variance, of the SPT data for repeated tests under identical conditions. Based on the data in the literature (Phoon and Kulhawy, 1999), CV_{SPT}^2 will be assumed to vary between 0.0 and 0.25, which does not differentiate for either safety or automatic hammers.

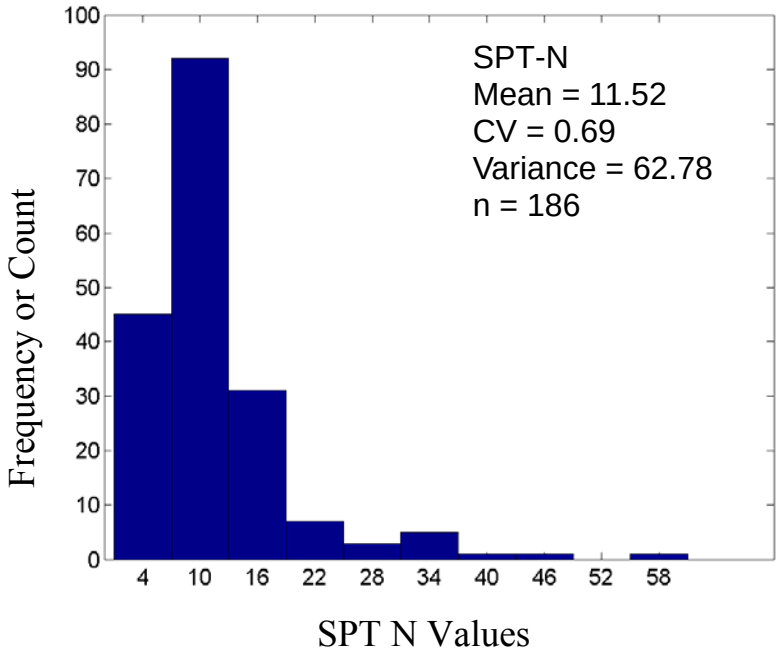

Figure 4.17 Frequency Distribution of SPT N Values for Sand in Dixie Highway, Florida

For this work, Eqs. 4.18, 4.19, 4.20 and 4.21 will be used to evaluate the method error for any analysis (i.e., skin friction or tip resistance). The mean square error MSELn given in Eq. 4.2 was used to control the GP algorithm's convergence, genetic operations, etc.

CHAPTER 5
ESTIMATION OF UNIT SKIN FRICTION AND END BEARING USING THE GP ALGORITHM

5.1 Description of Soils in FDOT Pile Database

In estimating the unit skin friction or end bearing vs. SPT N values, the separation of soils into representative groups with similar behavior is important. Typically, in the past FB-DEEP separated soil into 4 categories based on particle size: fine (clay, type 1), coarse grained (sand, type 3) and rock (Limestone, type 4). In the case of soil mixture, e.g., clayey sand, or sandy clay, they were usually lumped with silt (type 2).

With the increased use of the Unified Soil Classification System (USCS) for deep foundation design (FDOT plans and Geotechnical reports), separation of soil and rock into 4 representative groups is less subjective and more quantitative. For example, shown in Table 5.1 is separation of USCS descriptors into soil types of similar skin and tip resistance. Note, peats (Pt) are ignored in the analysis (i.e., identified as having no skin or tip resistance). Also, boring layers identified as Limestone (no USCS descriptor) were classified as soil type 4. Similarly, sandy clays (i.e., USCS: CL, CH) with more than 30% retained on #200 sieve were analyzed in both categories (i.e., one analysis in type 1 and another in type 2).

Table 5.1 Soil Type Based on USCS Description

Soil Type 1	Soil Type 2	Soil Type 3	Soil Type 4
CL	SM	SW	GW
ML	SC	SP	GP
CL-ML	SW-SC		GM
CH	SP-SC		GC
MH	SM-SC		GC-GM
OL	SW-SM		GW-GM
OH	SP-SM		GW-GC
			GP-GM
			GP-GC

Presented in Figures 5.1 to 5.4 are the frequency distributions of SPT N values based on soil type (Table 5.1) within 500 ft of all test piles within the database. The data represent SPT values along the length of the piles (i.e., side friction), with a total length of 8,030 feet of boring data. Figures 5.1 and 5.2 depict the case of no sandy clay correction on the left (i.e., CL and CH >30% retained on #200 sieve identified as Type 1) and with sandy clay correction on the right. Note, the values are presented in decimal (e.g., 0.15 represent 15% of all data = 0.15 x 8030' ~ 1200 ft, with N<10). Evident, the sandy clay had some effect on the lower bin counts (N<10, 10≤N<20, and 20≤N<30.). Note, since Sandy silts (e.g., ML or MH with more than 30% retained on a #200 sieve) did not occur in significant quantify, they were not analyzed separately as part of soil type 1 or 2 (all remained in soil type 1).

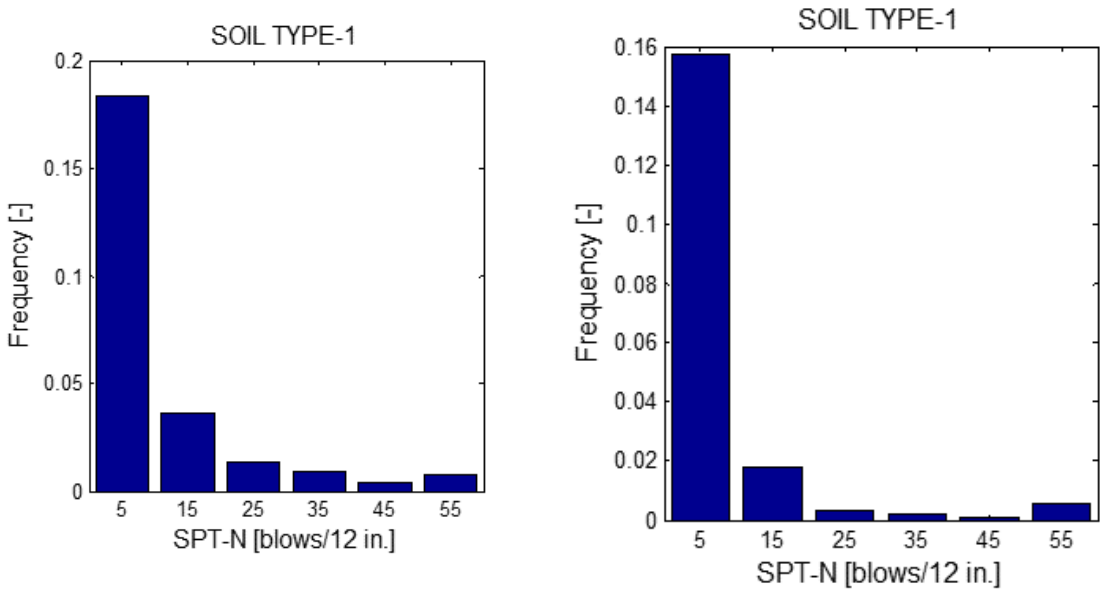

Figure 5.1 Frequency Distribution of SPT N Values alongside Piles for Soil Type 1(Without and With Sandy Clay Correction)

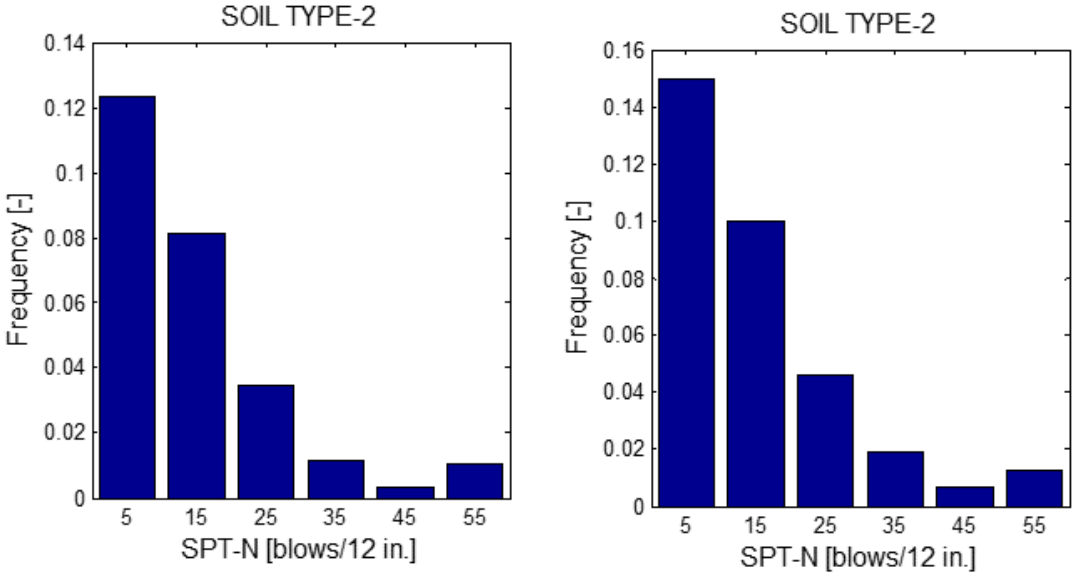

Figure 5.2 Frequency Distribution of SPT N Values alongside Piles for Soil Type 2(Without and With Sandy Clay Correction)

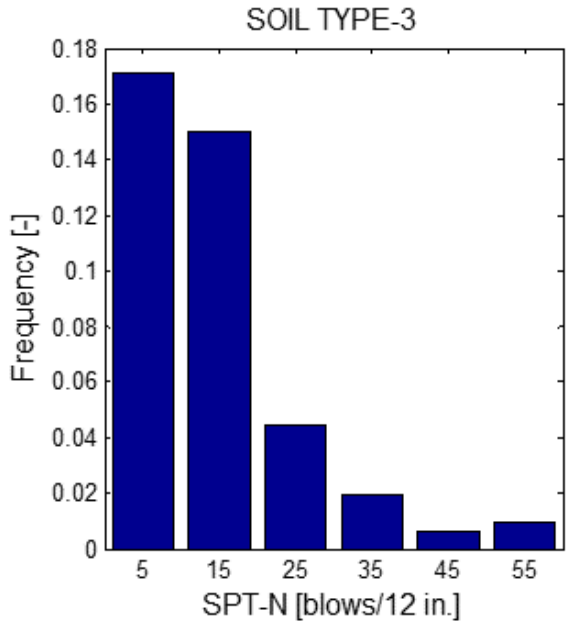

Figure 5.3 Frequency Distribution of SPT N Values alongside Piles for Soil Type 3

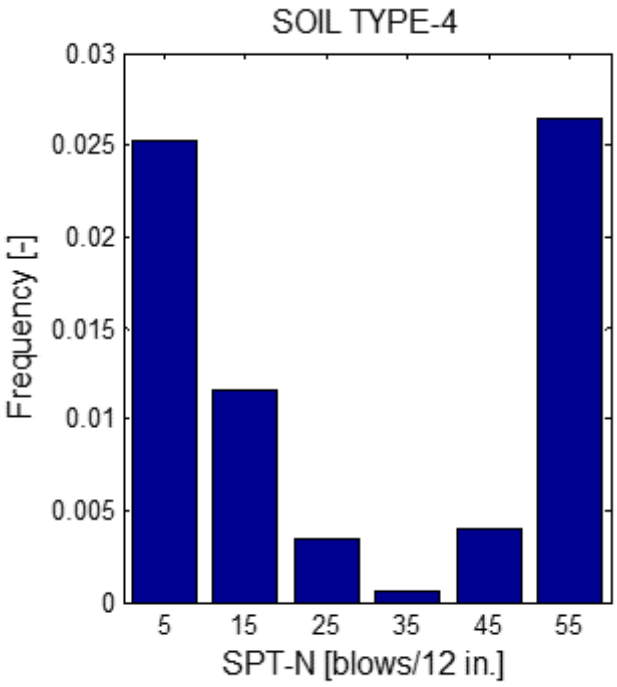

Figure 5.4 Frequency Distribution of SPT N Values alongside Piles for Soil Type 4

In the case of soil type 4, gravels and limestone, an increase in the data is observed in the last bin (50≤N<60). This was attributed to high blow counts (e.g., N> 60, 100, etc.) and refusals (e.g., 50/3"), as well as limiting blow to 60 (e.g., FB-DEEP). This limit was further investigated in the analyses sections.

Also of interest, is the distribution of SPT data below the tip of the piles used in assessing tip resistance. Given in Figures 5.5 through 5.8 are the distributions of SPT N values within 500 ft of the piles and located 3.5B below the tip of the piles. Again, Figures 5.5 and 5.6 depict the case of no sandy clay correction on the left (i.e., CL and CH >30% retained on #200 sieve identified as Type 1) and with sandy clay correction on the right. A total of 790 ft is represented (only 3.5B), and the values are presented in decimal format (e.g., 0.14 represent 14% of all data = 0.14 x 790' ≈ 111 ft, with 20 ≤ N <30, Figure 5.6).

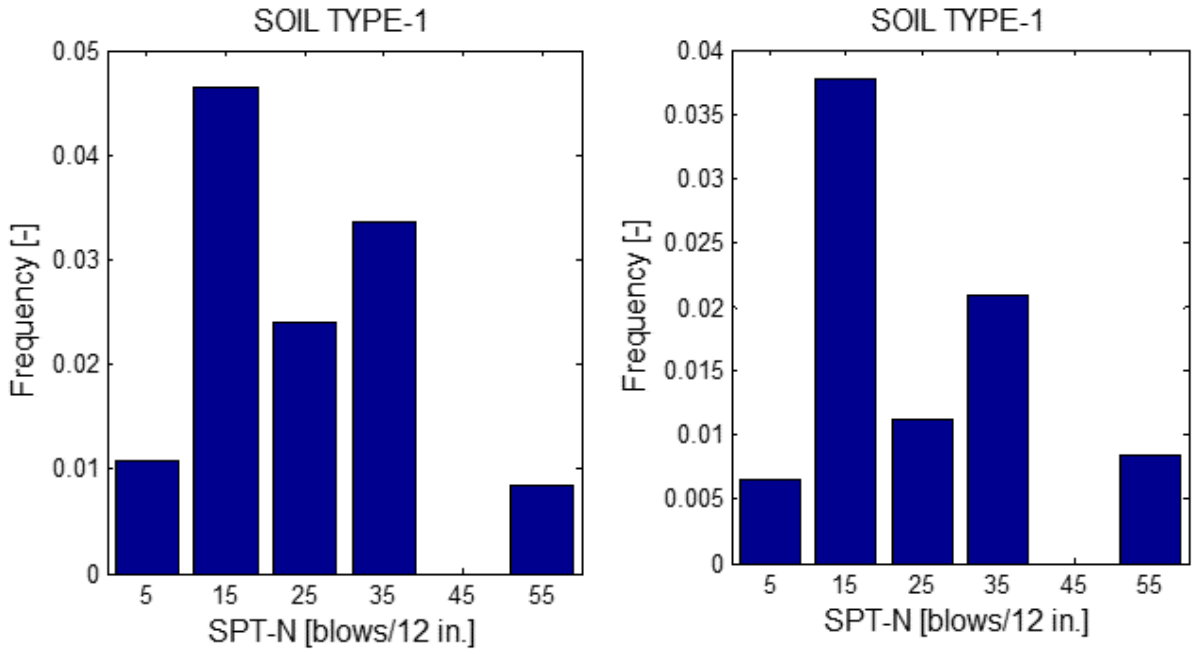

Figure 5.5 Frequency Distribution of SPT N Values only 3.5B beneath Pile Tip for Soil Type 1 (Without and With Sandy Clay Correction)

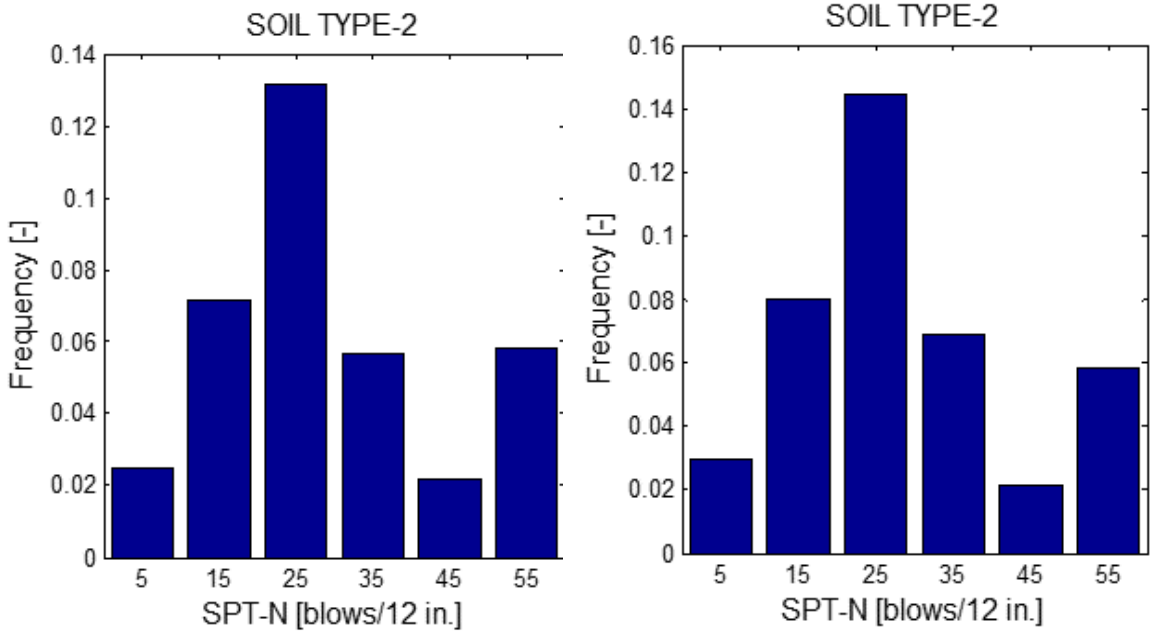

Figure 5.6 Frequency Distribution of SPT N Values only 3.5B beneath Pile Tips for Soil Type 2 (Without and With Sandy Clay Correction)

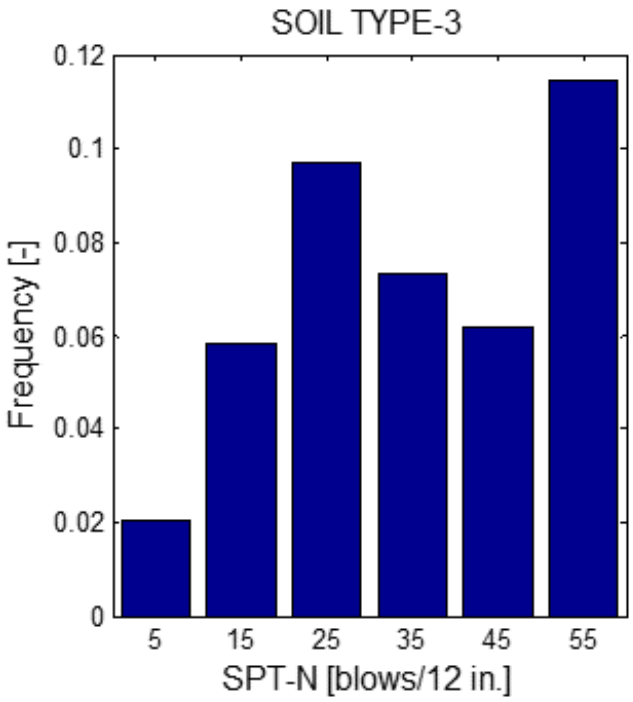

Figure 5.7 Frequency Distribution of SPT N Values 3.5B beneath Pile Tip for Soil Type 3

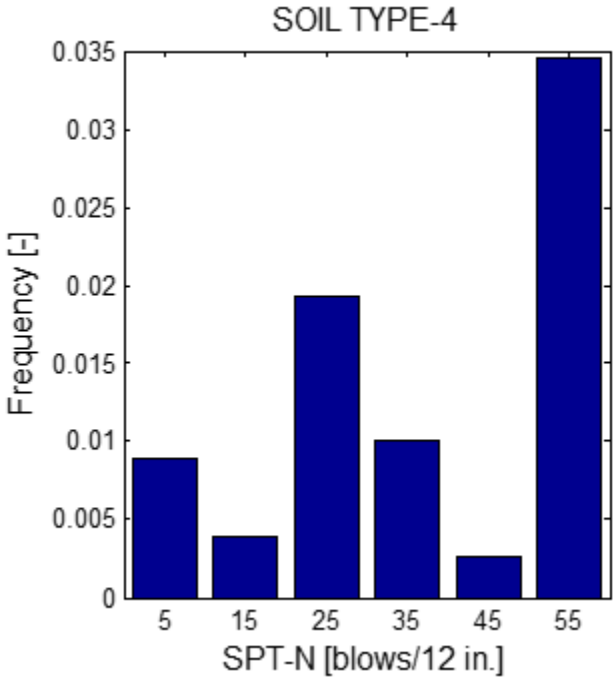

Figure 5.8 Frequency Distribution of SPT N Values 3.5B beneath Pile Tip for Soil Type 4

Evident, the sandy clay had some effect on the majority of the bin counts (N<10, 10≤N<20, and 20≤N<30, and 30≤N<40.). Also, both soil type 3 (sand) and soil type 4 (weathered limestone and limestone) have larger percentages of their blow counts in 50≤N<60. This may be attributed to refusals (e.g., 50/4"), as well blow counts above 60 (e.g., 70, 80, etc.); preliminary analysis limit all blow counts to 60 to agree with FB-DEEP. Higher limit values were also investigated.

5.2 Piles Used in the GP and FB-DEEP Investigation

All of the piles reported in chapter 2 (Table 2.5) were carefully reviewed to assess skin, tip and Davisson capacities. Shown in Table 5.2 are the individual resistances (kips) for each load test. Note, some of the piles were only uplift (e.g., 5th St Bascule Bridge), others did not reach Davisson capacity (some of Howard Frankland, Apalachicola River, etc.). Also, some of the piles did not report any distribution of skin and tip resistance (e.g., Buckman and Skyway Bridges), even though Davisson capacity was reported. Based on Table 5.1, a total of 48 piles reached Davisson Capacity, and of the 48 prestressed concrete piles, 28 had reported tip resistances, and 27 had reported skin frictions.

For the research, both the GP and the FB-DEEP software were run separately on the skin and tip resistances data. Once, the GP software established independent curves for skin and tip resistance based on soil type and SPT blow count, both the GP and FB-DEEP skin and tip resistance curves were used to predict the reported 48 Davisson capacities in the database. Also, for GP analysis, only borings within 100 ft were used to establish the skin and tip resistance curves. Once, the curves were established, the boring data within 500ft and 1000ft was used to evaluate method error, will be subsequently discussed in section 4.4.

Table 5.2 FDOT Database Piles Used for GP and FBDEEP Analysis

Project Site	Project Number	Pile	Skin Friction (kips)	End Bearing (kips)	Davisson (kips)	Issues
5th St. Bascule Bridge	412808-1-52-01	53	NA	NA	NA	Tension Test
		37	NA	NA	NA	Tension Test
		42	NA	NA	NA	Tension Test
		11	NA	NA	NA	Tension Test
Acosta Bridge	72160-3506	44	691.6	84.4	776	
		95	438	678	1116	
		26	NA	378.4	578	bad outlier
Apalachicola Bay	49010-3536	(B101) 3	320.4	493.6	814	
		(B133) 3	476.5	327.5	804	
		(B145) 3	491.4	488.6	980	
		(FSB22) 4	307.2	119.28	426	
		(B41) 3	NA	NA	524	Report that telltales did not give reliable analysis.
Apalachicola River	49010-3533	P3	617.3	336.7	954	
		P14	NA	NA	NA	Davisson not reached
		P25	401.3	316.7	718	
		FSB16	201.3	126.7	328	
Bayou Chico	48050-3536	P5	256.7	339.3	596	
		P10	127.5	672.5	800	
		P15	264.3	525.7	790	
Blackwater Bridge (I-10)	58002-3449	LT-1	NA	NA	658	Distribution of Side and Tip resistance not available
		TS2-2	NA	NA	908	Distribution of Side and Tip resistance not available
Buckman Bridge	72001-3462	TS13	NA	NA	1106	Distribution of Side and Tip resistance not available
		TS19	NA	NA	1312	Distribution of Side and Tip resistance not available
		TS24	NA	NA	1148	Distribution of Side and Tip resistance not available
		TS29	NA	NA	1264	Distribution of Side and Tip resistance not available
Caminida Bay	061-01-0040	TP1	415	135	550	
		TP4	NA	NA	NA	Davisson not reached
		TP7	610	44	654	

Table 5.2 Cont. FDOT Database Piles Used for GP and FB-DEEP Analysis

Project Site	Project Number	Pile	Skin Friction (kips)	End Bearing (kips)	Davisson (kips)	Issues
Choctawhatchee	60040-3527	FSB3 -24	NA	NA	NA	Distribution of Side and Tip resistance not available, Use of slurry mix
		P5- X	655	769	1424	
		P11- 38	910	582	1492	
		P17- 38	760	856	1616	
		P23- 13	523	269	792	
		P29- 7	713	277	990	
		P35- 7	564	920	1484	
		P41- X	NA	NA	1440	Distribution of Side and Tip resistance not available
		FSB26- 3	NA	NA	NA	Distribution of Side and Tip resistance not available, Use of slurry mix
Dixie Highway	230656-1-52-01	EB1/TP1	217	213	430	
		P8/TP2	232	143	370	
		P4/TP3	NA	NA	NA	Tension Test
Dodge Island	87000-3675	TP1	NA	NA	NA	Davisson not reached
Escambia River	48140-3509/ 58080-3516	27	NA	NA	850	Distribution of Side and Tip resistance not available
		399	NA	NA	NA	Davisson not reached
Howard Frankland	15190-3479	24 IN SQ	NA	NA	NA	Davisson not reached
		30 IN LONG	200	840	1040	
		30 IN SHORT	NA	NA	NA	Davisson not reached
		30 IN SQ	NA	NA	NA	Davisson not reached
Matanzas River (SR 312)	78002-3509	P14	989.8	74.2	1064	
		P17	NA	NA	NA	Davisson not reached
Port Orange	79180-3514	6	128.4	149.6	278	
		9	130	118	248	
Roosevelt Bridge	89010-3541	A-30	NA	NA	1209	No report available
		B-30W	NA	NA	1006	No report available

Table 5.2 (-Cont.-) FDOT Database Piles Used for GP and FB-DEEP Analysis

Project Site	Project Number	Pile	Skin Friction (kips)	End Bearing (kips)	Davisson (kips)	Issues
Sunshine Skyway	15170-3421	1-1	NA	NA	878	Distribution of Side and Tip resistance not available
		1-2	NA	NA	600	Distribution of Side and Tip resistance not available
		3-1	NA	NA	1060	Distribution of Side and Tip resistance not available
		10-11	NA	NA	1204	Distribution of Side and Tip resistance not available
		13-20	NA	NA	604	Distribution of Side and Tip resistance not available
		13-19	NA	NA	720	Distribution of Side and Tip resistance not available
West Bay Bridge	217911-5-52-01	3	NA	NA	NA	Davisson not reached
		9	NA	NA	950	Distribution of Side and Tip resistance not available
		15	NA	NA	850	Distribution of Side and Tip resistance not available
White City Bridge	51020-3514	3	304	326	630	
		6	186	274	460	

5.3 GP Prediction of Unit Side Friction for Prestressed Concrete Piles

Using the developed GP algorithm (chapter 3), the piles in Table 5.2 were analyzed for skin friction based on USCS soil types identified in section 1.1. For the analysis, each pile's total skin friction was divided by its surface area, Asurf (4B x total length), in order to remove influence pile size effects. Since only total unit skin friction (Qs /Asurf) was available, the GP algorithm had to optimize multiple unit skin friction curves (i.e., soil types) as a function of SPT N value.

Shown in Figure 5.9 (left figure) is the GP predicted (green data) unit skin friction vs. SPT N values plot along with FB-DEEP (blue data) curve for soil type 1. Presented in the right figure (Figure 5.9) is the percentage of the total SPT side data for 8030 ft boring that was used in the estimation of fs as a function of SPT N value. For instance, for SPT N < 5, 15% of all data (see Figure 5.1) was used to fit the GP model. Also evident from Figure 5.9 (right side), approximately 22% of all data used in the GP analysis had N ≤ 30; however, for N ≥30 (e.g., N = 40, 50, etc.) very little data (less than 2%) existed in the boring logs (Figure 5.1, and right side of Figure 5.9), which was available for the analysis. Consequently, a cutoff of 3000 psf (1.5 tsf) is warranted, which agrees with FB-DEEP's nonlinear limit value. The equation for GP predicted skin friction, fs, given in Figure 5.9,

$$f_s(tsf) = USF = 0.051 * N + 0.098 \quad < 1.5tsf\ (3000\,psf), (Soil\ Type\ 1) \qquad \text{Eq 5.1}$$

is linear with an intercept. The intercept suggest the use of a minimum unit skin friction in very soft clays, i.e., N ≤ 5, is 0.098tsf (102 psf), which is most likely due to of lateral displacement of the soil during pile driving and subsequent consolidation (i.e., increase in lateral effective stress).

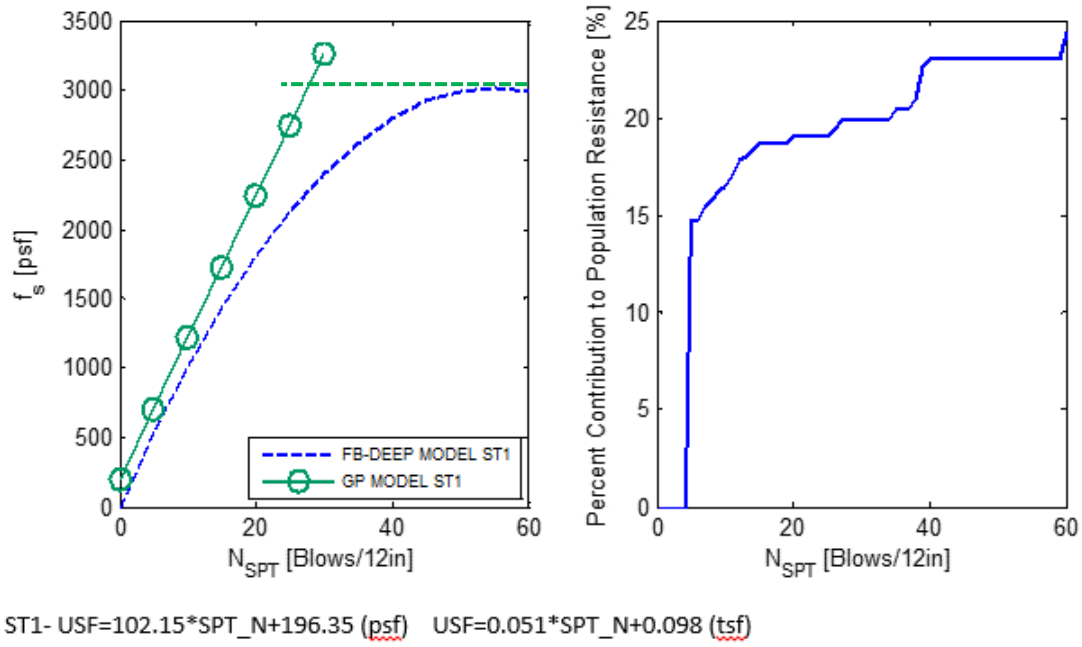

Figure 5.9 Unit Skin vs. SPT N Value for Soil Type 1 (Clays)

Presented in Figure 5.10 (left figure) is the GP (green data) predicted unit skin friction vs. SPT N values along with FB-DEEP (blue data) curve for soil type 2. Presented in the right figure (Figure 5.9) is the percentage of the total SPT side data for 8030 ft of boring that was used in the estimation of fs as a function of SPT N value. For instance, for SPT N < 20, 25% of all data (see Figure 5.2) was used to fit the GP model. Also evident from Figure 5.10 (right side) is for N ≤ 40, approximately 37% of all data was used in the GP analysis; however for N ≥40 (e.g., N = 50, 60, etc.) very little data (less than 2%) existed in the boring logs (Figure 5.1, and right side of Figure 5.9), which was available for the analysis. Consequently, a cutoff of 2750 psf (1.375 tsf) is warranted, which agrees with FB-DEEP's nonlinear limit value. The equation for the GP predicted skin friction, fs (Figure 5.10),

$$f_s(tsf) = USF = 0.037 * N \quad < 1.375 tsf\ (2750\ psf) \quad (Soil\ Type\ 2) \qquad \text{Eq 5.2}$$

is linear with no intercept. Evident, the GP prediction is slightly lower than FB-DEEP for N ≤ 25, but slightly higher for N ≥ 25. Thirty-five percent (Figure 5.10 right) of all boring data was used to fit the prediction.

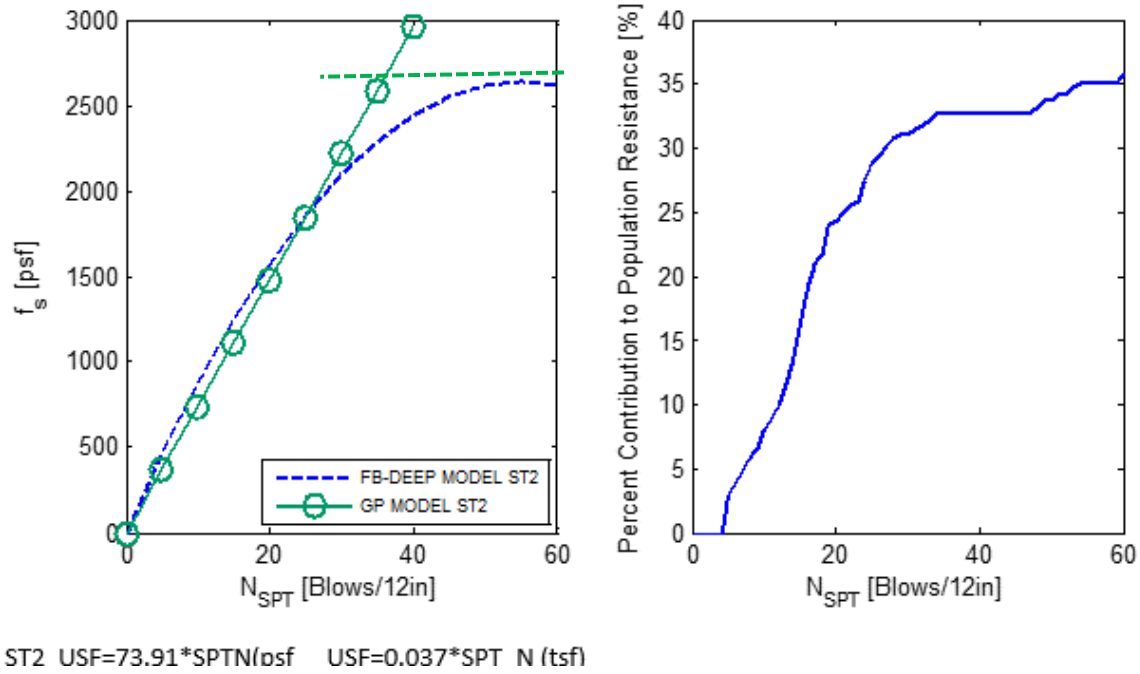

Figure 5.10 Unit Skin vs. SPT N Value for Soil Type 2 (Silts and Soil Mixtures)

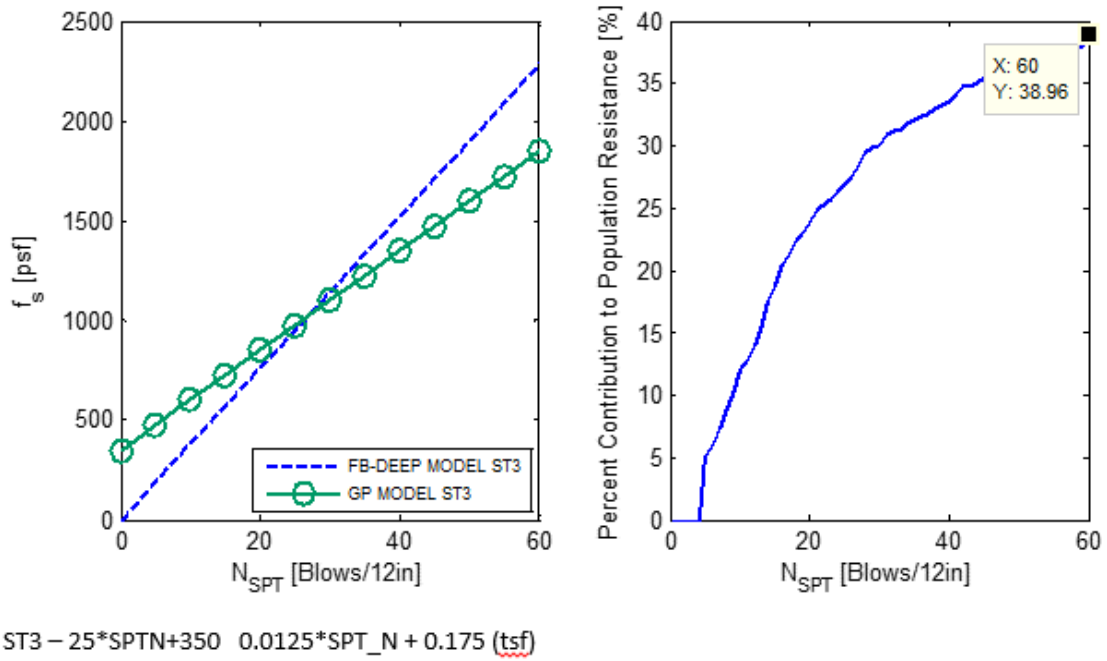

Figure 5.11 Unit Skin vs. SPT N Value for Soil Type 3 (Sands)

Shown in Figure 5.11 (left figure) is the GP predicted (green data) unit skin friction vs. SPT N values plot along with FB-DEEP (blue data) curve for soil type 3 (sand). Presented in the right figure (Figure 5.11) is the percentage of the total SPT side data for 8030 ft of boring that was used in the estimation of fs as a function of SPT N value. For instance, for SPT N < 20, 22% of all data (see Figure 5.3) was used to fit the GP model. Also evident from Figure 5.11 (right side) all SPT N values have some significant contribution (i.e. change is percent contribution > 0) in the estimated resistance such that it is no need to cut or limit the unit skin friction. A total of 37% of all data was used in evaluating the sand unit skin friction. The equation for GP predicted skin friction, fs, (Figure 5.11),

$$f_s(tsf) = USF = 0.0125 * N + 0.175 \qquad (Soil\ Type\ 3) \qquad \text{Eq 5.3}$$

is linear with an intercept. The intercept suggests that the minimum unit skin friction in loose sands, for N <5 is 0.175tsf (350 psf), and is most likely due to the densification of the sand as

result of the pile driving process. Also note that the slope of GP unit skin friction (0.0125) is less than the FB-DEEP value (0.019).

In the case of Limestone, the GP algorithm had very little (≤ 0.75%) soil type 4 data alongside the pile. Consequently, the GP algorithm for soil type 4 was set initially to FB-DEEP's representation (0.01∗ N), but the data generated very little if there was any changes (i.e., improvements to MSE_{Ln} , Eq. 4.2). Also, it should be noted, for all soil types (1 through 4), for SPT N values less than 5, the GP algorithm employed a limiting N value of 5.

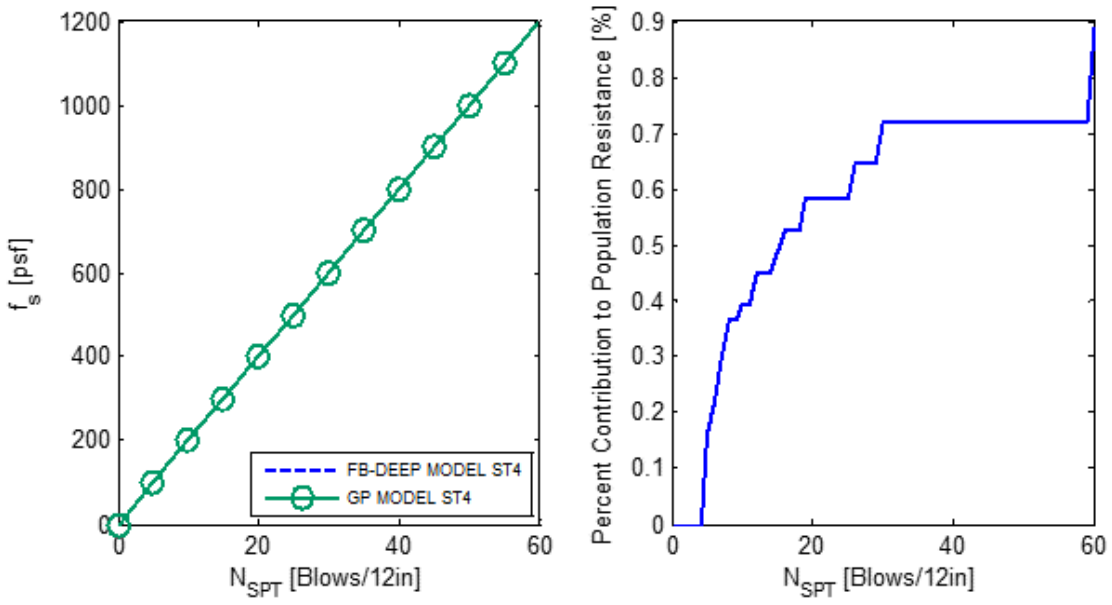

Figure 5.12 Unit Skin vs. SPT N Value for Soil Type 4 (Limestone)

Presented in Figure 5.13 (left) is the measured average unit skin friction on each pile (Table 5.2, Qs/A_{surf}), versus the GP predicted average unit skin friction, using Figures 5.9 through 5.12. The average bias, λ_R ($\frac{1}{N}\sum\frac{Measured_i}{Predicted_i}$) is 1.05 and the coefficient of variation, CV_R (σ_R / λ_R) is 0.27. Displayed in Figure 5.14 is the measured average unit skin friction vs. FB-DEEP's average predicted unit skin frictions. The latter has a bias, λ_R, of 1.23 and a CV_R of

0.31. The GP curves results in a 17% improvement in the bias, and a 15% improvement in the CV_R over FB-DEEP. Shown in the right side of Figure 5.13 is the convergence (MSE vs. iteration/generation step) of the GP algorithm for side friction.

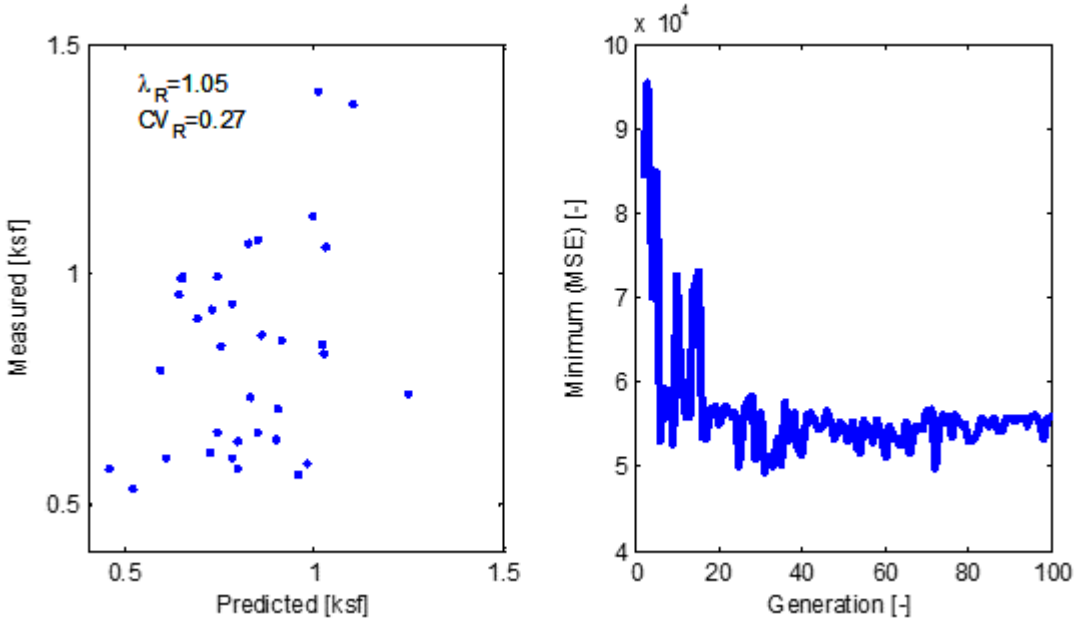

Figure 5.13 Average Measured Unit Skin Friction vs. Average GP Predicted Unit Skin Friction for All Piles

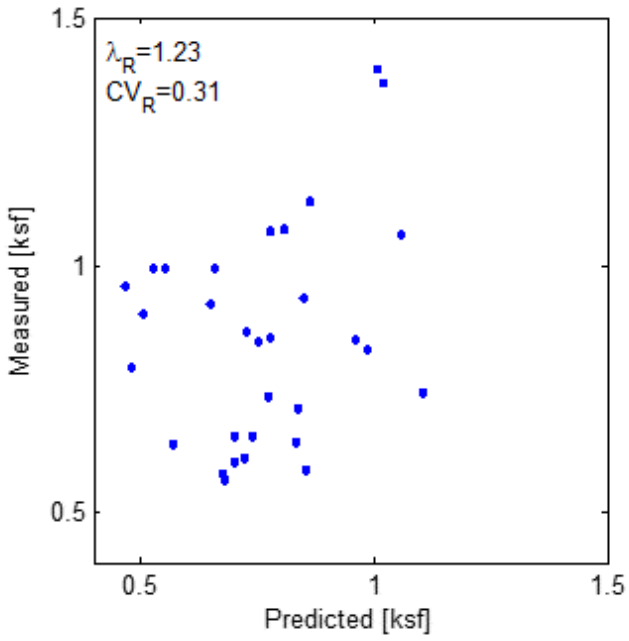

Figure 5.14 Average Measured Unit Skin Friction vs. Average FB-DEEP Predicted Unit Skin Friction for All Piles

5.4 GP Prediction of Unit End Bearing for Prestressed Concrete Piles

The GP algorithm was run on the developed tip resistance, Table 5.2. As with skin friction, the tip forces was first normalized [tip area (B^2)]. Since it wasn't known what averaging domain was appropriate, a number of different lengths and zones were considered: 1) traditional 8B above and 3.5B below; 2) 4B above and 4B below; 3) 4B below and finally 4) 2B below. Also two different averaging approaches were considered traditional arithmetic and harmonic,

$$\bar{q}_T = \left(\sum W_i \, q_{T_i}^k\right)^{\frac{1}{k}} \qquad \text{Eq. 5.4}$$

where

$$W_i = \frac{L_i}{L} \qquad \text{Eq. 5.5}$$

$$Q_{TIP} = A_{Tip}\,\bar{q}_T \qquad \text{Eq. 5.6}$$

In the case of k (1 – arithmetic; -1 – harmonic). Note, Li is the spacing between N values, and L is the total length (e.g., 3.5B + 8B, 4B, etc.).

Shown in Table 5.3 are the GP results of different averaging assumptions above and below the tip of the piles. Evident from the table, all averaging, which includes blow counts above the pile, for example, 4B and 8B results in conservative biases, λ_R , i.e., predicted results smaller than the measured values. The latter could be possibly attributed to smaller blow counts of the pile. For verification, the FB-DEEP unit tip curves were used to analyze the data set.

Table 5.3 GP Analysis of Unit Tip Resistances

Averaging Domain	Averaging Type	CV_R	λ_R
4B Below	Arithmetic	0.668	1.110
4B Below	Harmonic	0.690	1.384
4B Above and 4B Below	Arithmetic	0.614	1.568
4B Above and 4B Below	Harmonic	0.608	1.023
2B Below	Arithmetic	0.568	1.094
2B Below	Harmonic	0.586	1.287
8B Above and 3.5B Below	Arithmetic	0.614	1.569
8B Above and 3.5B Below	Harmonic	0.602	1.209

Shown in Figure 5.15 is the measured and predicted FB-DEEP tip resistance based on with or without sandy clay correction. Note, the large bias, λ_R (2.42), suggests that the FB-DEEP tip resistance curves are very conservative (i.e., under predict tip capacity).

One way to reduce the conservativeness of unit tip resistance curves are to increase the mean average of SPT blow counts in the vicinity of the pile tip, or possibly reducing the likelihood of obtaining lower SPT N values. Since pile bearing layers are generally stronger than overlying weaker layers, which SPT N $_{\text{bearing layer}}$ > SPT $_{\text{overlying layer}}$; averaging only beneath the pile would generally ensure higher average SPT N values. The latter is reflected in Table 5.3.

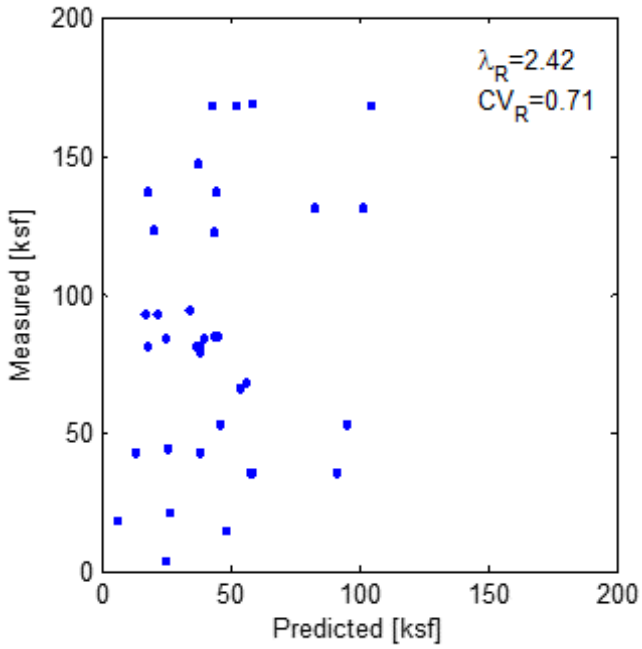

Figure 5.15 Average Measured Unit Tip vs. Average FB-DEEP Predicted Tip Resistance for All Piles

Note, the averaging of just 2B below the pile tip results in the lowest bias, λ_R (e.g., Arithmetic - 1.09). However, with 2B averaging, it is the concern of very limited number blow counts in this zone, which consist of only 2 to 3 N values. Consequently, the 4B averaging below the tip was considered more appropriate. For this case, the arithmetic average in Table 5.3 had the best bias and will be presented and discussed.

In the case of averaging (arithmetic) the blow counts 4B beneath the tip of individual pile, GP algorithm developed 4 unit tip resistance curves, Figure 5.16 to 5.19. In the case of

clays (soil type 1), the GP curve starts at 0 and follows the original FB-DEEP curve initially, but then increases significantly with blow count. Of concern with the curve, is the limited data for this soil type (8%) of all data (Figure 5.16 – right side). Due to the limited amount of data, it was decided to limit the maximum tip resistance to the observed maximum percentage change (N = 35) given by the GP algorithm, which is $7x10^4$ in Figure 5.17.

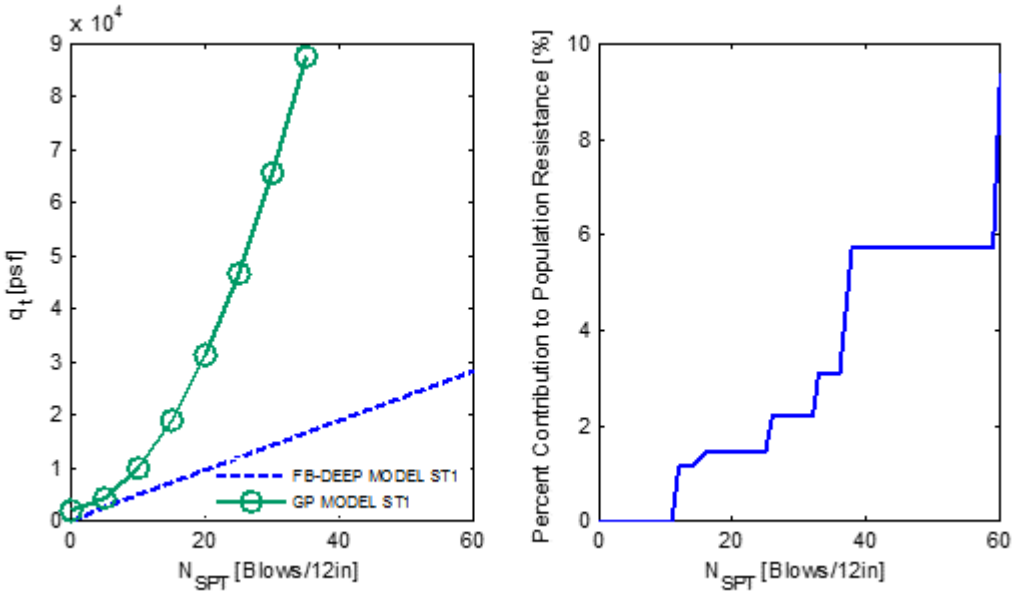

Figure 5.16 GP Unit Tip Resistance vs. SPT N Value for Soil Type 1 (Clay)

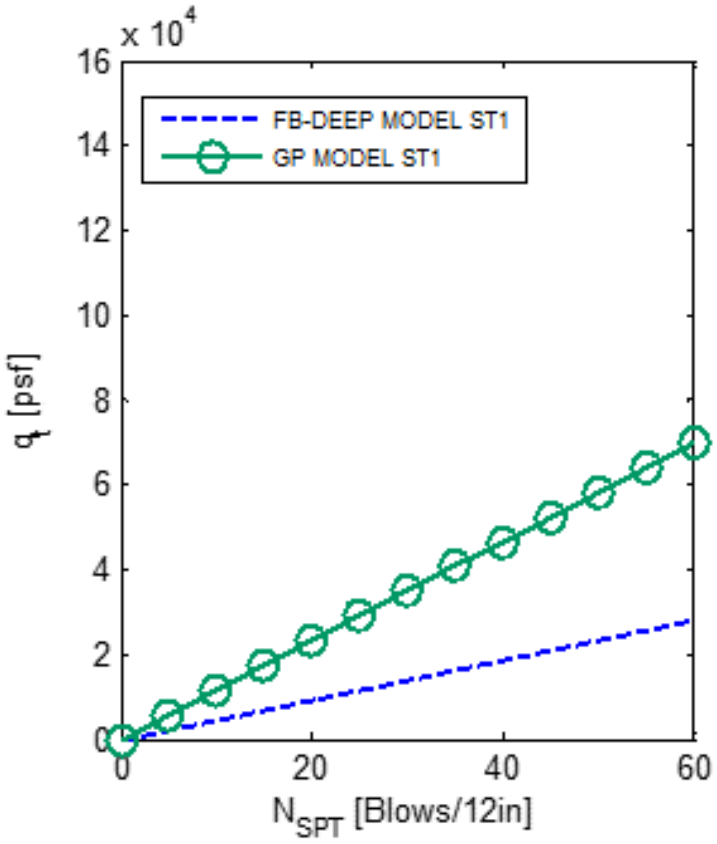

Figure 5.17 Recommended Unit Tip Resistance vs. SPT N Value for Soil Type 1 (Clay)

The recommended unit tip resistance for soil Type 1, may be expressed as,

$$q_T(tsf) = 0.58325 * N \qquad (Soil\ Type\ 1) \qquad \text{Eq. 5.7}$$

In the case of silt (soil type 2), the GP algorithm generated Figure 5.18. Again, the unit tip resistance is higher than FB-DEEP (i.e., bias correction), and the function is linear. In addition, over 40% of the boring data (Figure 5.18 – right) was used in the analysis. However, since the GP function didn't extend over the full range of blow counts (i.e., N=60), it was decided to adjust the curve (i.e., lower slope) to extend over the full blow count range, shown in Figure 5.19.

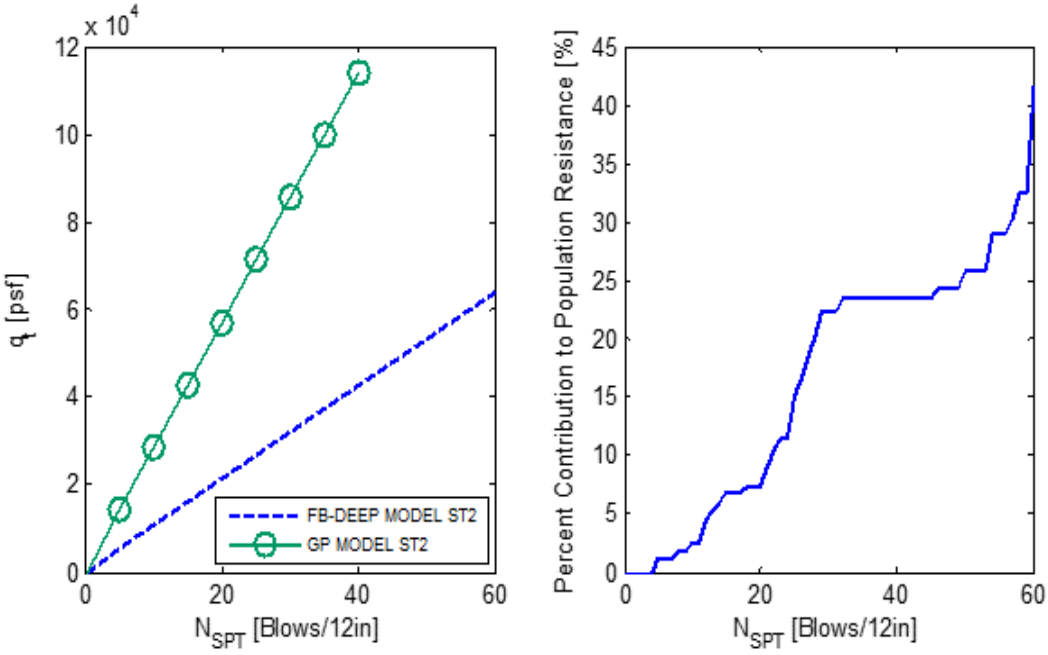

Figure 5.18 GP Unit Tip Resistance vs. SPT N Value for Soil Type 2 (Silt)

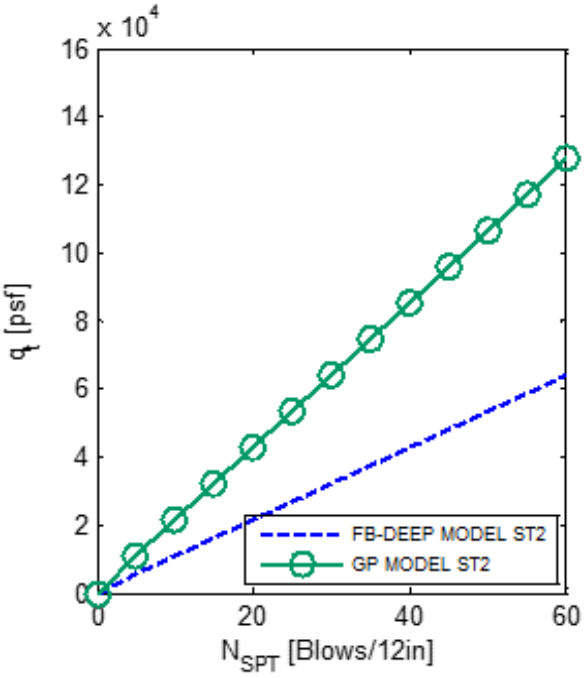

Figure 5.19 Recommended Unit Tip Resistance vs. SPT N Value for Soil Type 2 (Silt)

The recommended unit tip resistance for soil Type 2 (Figure 5.19) is given as,

$$q_T(tsf) = 1.08 * N \qquad (Soil\ Type\ 2) \qquad \text{Eq. 5.8}$$

In the case of sand (soil type 3), the GP algorithm generated Figure 5.20. Again, the unit tip resistance is higher than FB-DEEP (i.e., bias correction), and the function is linear. In addition, approximately 40% of the boring data (Figure 5.18 – right) was used in the analysis. For this case (soil type 3), the GP function extended over the full range of blow counts (i.e., N=60), and no adjustment to the curve was considered. The proposed unit tip resistance for soil Type 3 (Figure 5.20) is given as,

$$q_T(tsf) = 1.25 * N \qquad (Soil\ Type\ 3) \qquad \text{Eq. 5.9}$$

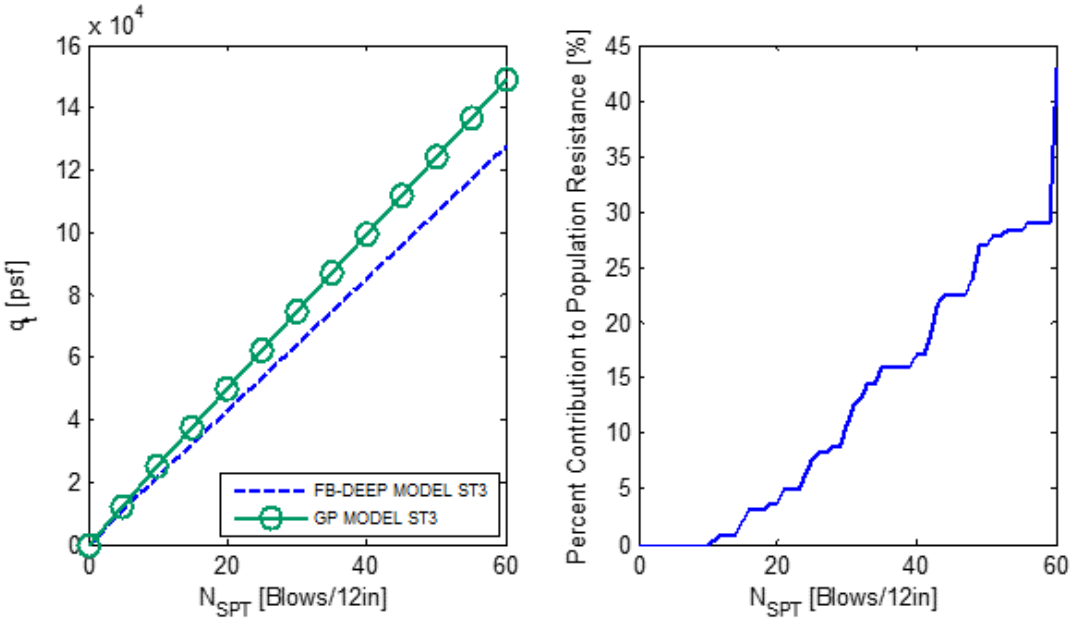

Figure 5.20 GP Unit Tip Resistance vs. SPT N Value for Soil Type 3 (Sand)

In the case of Limestone, soil type 4, the GP algorithm had very little (≤ 4%) data beneath the pile. Consequently, the GP algorithm for soil type 4 was set initially to FB-DEEP's representation (1.2∗ N), with little, if any, changes (i.e., improvements to MSE_{Ln} , Eq. 4.2) occurred, Figure 5.21. Consequently, the FB-DEEP's curve is recommended or the sand curve (Eq. 5.9) may be used, since they are very similar.

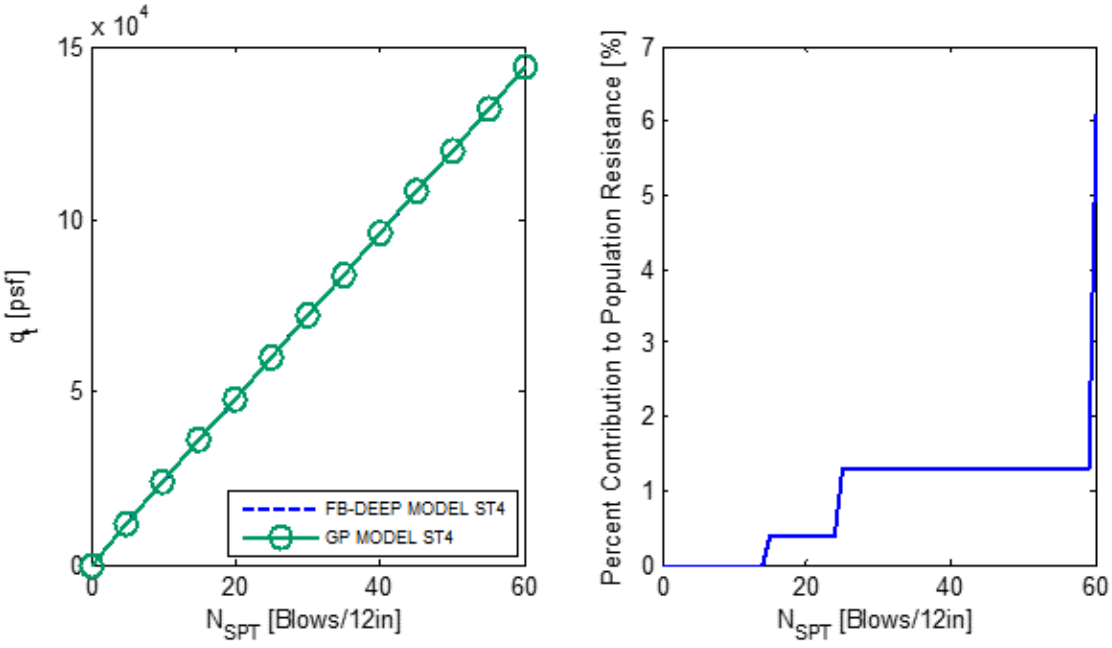

Figure 5.21 Unit Skin vs. SPT N Value for Soil Type 4 (Limestone)

5.5 GP vs. FB-DEEP Predicted Davisson Capacities for All Prestressed Concrete Piles

Of great interest is the comparison of GP/recommended predicted Davisson response with the measured (Table 5.2), Figure 5.22. Note, for unit tip resistance of clays and silts, the recommended Eq. 5.7 and 5.8 were employed. The mean bias, λ_R ($\frac{1}{N}\sum\frac{Measured_i}{Predicted_i}$) was 1.07, and the coefficient of variation, CV_R ($\frac{\sigma_R}{\lambda_R}$), was 0.37. Interestingly, this prediction includes all spatial

and method errors, and is based on the use of all boring data within 100ft of the load test. Also, the measured vs. prediction (Figure 5.22) is independent of whether or not separating the sandy-clay (Figures 5.1, 5.2, 5.5 and 5.6) from clay (i.e., same results).

Presented in Figure 5.23 is the current FB-DEEP's predicted capacity of the piles in Table 5.2, using all borings within 100 ft of each load test. There was no observed difference in the

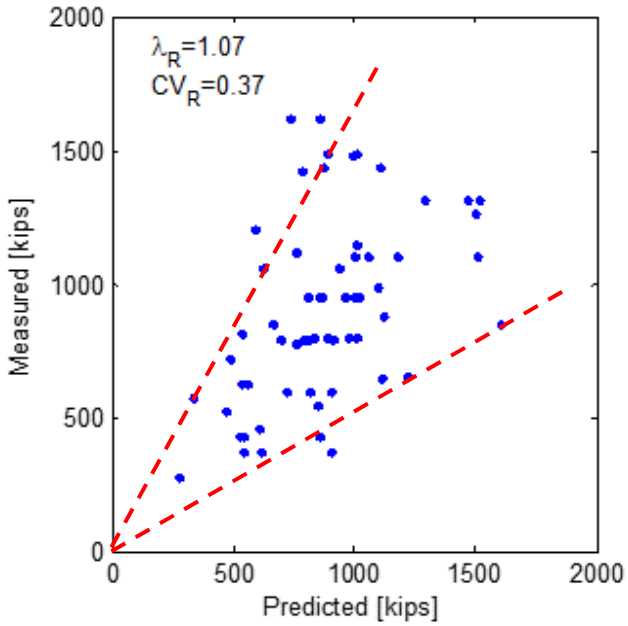

Figure 5.22 Measured Davisson Capacities (Table 5.2) vs. GP Predicted Pile Capacities

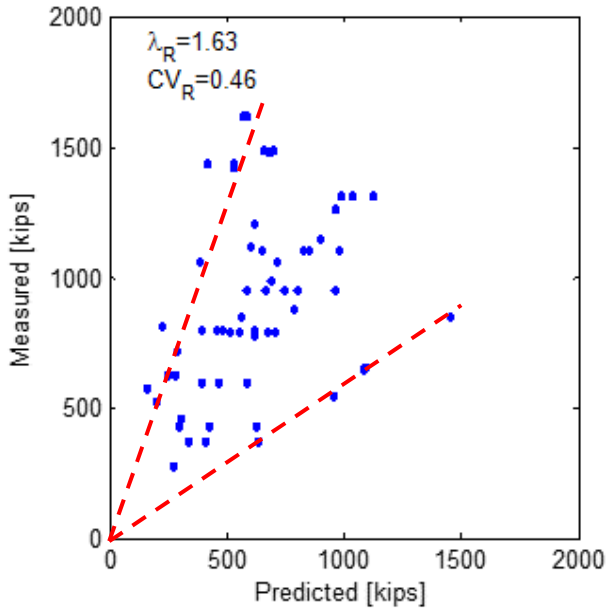

Figure 5.23 Measured Davisson Capacities vs. FB-DEEP (Sandy-Clay Adjustment)

Results if the sandy-clay soils were separated (Figures 5.1, 5.2, 5.5 and 5.6) from the clay (i.e., same results). It is interesting to compare, Figure 5.23 with earlier reported results (Styler, 2005, FDOT Report BD545-17) in Figure 5.24. In the earlier report, similar CV_R (0.433) and bias, λ_R, (1.53) was found. The slight difference is attributed to the increased number of piles (e.g., Dixie, Caminida Bay, etc.) in the newer database.

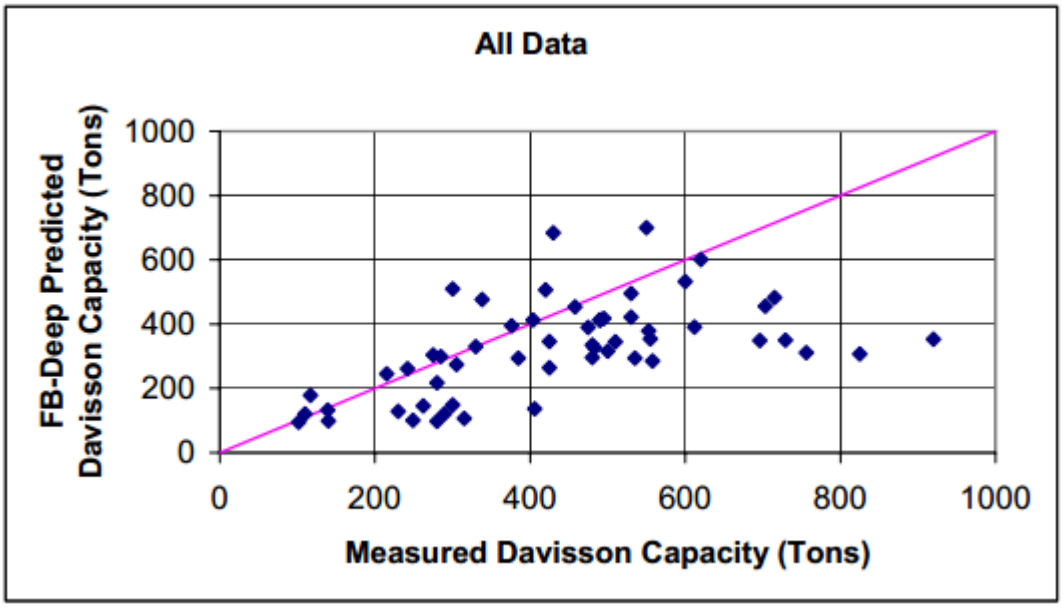

Figure 5.24 Measured Davisson Capacities vs. FB-DEEP (FDOT Report BD545-17)

Given the large bias for FB-DEEP, it was decided to remove the lower limit of assuming that all skin friction and tip resistance values are zero, if SPT N was less than 5. Note that the GP analysis (side and tip) were developed with N values defaulting to 5 in the case of $N < 5$. Consequently the FB-DEEP analysis was rerun on all borings within 100 ft using a default N=5 for the case of $N < 5$, (applied to both skin and tip resistance), Figure 5.25. Evident is the large drop in the bias (1.43) and the CV_R (0.39), versus the original FB-DEEP (bias = 1.63, and CV_R = 0.46).

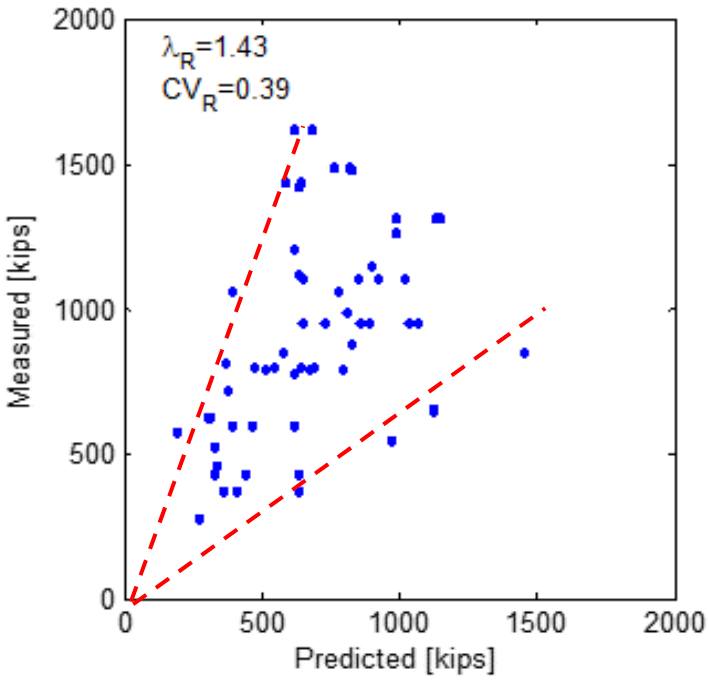

Figure 5.25 Measured Davisson Capacities vs. FB-DEEP (N ≤ 5, N =5)

5.6 Method Error and LRFD Φ Assessment for GP and FB-DEEP Resistances

In order to assess method error, the GP/recommended and FB-DEEP unit skin and tip resistances curves were applied to borings at various distances (100 ft, 500 ft and 1000 ft) from the load test piles (Table 5.2). Shown in Table 5.4 are the GP/recommended average bias, λ_R ($\frac{1}{N}\sum\frac{Measured_i}{Predicted_i}$) and the coefficient of variation, CV_R (σ_R / λ_R) for tip and side resistances individually, as well as for total Davisson (side and tip) capacity based on distance. Also, by using Eqs. 4.19 and 4.20, borings located at various distances (100 ft, 500 ft and 1000 ft) were used to calculate the error between prediction and load test, σ_ε^2, as well as prediction error between borings, $\sigma_{\varepsilon'}^2$, was found along with method error σ_m^2 for the GP/recommended curves. Presented in Tables 5.5 and 5.6 are the results for FB-DEEP with N=0 for N <5, and for FB-DEEP with N=5 for N <5.

Table 5.4 Uncertainty Estimations for GP/Recommended Tip, Side, and Davisson Capacities

a) Unit Tip Resistance:

Nearest Boring Search Distance (ft)	CV_R	λ_R	σ_e^2	$\sigma_{e`}^2$	σ_m^2
100	0.7395	1.3766	0.4258	0.0507	0.4963
500	1.0292	1.5640	0.5851	0.4855	0.2208
1000	1.3517	2.4288	0.9241	0.7878	0.2575

b) Unit Side Resistance:

Nearest Boring Search Distance (ft)	CV_R	λ_R	σ_e^2	$\sigma_{e`}^2$	σ_m^2
100	0.2742	1.0582	0.0855	0.0228	0.1839
500	0.5437	1.1496	0.2159	0.1366	0.2005
1000	0.6263	1.2238	0.2836	0.1201	0.2848

c) Davisson Capacity :

Nearest Boring Search Distance (ft)	CV_R	λ_R	σ_e^2	$\sigma_{e`}^2$	σ_m^2
100	0.3709	1.0743	0.1375	0.0155	0.2431
500	0.5081	1.0612	0.1749	0.1385	0.1575
1000	0.9136	1.2695	0.2760	0.2409	0.1563

Table 5.5 Uncertainty Estimations for FB-DEEP Tip, Side, and Davisson Capacities (N <5, N=0)

a) Tip Resistance:

Nearest Boring Search Distance (ft)	CV_R	λ_R	σ_e^2	$\sigma_{e`}^2$	σ_m^2
100	0.7656	2.4092	1.0367	0.0874	1.0705
500	0.9651	2.6764	1.1150	0.3237	0.9125
1000	3.6942	7.0788	2.0897	1.1549	1.0561

b) Side Resistance:

Nearest Boring Search Distance (ft)	CV_R	λ_R	σ_e^2	$\sigma_{e`}^2$	σ_m^2
100	0.4276	1.4926	0.2470	0.0735	0.2948
500	1.1733	2.1027	0.5390	0.3173	0.343
1000	1.4635	2.6264	1.0089	0.5110	0.6191

c) Davisson Capacity:

Nearest Boring Search Distance (ft)	CV_R	λ_R	σ_e^2	$\sigma_{e`}^2$	σ_m^2
100	0.4539	1.6207	0.3320	0.0293	0.4239
500	0.8695	1.7227	0.3979	0.1897	0.3294
1000	2.2648	2.6268	0.7611	0.4639	0.4184

Table 5.6 Uncertainty Estimations for FB-DEEP Tip, Side, and Davisson Capacities (N <5, N=5)

a) Tip Resistance:

Nearest Boring Search Distance (ft)	CV_R	λ_R	σ_e^2	$\sigma_{e`}^2$	σ_m^2
100	0.7197	2.4203	1.0874	0.0864	1.1222
500	0.8495	2.6349	1.1610	0.3264	0.9559
1000	1.5100	4.0108	1.7041	0.6856	1.1398

b) Side Resistance:

Nearest Boring Search Distance (ft)	CV_R	λ_R	σ_e^2	$\sigma_{e`}^2$	σ_m^2
100	0.3165	1.2315	0.1157	0.0518	0.1852
500	0.5782	1.4008	0.2335	0.1575	0.1972
1000	0.6219	1.4770	0.3276	0.1385	0.3103

c) Davisson Capacity:

Nearest Boring Search Distance (ft)	CV_R	λ_R	σ_e^2	$\sigma_{e`}^2$	σ_m^2
100	0.3952	1.4381	0.2337	0.0249	0.3300
500	0.4935	1.4068	0.2466	0.1085	0.2593
1000	0.8881	1.6443	0.3772	0.2027	0.2957

Evident from the tables (5.3 to 5.5), CV_R for Tip resistance are quite large for all methods at any distance, suggesting that borings at closer distances, or site specific spatial uncertainty assessment of tip resistance is warranted. However, in the case of side resistance, or Davisson total capacity, borings within 100ft will result in reasonable LRFD Φ values as shown in Table 5.7. That is LRFD Φ values are greater than 0.49; however, at borings located at greater distances (D > 100ft, e.g., 500ft), the spatial error becomes so large that useful LRFD Φ will not be calculated. Also, shown in Table 5.7 are Φ/λ values, which represent the percentage of the measured Davisson Capacity available for design. It also characterizes a means of comparing one design method to another with the bias, λ, removed. Consequently, the method, which

should result in the shorter pile lengths on average are: 1) GP/Recommended; 2) FB-DEEP (N<5, N=5) and 3) FB-DEEP (N<5, N=0).

Table 5.7 LRFD Φ and Percentage of Measured Resistance Available for Design

Method	LRFD Φ	Φ/λ
GP/Recommended		
Side – 100ft	0.66	0.62
Side -500ft	0.35	0.30
Davisson -100ft	0.49	0.52
Davisson -500ft	0.34	0.36
FB-DEEP(N<5,N=0)		
Side – 100ft	0.60	0.40
Side -500ft	--	---
Davisson -100ft	0.63	0.39
Davisson -500ft	0.25	0.15
FB-DEEP(N<5,N=5)		
Side – 100ft	0.65	0.54
Side -500ft	0.39	0.28
Davisson -100ft	0.61	0.43
Davisson -500ft	0.42	0.35

Also of great interest is the method error for side, tip and Davisson for the GP/recommended and FB-DEEP algorithms. Using the log variances (σ_{ε}^2, $\sigma_{\varepsilon\prime}^2$, and σ_m^2) given in Tables 5.4 and 5.5, the coefficient of variation of method error (CV_m) was found. Shown in

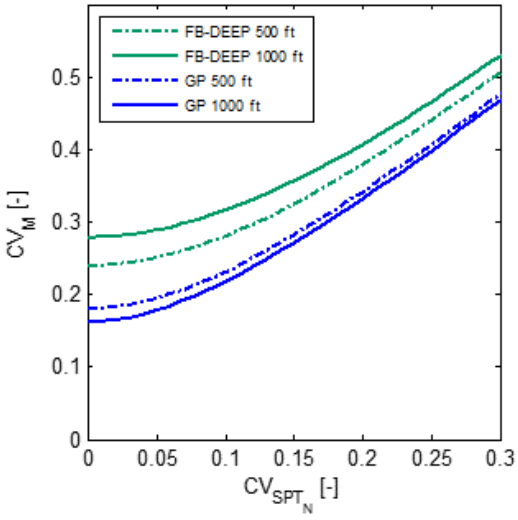

Figure 5.26 Method Error for GP/recommended and FB-DEEP (N<5, N=5) for Davisson Capacity as Function of CV_{SPT}

Figure 5.26 is the CV_m for both the GP/recommended and FB-DEEP (N<5, N=5) for Davisson Capacity at various distances from the pile. An example of the use of the figure would be the case of borings in the footprint of a pile. Assuming CV_{SPT} of 0.12 (e.g., use of automatic and safety hammer on a site), the GP would result in a CV_M of 0.21 and FB-DEEP would give 0.28 (500 ft). Next, using the standard AASHTO Φ/λ plot (Figure 5.27, β =2.5), the GP/recommended Φ/λ is 0.7 and the FB-DEEP value is 0.6. Note, $CV_R = \sqrt{(CV_s)^2 + (CV_M)^2}$ and CV_S is equal to zero when the boring is in the footprint of the pile. The difference between the computed Φ/λ values (0.7 & 0.6) and those given in Table 5.7 (0.36 and 0.35) are attributed to spatial error. Spatial error (CV_S) for any site may be evaluated by running the borings (distances of interest) through the algorithms (e.g., FB-DEEP & GS-DEEP - FDOT BDK-75-977-23) and assessing the standard deviation of the predictions divided by the mean prediction.

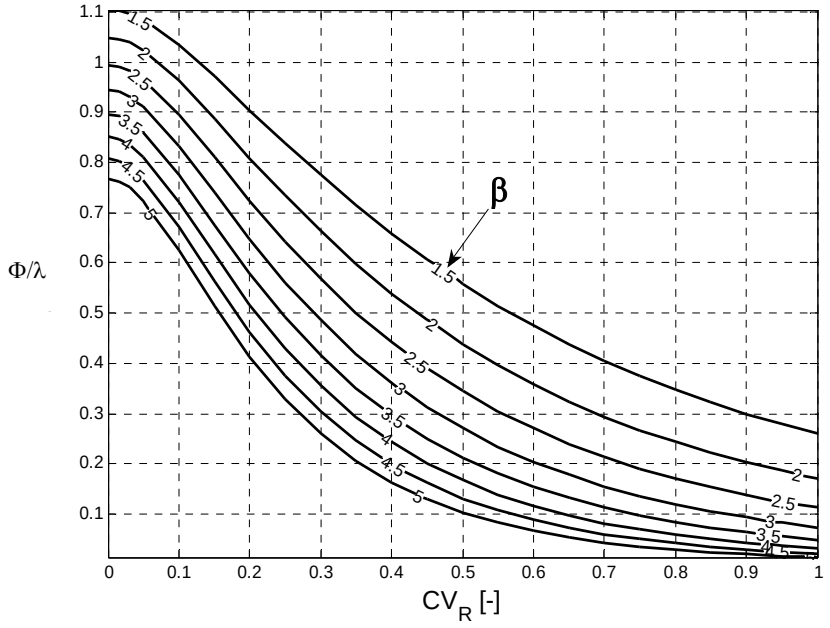

Figure 5.27 Normalized AASHTO Φ/λ vs. CV_R for Different Reliability Values, β

Presented in Figure 5.28 is the method error (CV_M) for side and tip resistances if the GP/recommended or FB-DEEP (N<5, N=5) algorithms are used. Note, both the GP/recommended and FB-DEEP have the same CV_M for side friction at 500ft (left figure). Note, each of the figures may be used to assess total uncertainty, $CV_R = \sqrt{(CV_s)^2 + (CV_M)^2}$ for skin and tip separately. Interestingly, the method error (CV_M) for tip resistance (Figure 5.28, right side) for the GP method is significantly smaller than FB-DEEP. This may be attributed to the bias (FB-DEEP > GP) and the variability of tip resistance over zones of interest (i.e., 8B above and 3.5B below tip vs. 4B below the tip).

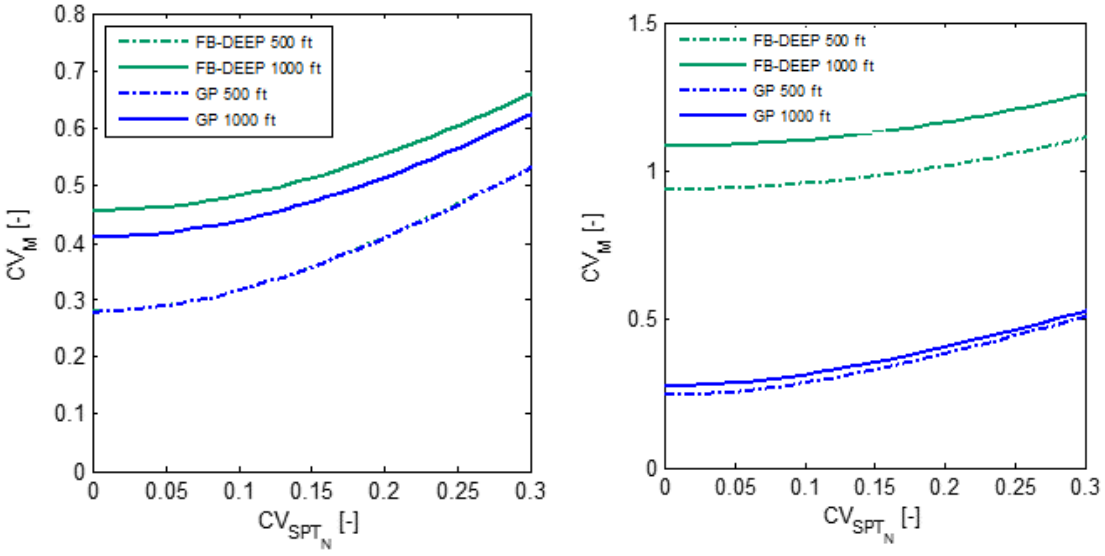

Figure 5.28 Method Error for GP/recommended and FB-DEEP (N<5, N=5) side (left) and tip (right) as Function of CV_{SPT}

5.7 GP Assessment of Mobilized Side Friction of a Drilled Shaft in Limestone

Besides piles, the GP algorithm was run on the drilled shaft database, Table 5.7, to assess the normalized mobilized unit skin friction and displacements (i.e., T-Z) curves for shafts embedded in Florida Limestone. For normalization, the mobilized unit skin friction was divided by the measured ultimate skin friction and the shaft displacement was divided by the diameter of the drilled shaft. A total of 33 curves (Figure 5.29) were considered in GP analysis. Shown in Figure 5.29 is the GP predicted (red line) T-Z curve (normalized) along with the MSE error versus iteration number for the analysis. The equation describing the curve is,

$$\frac{f_s}{f_{s,ult}} = \left[\frac{4*r}{4*r+1}\right]^{0.5} \qquad \text{Eq. 5.10}$$

where r = (z, displacement) / B (shaft Diameter). Of interest is a comparison between FB-DEEP's (Kim 2001) mobilized unit skin friction vs. displacement curve with the GP results, Figure 5.30. Evident, the curves are quite similar on average; however, the mean square error (MSE) for the GP curve (0.0198) is slightly better than Kim (2001) curve (0.1359).

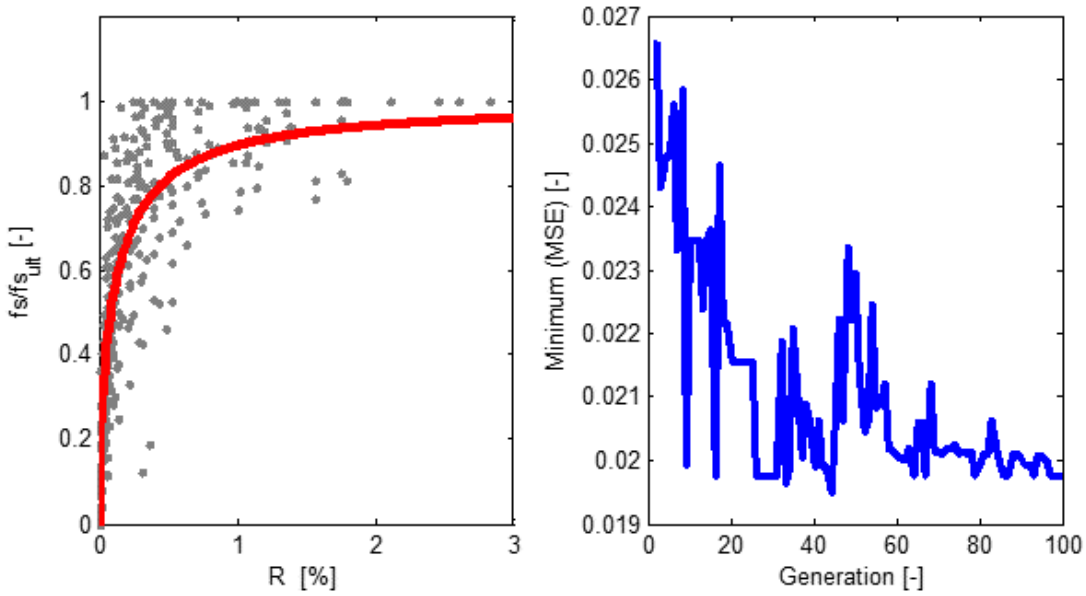

Figure 5.29 GP Mobilized Unit Skin Friction vs. Displacement (Normalized) and MSE vs. Generation (i.e., Iteration)

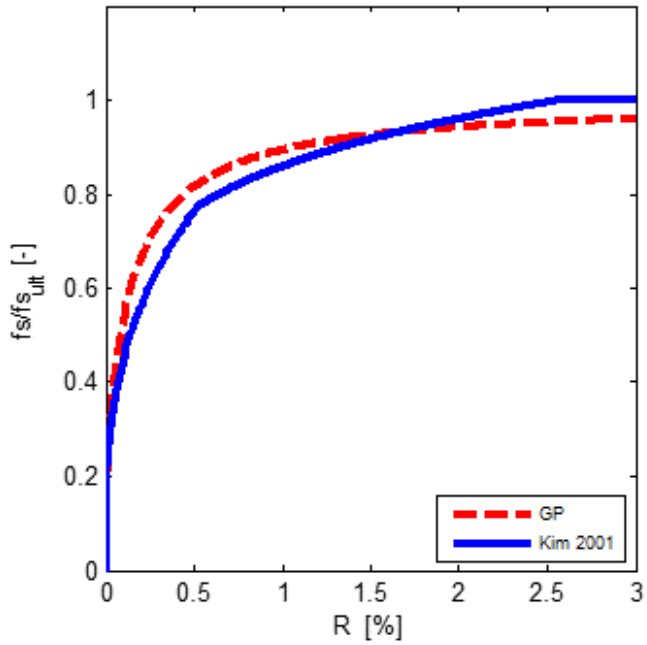

Figure 5.30 Comparison of GP with Kim (2001) Mobilized Skin Friction vs. Displacement Curve (Normalized)

5.8 GP Assessment of Ultimate Skin Friction in Limestone

Using the measured ultimate skin friction from segments of the load tests with the report rock strengths (q_u and q_t), and recoveries, the relationship between the measured and predicted skin friction was investigated. Initially, all rock strengths were considered, but only limited correlation was observed. Then as identified in FDOT BC354-08, limiting rock strengths (q_u and q_t) were investigated. Since peak ultimate skin frictions at a point was 24 tsf, observed in Gandy and Fuller Warren, then associated peak rock strengths of 120 tsf (q_u) and 20 tsf (q_t) were selected [i.e., limiting ½ sqrt(q_u x q_t)]. In addition, since rock strength data is lognormal distributed, the log of all rock data (e.g., q_u and q_t) was taken, as well as mean and one plus and minus standard deviation of the data was used for the analysis. Specifically, the mean strengths (μ_{qu} ,μ_{qt}) , as well as mean plus one standard deviation ($\mu_{qu} + \sigma_{qu}$,$\mu_{qt} + \sigma_{qt}$) and mean minus one standard deviation ($\mu_{qu} - \sigma_{qu}$,$\mu_{qt} - \sigma_{qt}$) of both q_u and q_t were found and converted back to normal space. Similarly, the unit skin friction along any shaft (T-Z curves) for all of the sites were converted to log space (i.e., log of values), and the mean (μ_{fs}) as well as mean plus one standard deviation ($\mu_{fs} + \sigma_{fs}$) and mean minus one standard deviation ($\mu_{fs} - \sigma_{fs}$) was found and converted back to normal space. Next, the pairs (means), (means + standard deviation), and (means – standard) deviation of both strengths and unit skin friction, as well as recoveries were analyzed with the GP algorithm. Presented in Figure 5.31 is a comparison of the measured and predicted unit skin for all pairs considered. For the predicted, the FDOT equation,

$$f_{s,predicted} = \frac{1}{2}\sqrt{q_u}\sqrt{q_t} \text{ x Recovery} \qquad \text{Eq. 5.11}$$

was found to give a good fit to the data using the following bias correction, $f_{s,bias\_corrected,}$

$$f_{s,bias\_corrected} = 0.768\left(\frac{1}{2}\sqrt{q_u}\sqrt{q_t}\, x\, Recovery\right) \qquad \text{Eq. 5.12}$$

The method error, σ_{LF} (spread of data about trend line) was found to be 1.96 tsf.

Shown in Figure 5.32 is FDOT current practice of removing one standard deviation of the data (q_u and q_t), revaluate the mean and standard deviations, and then computing the mean unit skin friction (Eq. 5.11) and one standard lower bound (Eq. 5.11 mean – one standard deviation). The CV_R (measure/predicted) of pairs were 0.77. The larger spread (Figs. 5.32 vs. 5.31) is attributed to truncation of tails of the strength data, which effects the bias of the predictions.

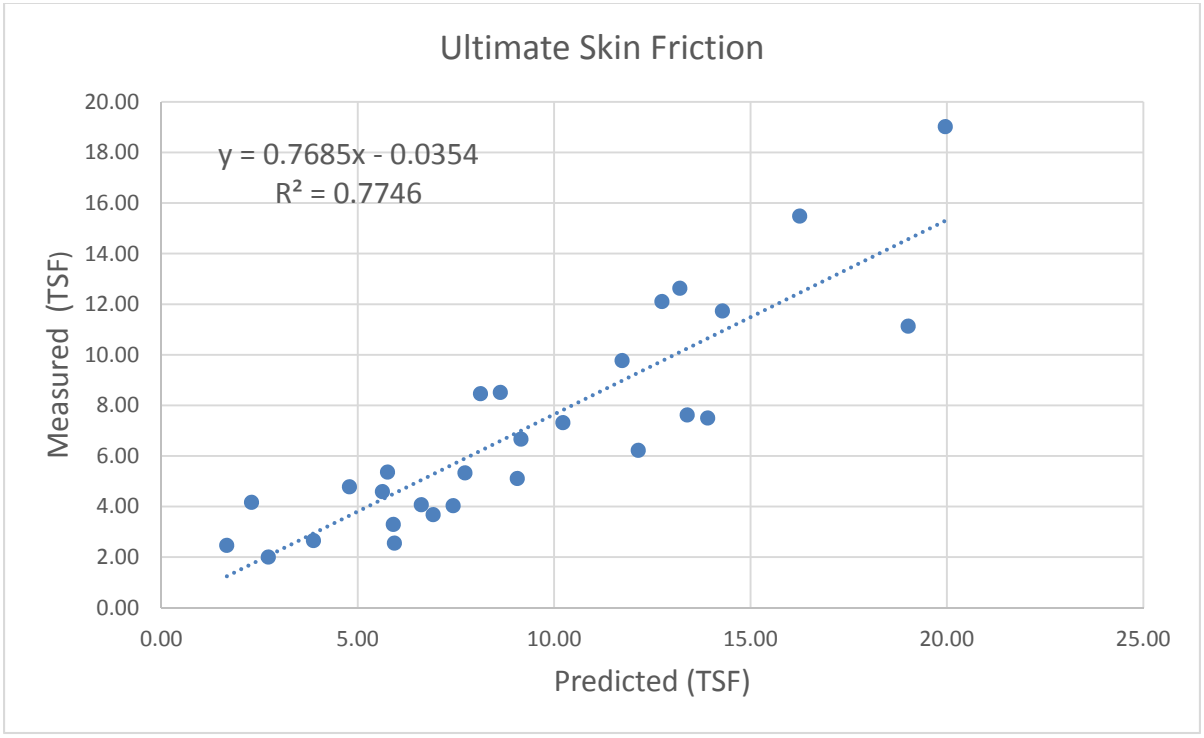

,

Figure 5.31 Measured and Predicted Unit Skin Friction for Florida Limestone

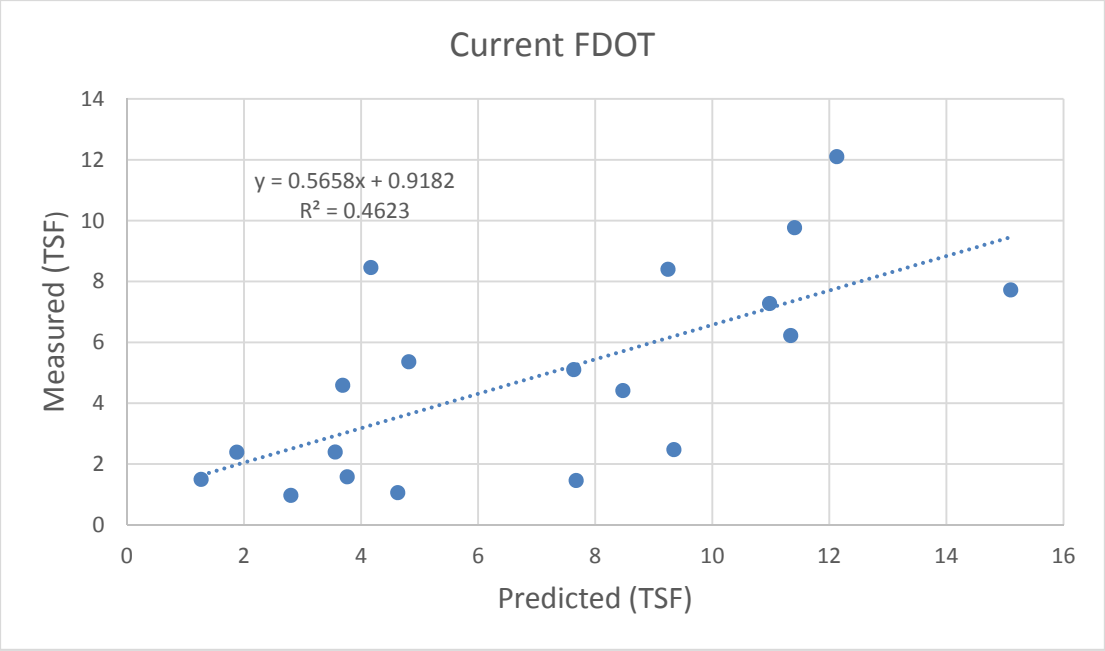

Figure 5.32 Measured and Predicted Unit Skin Friction for Florida Limestone

CHAPTER 6
SUMMARY AND CONCLUSIONS

6.1 FDOT Database of Prestressed Concrete Piles and Drilled Shaft

For this work, 64 static load tests on 18 sites in Florida and Louisiana (1 site) were collected from district reports and plans. For each site, SPT borings and Laboratory (e.g., USCS) data (State Materials Office) was also collected. A total of 458 borings on the 19 sites with known locations (e.g., station and offset, or GPS) was digitized and uploaded into the FDOT online database. For the 64 static load tests, 48 reached the Davisson capacity, and 28 had separate assessment of skin friction and tip resistance using either strain gages or tip telltales. Individual load vs. displacement curves, as well as mobilized skin and tip resistance at Davisson Capacity were digitized and uploaded into the online database.

In the case of drilled shafts, 66 load tests (33 Osterberg, 15 top down static, and 15 Statnamic tests) were collected from the Districts on 18 Florida Bridge sites. For all the drilled shaft sites, a total of 815 borings with laboratory data (e.g., USCS, rock strength, etc.) were collected along with their locations (station and offset or GPS). Each of the borings and laboratory data was digitized and subsequently uploaded into the database. In the case of the load tests, individual T-Z (unit skin friction vs. displacement) curves along with the Load vs. Displacement response of each shaft were also digitized and uploaded.

6.2 GP Algorithm

An integral component to this research was the development of a GP algorithm to back compute unit skin and tip resistance curves for piles as well as drilled shafts. Using concepts of genetic evolution (Cross Over, Mutation, and Reproduction), the algorithm altered arithmetic operators (+, -, x, /), and constants to generate unit resistance curves based on minimization of the log of the mean square error (MSE_{Ln}). For instance, Figure 6.1 shows a Cross- over

Operation. Use of minimization of MSE was selected because it reduced both the bias (measured/predicted) as well as its variance.

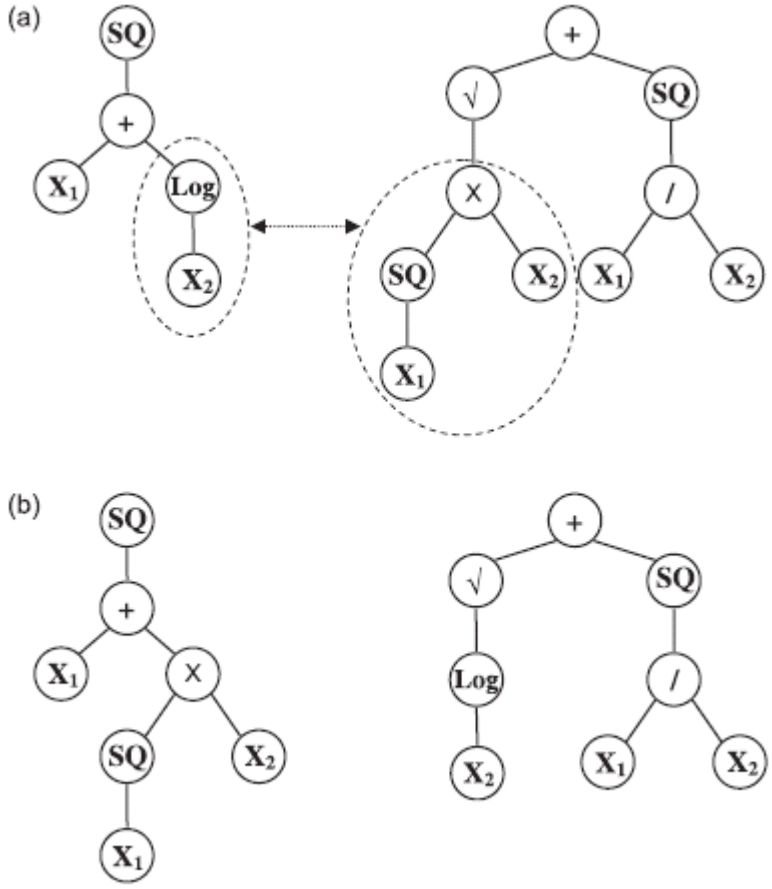

Figure 6.1 Cross-Over Operation in Genetic Programming Showing (a) Parents and (b) Children (Rezania and Javadi, 2007)

In the estimation of the unit side and tip resistance curves, multiple averaging concepts were investigated. For instance for side resistance, Figure 6.2, both arithmetic and harmonic averaging were considered,

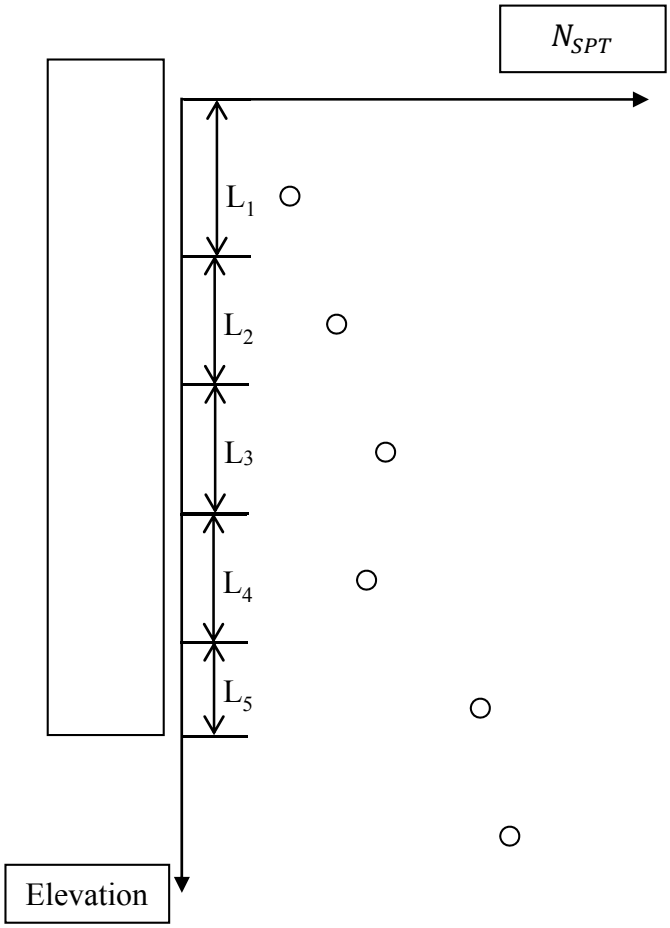

Figure 6.2 Determination of L_i Along Pile Side for each N_{SPT}

$$\bar{f}_{ST} = \frac{1}{\sum L_{ST_i}} \left(\sum L_{ST_i} f_{ST_i}^{k} \right)^{\frac{1}{k}} \quad \text{Eq. 6.1}$$

$$Q_{side} = P \sum_{ST=1:n} \bar{f}_{ST} \sum L_{ST_i} \quad \text{Eq. 6.2}$$

where k in Eq. 3.3 is the averaging process (Renard and de Marsily, 1997), ranging from -1 to +1; in the case where k = -1, harmonic averaging is occurring (i.e., reciprocal of unit skin frictions), k = 0 is geometric averaging (which can be shown through limit analysis) and k = 1 is arithmetic averaging (currently used in FB-DEEP).

6.3 GP/Recommended Unit Skin and Tip Resistance Curves for Concrete Piles

All borings within 100 ft of the load tests were run through the GP algorithm to assess unit skin and tip resistance curves for concrete piles. The following unit skin friction curves were developed:

$$f_s(tsf) = USF = 0.051 * N + 0.098 \quad < 1.5tsf\ (3000\ psf), (Soil\ Type\ 1) \qquad \text{Eq 6.3}$$

$$f_s(tsf) = USF = 0.037 * N \quad < 1.375tsf\ (2750\ psf) \quad (Soil\ Type\ 2) \qquad \text{Eq 6.4}$$

$$f_s(tsf) = USF = 0.0125 * N + 0.175 \qquad (Soil\ Type\ 3) \qquad \text{Eq 6.5}$$

$$f_s(tsf) = USF = 0.0125 * N \qquad (Soil\ Type\ 4) \qquad \text{Eq 6.6}$$

In the case tip resistance, the following linear representations were developed:

$$q_T(tsf) = 0.58325 * N \qquad (Soil\ Type\ 1) \qquad \text{Eq. 6.7}$$

$$q_T(tsf) = 1.08 * N \qquad (Soil\ Type\ 2) \qquad \text{Eq. 6.8}$$

$$q_T(tsf) = 1.25 * N \qquad (Soil\ Type\ 3\ \&\ 4) \qquad \text{Eq. 6.9}$$

For the analysis, the Unified Soil Classification System (USCS) was used to characterize all soils. Selection of silty-clays (e.g., clays with silt content >30) characterized as either soil type 1 or 2 revealed little if any difference in the results. However, the algorithm found that reducing all SPT N values to 0 when N <5 was very conservative. This conservatism was also found for FB-DEEP, bias (λ, measured/predicted), reduced from 1.6 to 1.4 for N < 5, N=5. This bias was observed in both skin and tip estimates. Consequently, it is proposed that all SPT N values should have a minimum limit of 5 when estimating skin and tip resistance.

In the case of averaging, arithmetic (vs. geometric and harmonic) was found to result in the lowest MSE_{Ln}, $CV_{R,}$ and bias for both skin and tip resistance assessment (Eqs. 6.3 to 6.9). Also, it was discovered that FB-DEEP's estimate of tip resistance was very conservative (even for N < 5, N=5) attributed not only to the unit tip resistance curves, but also the averaging

process 8B above and 3.5B below the tip. In order to increase the mean SPT blow count, as well as reduce the error, averaging just 4B below the tip (Eqs. 6.7 to 6.9) was found to results in the lowest MSE_{Ln}, $CV_{R,}$ and bias.

6.4 Method Error and LRFD Φ Assessment for GP and FB-DEEP Resistances of Piles

Using both the GP/recommended curves, and FB-DEEP (for N < 5, N=5), the borings at various distances (100ft, 500ft and 1000ft) were used to evaluate side, tip and total Davisson capacity of all the test piles. It was found that by using borings within 100ft of test piles that LRFD resistance,Φ, values of 0.66 (side) and 0.49 (Davisson) were appropriate for the GP curves, and 0.65 (side) and 0.61 (Davisson) were acceptable for the FB-DEEP (for N < 5, N=5) for β=2.5. For comparison (i.e., bias removed), the Φ/λ values were 0.62 (side) and 0.52 (Davisson) for the GP, and 0.54 (side) and 0.43 (Davisson) for FB-DEEP (for N < 5, N=5). Note, these values considered both spatial and method error and are recommended for borings within 100ft.

To improve the LRFD Φ assessment (e.g., borings closer to pile - reduce spatial uncertainty, required for tip assessment), the method error for side, tip and Davisson capacity was assessed for each method (GP and FB-DEEP). Using both the boring and load tests, the error between prediction and load test, σ_{ε}^2, as well the prediction error between borings, $\sigma_{\varepsilon\prime}^2$, was found along with the method error σ_m^2 (or CV_m) for both the GP and FB-DEEP algorithms based on distance (100ft, 500ft and 1000ft). For instance shown in Figure 6.3 is the CV_m for both GP and FB-DEEP algorithms based on distance, and SPT uncertainty, CV_{SPT} (e.g., automatic vs. safety hammer).

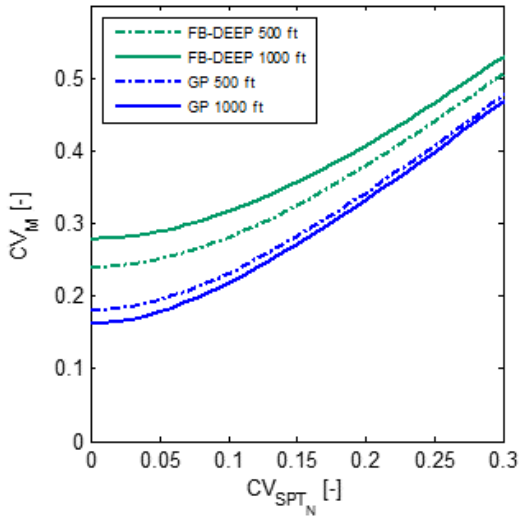

Figure 6.3 Method Error for GP/recommended and FB-DEEP (N<5, N=5) for Davisson Capacity as Function of CV_{SPT}

A simple use of the figure would be the case of borings in the footprint of a pile. Assuming CV_{SPT} of 0.12 (e.g., use of automatic and safety hammer on site), the GP would result in a CV_M of 0.21 and FB-DEEP would give 0.28 (500 ft). Next, using the standard AASHTO Φ/λ plot (Figure 5.27, β =2.5), the GP/recommended Φ/λ is 0.7 and the FB-DEEP value is 0.6. Note, for $CV_R = \sqrt{(CV_s)^2 + (CV_M)^2}$, the CV_S value is zero when the boring is in the footprint of the pile (i.e., no spatial uncertainty). In the case of borings away from the pile, the spatial error (CV_S) for any site may be evaluated by running the borings (any distances of interest) through the algorithms (e.g., GP & FB-DEEP) and assessing the standard deviation of the predictions divided by the mean prediction. Similar curves (Figure 5.28) were developed for both side and tip resistance methods, Figure 5.28.

6.5 GP Assessment of Side Friction of Drilled Shafts in Florida Limestone

Besides piles, the GP algorithm was run on the drilled shaft database to assess the normalized mobilized unit skin friction and displacements (i.e., T-Z) curves for shafts embedded in Florida Limestone. For normalization, the mobilized unit skin friction was divided by the measured ultimate skin friction and the shaft displacement was divided by the diameter of the drilled shaft. The GP algorithm developed the following normalized equation,

$$\frac{f_s}{f_{s,ult}} = \left[\frac{4*r}{4*r+1}\right]^{0.5} \qquad \text{Eq. 6.10}$$

where r = (z, displacement) / B (shaft Diameter). A comparison between FB-DEEP's (Kim 2001) mobilized unit skin friction vs. displacement curve with the GP results, is shown in Figure 6.4 Evident, the curves are quite similar on average; however, the mean square error (MSE) for the GP curve (0.0198) is slightly better than Kim (2001) curve (0.1359).

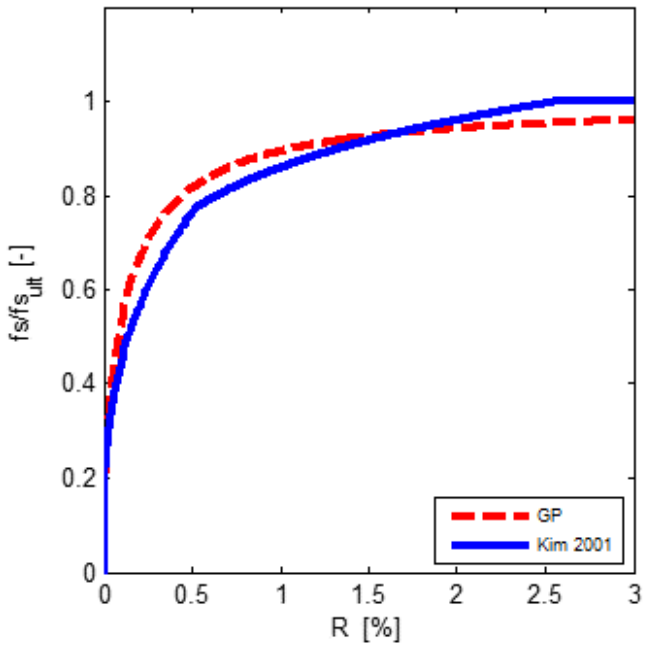

Figure 6.4 Comparison of GP with Kim (2001) Mobilized Skin Friction vs. Displacement Curve (Normalized)

For the case of ultimate skin friction, the following bias corrected unit skin friction from rock strength is proposed.

$$f_{s,bias\_corrected} = 0.768\left(\frac{1}{2}\sqrt{q_u}\sqrt{q_t}\ x\ Recovery\right) \quad \text{Eq. 6.12}$$

For the rock strengths, limits on unconfined (q_u < 120 tsf) and split tension (q_t <20) are warranted, that higher values are set to the limits. Also, when estimating the upper and lower bounds of unit skin friction, the log of the data should be used. That is, the log of unconfied and split tension data should be determined, then the mean standard deviation of each should be found and then converted back to normal space and substitute into Eq. 6.12 to find the range.

REFERENCES

Alkroosh, I. and Nikraz, H. (2011). Correlation of Pile Axial Capacity and CPT Data Using Gene Expression Programming. *Geotechnical Geological Engineering*, 29(5), 725-748.

Chung, J.H., Ko, J. Klammler, H., McVay, M., and Lai, P. (2011). A Numerical and Experimental Study of Bearing Stiffness of Drilled Shafts Socketed in Heterogeneous Rock. *Computer and Structures*, 90, 145-152.

Evett, M., & Fernandez, T. (1998, July). Numeric mutation improves the discovery of numeric constants in genetic programming. In *Genetic Programming 98: Proceedings of the Third International Conference* (pp. 223-231).

Kim, M. H. (2001). *Analysis of Osterberg and statnamic axial load testing and conventional lateral load testing* (Master thesis, University of Florida).

Koza, J. R. (1992). *Genetic programming: on the programming of computers by means of natural selection* (Vol. 1). MIT press.

McVay, M. C., Ellis Jr, R. D., Kim, M., Villegas, J., Kim, S. H., & Lee, S. (2003). *Static and dynamic field testing of drilled shafts: Suggested guidelines on their use for FDOT structures* (No. WPI No. BC354-08,).

McVay, M. C., Klammler, H., Faraone, M. Dase, K., Jenneisch, C. (2012). *Development of Variable LRFD PHI Factors for Deep Foundation Design Due to Site Variability* (FDOt Contract No BDK75-977-23).

Nawari, N.O., Liang, R., Nusairat, J. (1999) Artificial Intelligence Techniques for the Design and Analysis of Deep Foundations, *Electronic Journal of Geotechnical Engineering*, http://geotech.civeng.okstate.edu/ejge/ppr9909/index.html

Phoon, K. K. & Kulhawy, F. H. (1999). Characterization of geotechnical variability. *Canadian Geotechnical Journal*, 36(4), 612-624.

Renard, P. & De Marsily, G. (1997). *Calculating Equivalent Permeability: A Review*, Advances in Water Resources, 20 (5), 253-278.

Rezania, M., & Javadi, A. A. (2007). A new genetic programming model for predicting settlement of shallow foundations. *Canadian Geotechnical Journal*,*44*(12), 1462-1473.

Shahin, M. A., & Jaksa, M. B. (2005). Neural network prediction of pullout capacity of marquee ground anchors. *Computers and Geotechnics*, *32*(3), 153-163.

Styler, M. A. (2006). *Development and implementation of the DIGGS format to perform LRFD resistance factor calibration of driven concrete piles in Florida* (Master Thesis, University of Florida).